MIT-4105-2
MITNE-110

MASSACHUSETTS INSTITUTE OF TECHNOLOGY
DEPARTMENT OF NUCLEAR ENGINEERING
Cambridge, Massachusetts 02139

DESIGN, CONSTRUCTION AND EVALUATION OF A FACILITY FOR THE SIMULATION OF FAST REACTOR BLANKETS

by
I.A. Forbes, M.J. Driscoll, T.J. Thompson,
I. Kaplan and D. D. Lanning

February 1970

Contract AT (30-1) 4105
U.S. Atomic Energy Commission

ERRATA

Page	Correction
11	3rd line from bottom: delete "Since".
12	2nd line from bottom: change "respect" to "report"
110	Table A.1: change "x" to "χ"

MASSACHUSETTS INSTITUTE OF TECHNOLOGY

DEPARTMENT OF NUCLEAR ENGINEERING

Cambridge, Massachusetts

DESIGN, CONSTRUCTION AND EVALUATION OF A FACILITY FOR THE SIMULATION OF FAST REACTOR BLANKETS

by

I. A. Forbes, M. J. Driscoll, T. J. Thompson,

I. Kaplan and D. D. Lanning

February, 1970

MIT - 4105 - 2

MITNE - 110

AEC Research and Development Report

UC - 34 Physics

Contract AT(30-1)4105

U. S. Atomic Energy Commission

DISTRIBUTION

MIT-4105-2 MITNE-110

AEC Research and Development Contract

UC-34 Physics

1-3. U. S. Atomic Energy Commission, Headquarters,
Division of Reactor Development and Technology,
Reactor Physics Branch.

4. Argonne National Laboratory,
Liquid Metal Fast Breeder Reactor Program Office,
9700 South Cass Avenue
Argonne, Illinois, 60439.

5. H. S. Potter, New York Patent Group,
U. S. Atomic Energy Commission,
Brookhaven Office,
Upton, New York, 11973.

6, 7. U. S. Atomic Energy Commission,
Cambridge Office.

ABSTRACT

A facility has been designed and constructed at the MIT Reactor for the experimental investigation of typical LMFBR breeding blankets. A large converter assembly, consisting of a 20-cm-thick layer of graphite followed by a 17.5-cm-thick UO_2 fuel region, is used to convert thermal neutrons into fast neutrons to drive a blanket mockup. Operating at 55 watts, the converter generates blanket fluxes at an equivalent LMFBR core power of about 350 watts, with as little as one-tenth of the blanket material required for a critical assembly. Calculations show that the converter leakage spectrum is a close approximation to the core leakage spectrum from reference LMFBR designs, and that the axial distribution of the neutron flux in the blanket assembly simulates that in the radial blanket of a large LMFBR when the effective height and width of the blanket assembly are correctly chosen.

Testing of the completed facility with a blanket composed of 50 v/o iron and 50 v/o borax showed that the lateral flux distributions were cosine-shaped, and that lateral spectral equilibrium was achieved in a large central volume of the blanket. Backscattering from concrete shielding surrounding the experiment was found to affect no more than the outer 30 cm of the blanket assembly, confirming the results of two-dimensional multigroup calculations. Measurements of the axial activity of gold and indium show good agreement with 16-group, S_8 ANISN calculations.

ACKNOWLEDGMENTS

The successful completion of the Blanket Test Facility is due to the support of both M. I. T. and the U. S. Atomic Energy Commission, and to the contributions of a large number of individuals. The work described in this report has been performed primarily by the principal author, I. A. Forbes, who has submitted substantially the same report in partial fulfillment of the requirements for the Ph. D. degree at M. I. T.

Overall direction of the project has been shared by Professors M. J. Driscoll, T. J. Thompson (now on leave of absence) and, more recently, D. D. Lanning. Professors I. Kaplan, N. C. Rasmussen and F. M. Clikeman are contributing investigators.
Messrs. Albert T. Supple, Jr., Ed Barnett and George Sullivan have provided great assistance during construction and initial operation of the facility, as have a large number of the students in the M. I. T. Nuclear Engineering Department, including Dug Choi, Jack Donohew, Jr., James Klucar, Timothy Leung, Nestor Ortiz, Shivaji Seth and Joseph Synan.

Much of the equipment for the Blanket Test Facility was fabricated in the Reactor Machine Shop. The staff of the Machine Shop, and also those of the M. I. T. Reactor, the Reactor Electronics Shop and the Radiation Protection Office have provided assistance and advice throughout the design, construction and startup of the facility. Mrs. Mary Bosco has ably prepared the final manuscript.

All computer calculations were done at the M. I. T. Information Processing Center.

TABLE OF CONTENTS

LIST OF TABLES

LIST OF FIGURES

Chapter 1

INTRODUCTION

1.1 FOREWORD

In the international program to develop an economical fast breeder reactor, considerable effort has been expended on experimental fast reactor physics. Most of this research has been conducted with low-power fast critical assemblies such as ZPR-III, ZPR-VI, VERA, ZEBRA, MASURCA and SNEAK.[1, 2] To a lesser extent, work has also been done with subcritical assemblies such as Chezem's uranium metal exponential experiment,[3] the Argonne Fast Exponential Experiment,[4] the pulsed subcritical assembly, SUAK,[5] and HARMONIE.[2]

Nearly all of this research, however, has been core-oriented: measurements of such parameters as breeding and fission ratios, neutron spectra and heterogeneity effects have generally been limited to the core region, and very little work has been done in extending these measurements out into the breeding blanket region. In fact, in many of the assemblies no blanket is used, or a crude approximation to realistic blanket compositions is made, and reflector material at the outer periphery of the blanket is seldom included.

Since the axial and radial blankets of proposed LMFBR designs typically contribute one quarter to one third of the total breeding ratio, and thus, in a manner of speaking, the entire breeding

gain. In addition, theoretical prediction of reactor physics parameters is considerably more complex and unreliable in the blanket region than it is in the core, due mainly to the strong spatial dependence of the neutron energy spectrum. It has consequently become increasingly evident that a systematic experimental study of the blanket region would be extremely desirable. Indeed, the measurement of reaction rates and neutron energy spectra in the blanket and the determination of the effects of blanket and outer reflector composition and thickness have been assigned Priority 1 under the USAEC's LMFBR Program Plan.[6]

1.2 INTRODUCTION TO THE PRESENT WORK

Early in 1967, steps were taken to initiate experimental fast reactor blanket research at M.I.T.[7] To eliminate the necessity for a critical assembly, an investigation was made involving the use of a uranium-loaded fission (or converter) plate powered by the thermal neutron flux from the MITR thermal column to generate a fast neutron flux for testing a blanket mockup. It was required as a primary design objective that the converter plate have a leakage spectrum and albedo typical of the core of a large LMFBR. These requirements were considerably more stringent than those imposed on most previous fission plate designs, where the stress has been only on thermal to fast conversion and not on concurrent spectrum shaping.[4, 8] Calculations to determine the optimum design of the converter assembly comprised the major portion of the theoretical work discussed in this respect. The results of these analytical and numerical studies showed that this

special type of exponential facility has certain advantages over a critical facility for blanket studies. Apart from the obvious ones of low cost and safety, it requires only one tenth of the volume of material needed for a critical mockup, while at the same time, a 50-watt converter is capable of generating blanket region fluxes equivalent to a critical assembly operating at about 350 watts.

Failure to attain true spectral equilibrium in the ANL Fast Exponential Experiment was attributed to both poor source matching by the converter plate and to backscattering.[10] Considerable attention was therefore given to determining the size of the blanket assembly in order to correctly simulate leakage effects and to minimize the detrimental effect of the backscattering of leakage neutrons by the biological shielding surrounding the experiment. In most critical facilities, the backscatter problem is reduced by locating the assembly in the center of a large shielded cell, leaving as much free volume around the experiment as is practicable.[9] For an installation in the MITR, however, this solution was not possible. Thus the design philosophy had to be to accept biological shielding in close proximity to the experiment, and to reduce backscatter effects by the use of neutron absorbers, by minimizing the streaming of neutrons around the assembly, and by making the blanket dimensions large enough to prevent backscattered neutrons from penetrating to the central blanket region used for experimental purposes.

Construction of the Blanket Test Facility was begun in July, 1968, funded by an M.I.T. research grant until July, 1969, at which time support under USAEC Contract AT(30-1)4105 commenced.

Construction was completed in September, 1969, and testing of the facility with the first simulated blanket started in October, 1969.

Location of the experiment at the rear of the MITR graphite-lined hohlraum was achieved by removing the former thermal column door and adding new heavy concrete shielding to form an irradiation cave approximately 6 ft. X 6 ft. X 6 ft. (see Figure 1.1). Access to the cavity is gained by removing two 15-ton shield doors using the reactor building's overhead crane. The converter plate and simulated blanket assembly are mounted on separate carts which run on rails extending from the front of the irradiation cave out to the containment wall, allowing the carts to be rolled into, or removed from, their operating position. Since the converter plate becomes considerably more radioactive than the blanket assembly during irradiation, mounting them on separate carts reduces personnel radiation exposure by permitting work on the blanket to be performed on the reactor floor at a safe distance from the converter. A third cart, loaded with graphite to form a wall $53\frac{1}{2}$ in. high, 64 in. wide and 20 in. thick, replaces the converter at the front of the cave and restores the reflective properties of the hohlraum for operation of the D_2O thermal lattice facility and other experiments utilizing the MITR thermal column. The converter is stored in the cave behind the graphite cart during such operations.

The third and final part of this report describes the testing of the completed facility with the first simulated blanket assembly. For reduced cost and ease of construction, it was decided that the subassemblies of the first blanket mockup would be loaded with a mixture

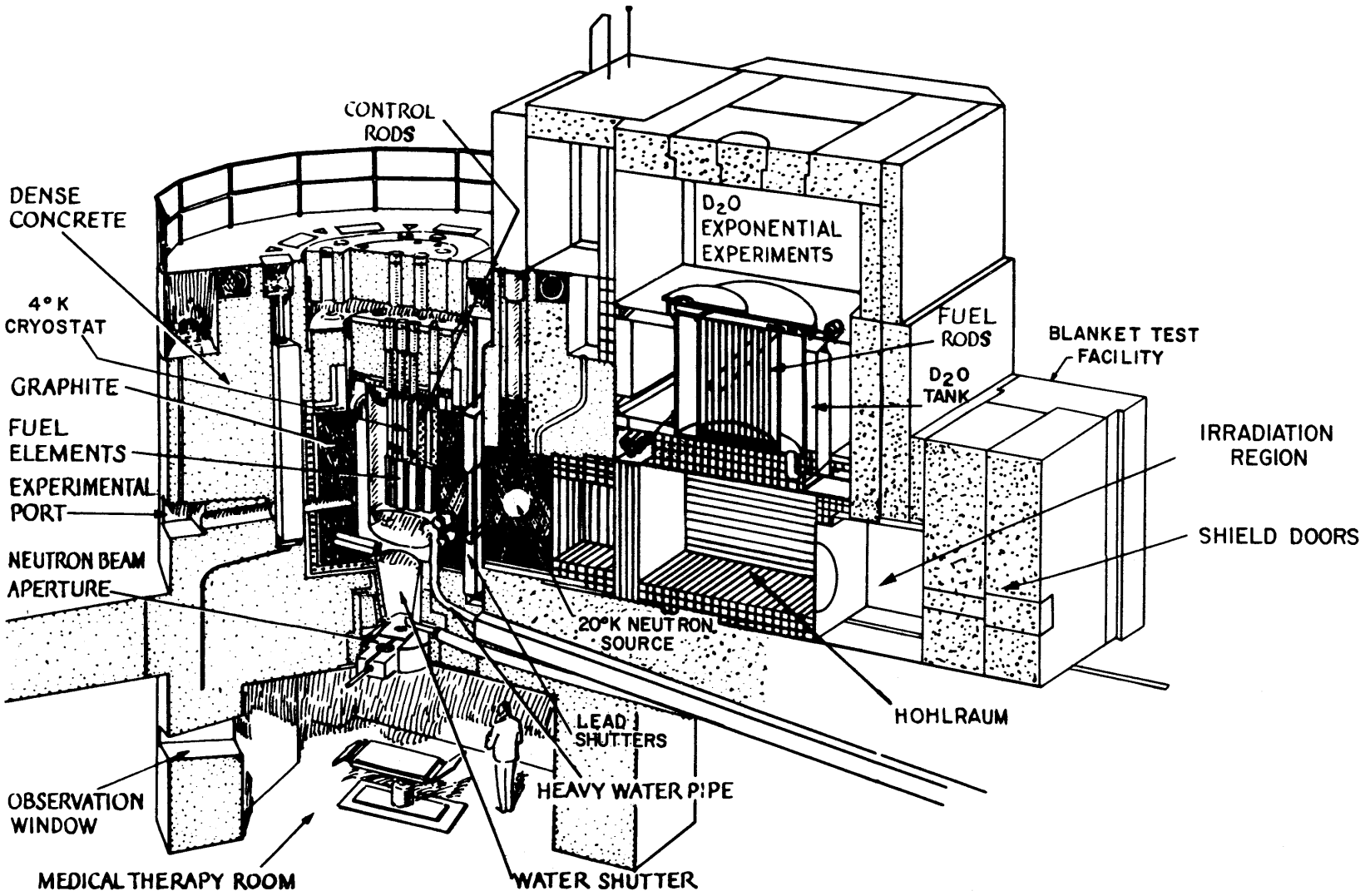

FIG. I.I VIEW OF M.I.T. RESEARCH REACTOR SHOWING THE HOHLRAUM AND BLANKET FACILITY IRRADIATION ROOM.

of iron and anhydrous borax ($Na_2 B_4 O_7$), rather than the more realistic loadings to be used in subsequent blanket assemblies. This mixture contains oxygen, sodium and iron (typical blanket constituents), and simulates the neutronic properties of uranium with iron and boron so that the neutron spectra and overall spatial flux shapes generated are quite similar to those in realistic blanket assemblies. This permitted testing of the facility for correct converter spectrum and source shape generation, for correct transverse equilibrium and leakage effects in the blanket, for streaming and backscattering, and for biological shielding, residual activation and accessibility.

The three major topics introduced above – theoretical calculations, design and construction, and initial testing – are described in detail in the following chapters.

Chapter 2

ANALYTICAL AND NUMERICAL CALCULATIONS

2.1 INTRODUCTION

The principal aims of the analytical and numerical calculations described in this chapter were to establish the feasibility of the converter concept and then to optimize the design of the converter plate and the blanket assembly for the generation of neutron spectra and spatial flux shapes typical of those in the blankets of large LMFBR's. Optimization was accomplished by comparing one- and two-dimensional analyses of the converter plate and blanket assemblies with similar calculations for typical "reference" LMFBR designs and varying the converter plate dimensions and composition to obtain the best possible flux match in the blanket region.

The two-dimensional calculations were performed with the TWENTY GRAND[11, 12] multigroup diffusion theory code using a six-group fast-thermal cross-section set adapted from I. P. Moorhead's five-group set,[13] by the addition of a thermal group (see Appendix A). The one-dimensional calculations were performed with the AIM-6[14, 15] multigroup diffusion theory code and the ANISN[16, 17, 18] multigroup transport theory code using a modified Hansen-Roach sixteen-group fast-thermal cross-section set.[19] The lower boundaries of the energy groups in the Hansen-Roach set are given in Table 2.1.

TABLE 2.1

Group Lower Energy Boundaries for the Hansen-Roach Cross-Section Set

Group	E_L	Group	E_L
1	3 Mev	9	100 ev
2	1.35 "	10	30 "
3	0.9 "	11	10 "
4	0.4 "	12	3 "
5	100 kev	13	1 "
6	17 "	14	0.4 "
7	3 "	15	0.1 "
8	0.55 "	16	thermal

In addition to the optimization studies, a two-dimensional six-group calculation was made with TWENTY GRAND primarily to establish the effects of backscatter from the graphite and concrete shielding surrounding the converter-blanket assembly upon the blanket neutron spectrum.

Finally, a comparative study of various blanket compositions was made to see if any mixture of simple and inexpensive materials could provide neutron spectra and spatial flux shapes sufficiently similar to those in real blanket assemblies. A mixture of 50 v/o iron and 50 v/o anhydrous borax ($Na_2B_4O_7$) was finally specified for the first blanket assembly.

2.2 SLAB SIMULATION OF CYLINDRICAL GEOMETRY

It is desirable that the neutron flux in the slab geometry of the blanket assembly have the same spatial shape in the z-direction (see Figure 2.2) as the neutron flux in the cylindrical geometry of an LMFBR radial blanket in the r-direction (see Figure 2.1), in order to increase the practical value of the experimental data.

In a one-group model, the flux in the blanket region of either system is given by

$$\nabla^2\phi - \alpha^2\phi = 0\,, \tag{2.1}$$

where

$$\alpha^2 = \frac{\Sigma_a - \nu\Sigma_f}{D}\,. \tag{2.2}$$

For the LMFBR blanket,

$$\nabla^2\phi = \frac{d^2\phi(r)}{dr^2} + \frac{1}{r}\frac{d\phi(r)}{dr} - \left(\frac{\pi}{A}\right)^2\phi(r)\,, \tag{2.3}$$

and for the simulated blanket assembly,

$$\nabla^2\phi = \frac{d^2\phi(z)}{dz^2} - \left(\frac{\pi}{H}\right)^2\phi(z) - \left(\frac{\pi}{A}\right)^2\phi(z)\,, \tag{2.4}$$

where H is the effective height of both systems (assumed to be the same) and A is the effective width of the blanket assembly. Thus, the solution of Eq. 2.1 will be the same for both systems if a value of A can be found such that

$$\left(\frac{\pi}{A}\right)^2\phi(z) = -\frac{1}{r}\frac{d\phi(r)}{dr}\,. \tag{2.5}$$

But if $\phi(z) \sim \phi(r)$, then

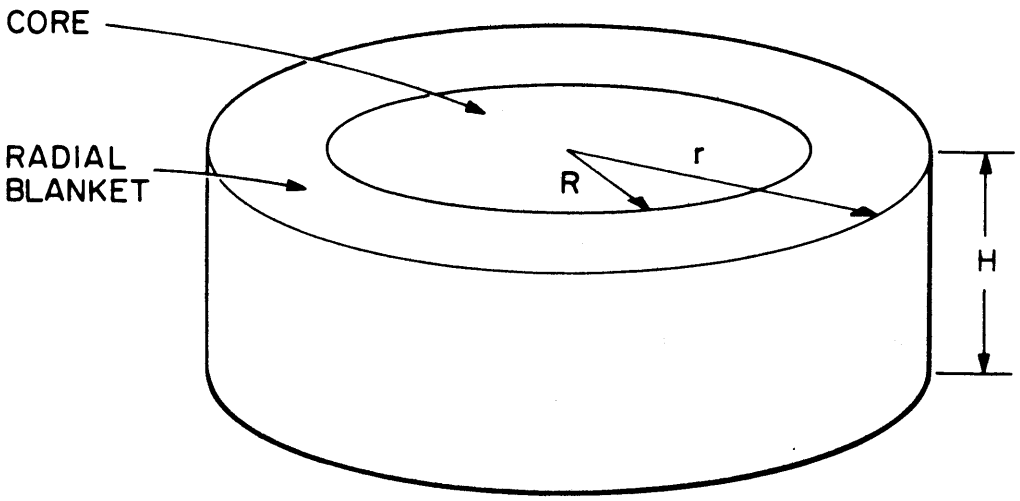

FIG. 2.1 SCHEMATIC REPRESENTATION OF LMFBR CYLINDRICAL GEOMETRY.

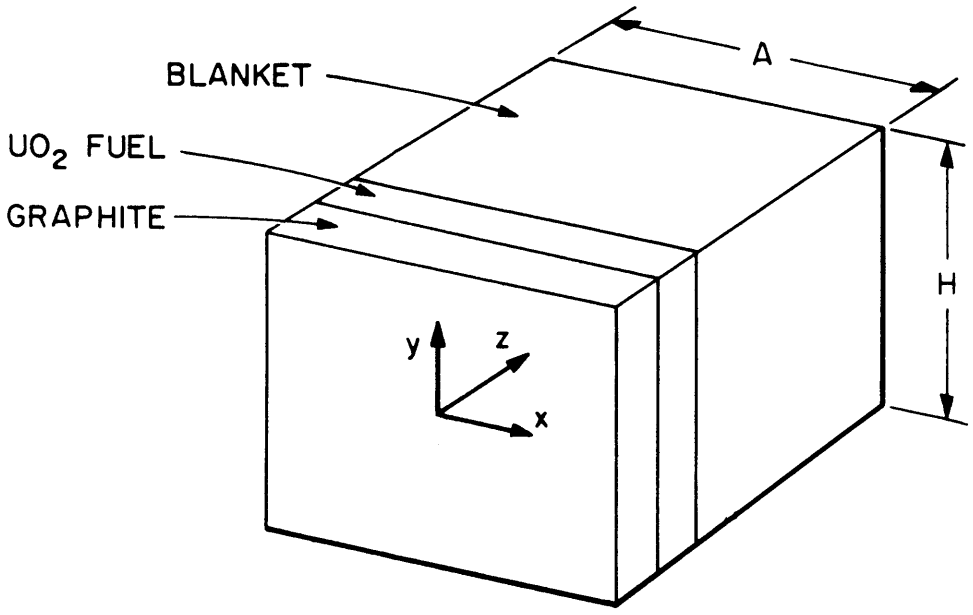

FIG. 2.2 SCHEMATIC REPRESENTATION OF BLANKET FACILITY SLAB GEOMETRY.

$$\phi(z) \sim K_o(\beta r), \tag{2.6}$$

and

$$-\frac{d\phi(r)}{dr} \sim \beta K_1(\beta r), \tag{2.7}$$

where

$$\beta^2 = \alpha^2 + \left(\frac{\pi}{H}\right)^2. \tag{2.8}$$

Substituting Eq. 2.6 and Eq. 2.7 into Eq. 2.5 yields

$$\left(\frac{\pi}{A}\right)^2 = \frac{\beta}{r} \cdot \frac{K_1(\beta r)}{K_o(\beta r)}. \tag{2.9}$$

For values of βr greater than unity, $K_o(\beta r)$ and $K_1(\beta r)$ may be expanded as

$$K_o(\beta r) = e^{-\beta r}\sqrt{\frac{\pi}{2\beta r}}\left(1 - \frac{1}{8\beta r}\right), \tag{2.10}$$

$$K_1(\beta r) = e^{-\beta r}\sqrt{\frac{\pi}{2\beta r}}\left(1 + \frac{3}{8\beta r}\right). \tag{2.11}$$

With these relations, Eq. 2.9 reduces to the form

$$\left(\frac{\pi}{A}\right)^2 \simeq \frac{\beta}{r}\left(1 + \frac{1}{2\beta r}\right). \tag{2.12}$$

Hence, the determining equation for the effective width required for the blanket assembly is

$$A(r) \simeq \frac{\pi\sqrt{2}\, r}{\sqrt{1 + 2\beta r}}, \tag{2.13}$$

or

$$A(z) \simeq \frac{4.43(z+R)}{\sqrt{1 + 2\beta(z+R)}}, \tag{2.14}$$

where R is the radius of the LMFBR core.

For a core radius of 100 cm, an effective height of 138 cm (equivalent to a core height of 95 cm plus 43 cm (21.5 cm each end) axial reflector savings), and a blanket composed of 50 v/o depleted UO_2, 30 v/o sodium and 20 v/o stainless steel,

$$\beta = 0.0409 .$$

At z = 0, Eq. 2.14 yields

$$A = 146 \text{ cm},$$

and at z = 45 cm,

$$A = 179 \text{ cm}.$$

Thus a tapered blanket assembly having an effective width of 146 cm at z = 0 and an effective width of 179 cm at z = 45 cm would accurately simulate the radial blanket of an LMFBR with a 3000-liter core. However, since the lateral neutron leakage in the x-direction from the simulated blanket constitutes less than 10% of the neutron balance, it appeared reasonable to adopt a blanket assembly having a constant effective width. The average value of A for a blanket 45 cm thick is 163 cm ($\simeq 0.5$ (146 cm + 179 cm)), and this value was therefore used for the subsequent multigroup analyses of the converter-blanket assembly.

2.3 THE REFERENCE LMFBR DESIGNS

2.3.1 Selection of the Reference LMFBR Designs

In order to optimize the converter plate design, it was necessary to have "reference" LMFBR designs so that predicted multigroup flux distributions in the simulated blanket assembly could be compared with those in a typical LMFBR blanket. Two reference LMFBR designs

were used, one with a single region core (reference LMFBR No. 1), and one with a two region core (reference LMFBR No. 2). Dimensions and material compositions for these two designs were compiled by averaging data from the considerable number of 1000-MWe LMFBR design studies presented at international conferences in the last eight years,[20, 21, 22, 23] and also from other reference designs.[24, 25, 26] The Karlsruhe 1000-MWe LMFBR design[22] was particularly useful since its dimensions and material compositions were very close to this average.

Table 2.2 gives the dimensions of the reference LMFBR's, and Tables 2.3 and 2.4 give the material compositions of LMFBR No. 1 and LMFBR No. 2, respectively. Both designs have a cylindrical core with an L/D ratio of 0.475, and axial and radial blankets surrounded by a sodium reflector 50 cm thick. LMFBR No. 2 has an outer core to inner core fissile material ratio of 1.3 (for power flattening). The effective core height for one-dimensional calculations of 138 cm given

TABLE 2.2
Reference LMFBR Dimensions

Inner core diameter (LMFBR No. 2 only)	140 cm
Outer core diameter	200 cm
Core height	95 cm
Effective core height for one-dimensional calculations	138 cm
Radial blanket thickness	45 cm
Axial blanket thickness	40 cm
Sodium reflector thickness	50 cm

TABLE 2.3

Reference LMFBR No. 1 Material Compositions

Material	Core	Axial Blanket	Radial Blanket	Reflector
Na	50 v/o	50 v/o	30 v/o	100 v/o
S. S.	15 v/o	15 v/o	20 v/o	–
UO_2*	28.47 v/o	35 v/o	50 v/o	–
$Pu^{239}O_2$	4.35 v/o	–	–	–
$Pu^{240}O_2$	2.18 v/o	–	–	–

TABLE 2.4

Reference LMFBR No. 2 Material Compositions

Material	Inner Core	Outer Core	Axial Blanket	Radial Blanket	Reflector
Na	50 v/o	50 v/o	50 v/o	30 v/o	100 v/o
S. S.	15 v/o	15 v/o	15 v/o	20 v/o	–
UO_2*	28.94 v/o	27.10 v/o	35 v/o	50 v/o	–
$Pu^{239}O_2$	4.04 v/o	5.27 v/o	–	–	–
$Pu^{240}O_2$	2.02 v/o	2.63 v/o	–	–	–

* Depleted UO_2, 87% of theoretical density.

in Table 2.2 assumes an axial reflector savings of 21.5 cm (at each end), a value given in Ref. 27 and confirmed by calculations with the ANISN code.

2.3.2 Multigroup Calculations for the Reference LMFBR Designs

The ANISN code was used to perform one-dimensional, 16-group, S_8 transport theory calculations on the reference LMFBR's. Criticality was achieved by varying the concentration of fissile material in the core while keeping the fissile plus fertile volume percentage constant. The critical enrichment, $Pu^{239}/(Pu+U)$, calculated by ANISN was 12.85 a/o for LMFBR No.1, 11.94 a/o for the inner core of LMFBR No.2, and 15.53 a/o for the outer core. Similar multigroup diffusion theory calculations with the TWENTY GRAND and AIM-6 codes and the two cross-section libraries predicted critical masses about 5% smaller than those calculated with ANISN.

Figures 2.3 and 2.4 show the 16-group radial flux distributions through the core, radial blanket and sodium reflector of LMFBR No. 1 and LMFBR No. 2, respectively. Only the first nine groups are shown; groups ten through sixteen (100 ev to thermal) are not significant for fast reactor calculations but were required for analysis of the converter-blanket assembly. It is evident that the group flux distribution in the radial blanket of the two reference LMFBR's are very similar.

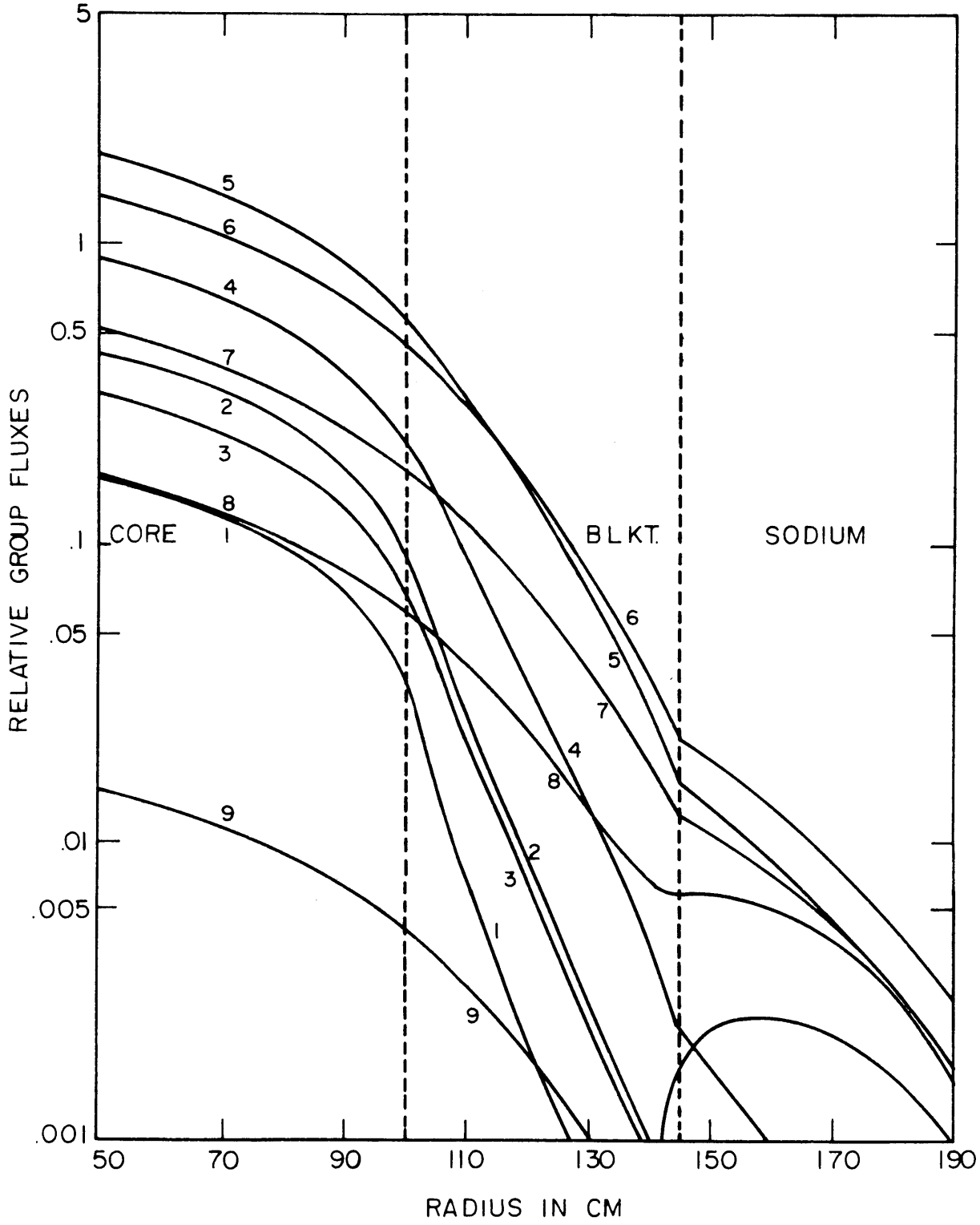

FIG. 2.3 ANISN 16-GROUP RADIAL FLUX DISTRIBUTIONS IN LMFBR # 1

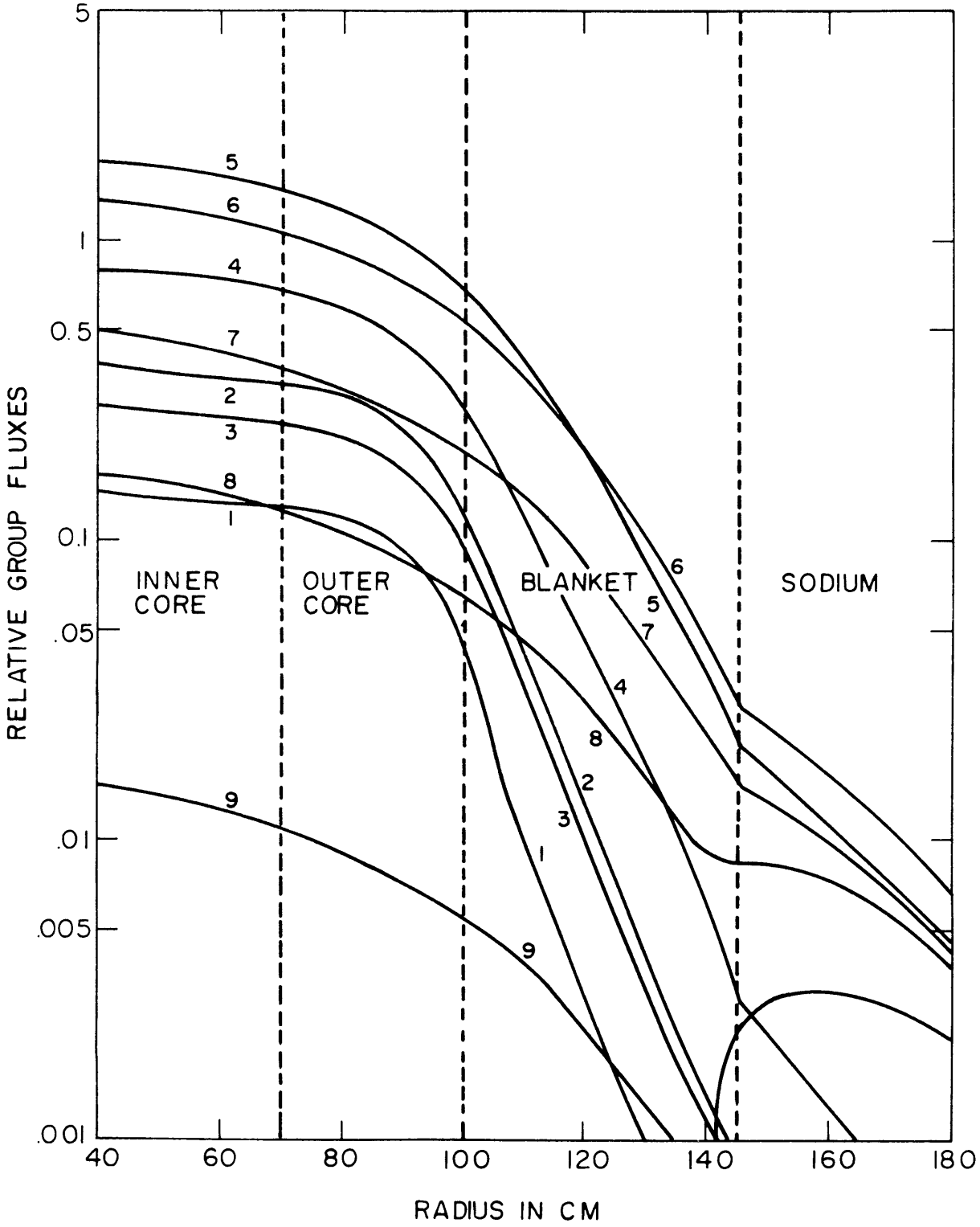

FIG. 2.4 ANISN 16-GROUP RADIAL FLUX DISTRIBUTIONS IN LMFBR# 2

2.4 OPTIMIZATION OF THE CONVERTER PLATE DESIGN

2.4.1 Multigroup Calculations for the Converter-Blanket Assembly

For calculational purposes, the converter-blanket assembly was assumed to be a slab with an effective width of 162.5 cm, as determined in section 2.2, and an effective height of 138 cm, the same as for the reference LMFBR designs (see Figure 2.2). Composition and thickness of the simulated blanket and reflector were also the same as those of the radial blanket and reflector of the reference LMFBR's. The converter plate fuel was taken to be a close-packed array of 1/2-in.-diameter, aluminum-clad UO_2 fuel rods with a U^{235} enrichment of 1.99%, since the fuel inventory of the D_2O Thermal Lattice Project at M.I.T. included a large number of these fuel rods.

Initial calculations with TWENTY GRAND showed that a UO_2 converter assembly 20 cm thick could provide a leakage spectrum similar to that from the reference LMFBR cores from 10 Mev down to 100 kev, but that at lower energies the neutron flux decreased more rapidly with decreasing energy than the flux in the reference LMFBR cores. Furthermore, the leakage current from the converter became negative (i.e., there was a net current back into the converter) at energies below about 10 kev, whereas the leakage current from the reference LMFBR cores is positive at all energies (see Figures 2.3 and 2.4). Therefore, for subsequent calculations a slab of graphite was inserted in front of the converter (see Figure 2.2) to enhance the low energy tail of the converter leakage spectrum by providing external moderation.

Optimization of the converter assembly was achieved by varying the thickness of the graphite and fuel regions to obtain the best possible comparison between the multigroup flux distributions in the simulated blanket and the reference LMFBR radial blanket. The optimum thicknesses were found to be 20 cm of graphite and 16.5 cm of UO_2 fuel, the latter corresponding to 15 rows of the 1/2-in.-diameter UO_2 fuel rods. Figure 2.5 shows the 16-group (S_8 transport theory) flux distributions through the converter and simulated blanket for this optimum configuration as calculated by ANISN. The boundary and incident thermal flux conditions provided by the graphite-lined cavity or "hohlraum" of the MIT Reactor (the neutron flux in the hohlraum is about 5×10^9 n/cm^2-s at a reactor power of 5 Mw and has a cadmium ratio greater than 2000[28]) are simulated by a vacuum boundary condition and a thermal Maxwellian source at the outer edge of the graphite slab. This thermal source flux (groups 15 and 16) diffuses through the graphite and produces a fission source in the first few centimeters of the fuel region. The graphite external moderator and the bulk of the fuel region then provide the correct slowing-down and absorption characteristics to yield the desired leakage spectrum at the converter-blanket interface.

2.4.2 Comparison with Reference LMFBR No. 2

Figure 2.6 is a comparison of the 16-group flux distributions in the simulated blanket and the radial blanket of LMFBR No. 2, normalized by setting $\int \phi(E)\, dE = 1$ at a distance of 24.75 cm into both blankets. The comparison between the two is good; small interfacial discrepancies due to incorrect converter source-matching disappear

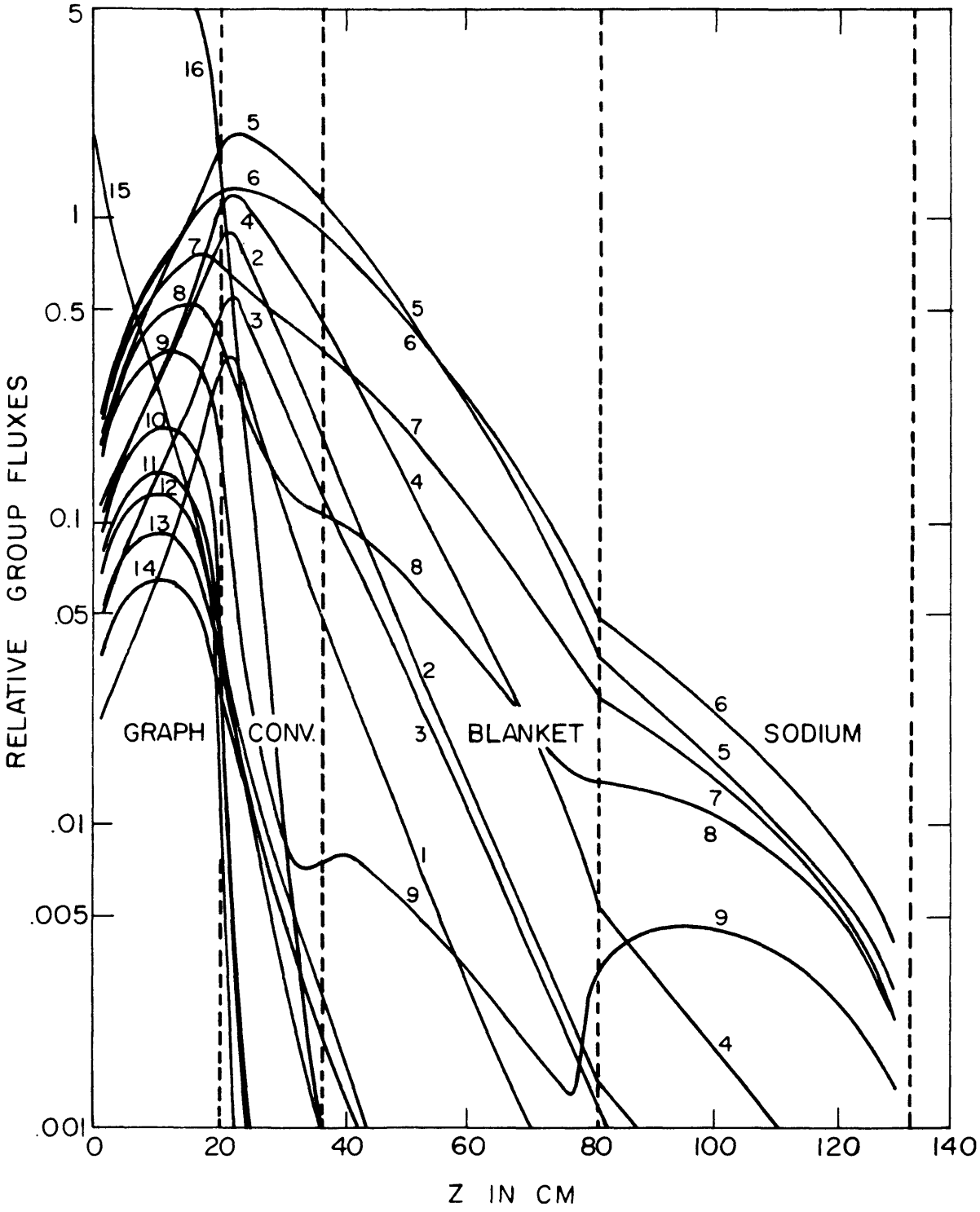

FIG. 2.5 16 GROUP Z-DIRECTION FLUX DISTRIBUTIONS IN THE CONVERTER-BLANKET ASSEMBLY

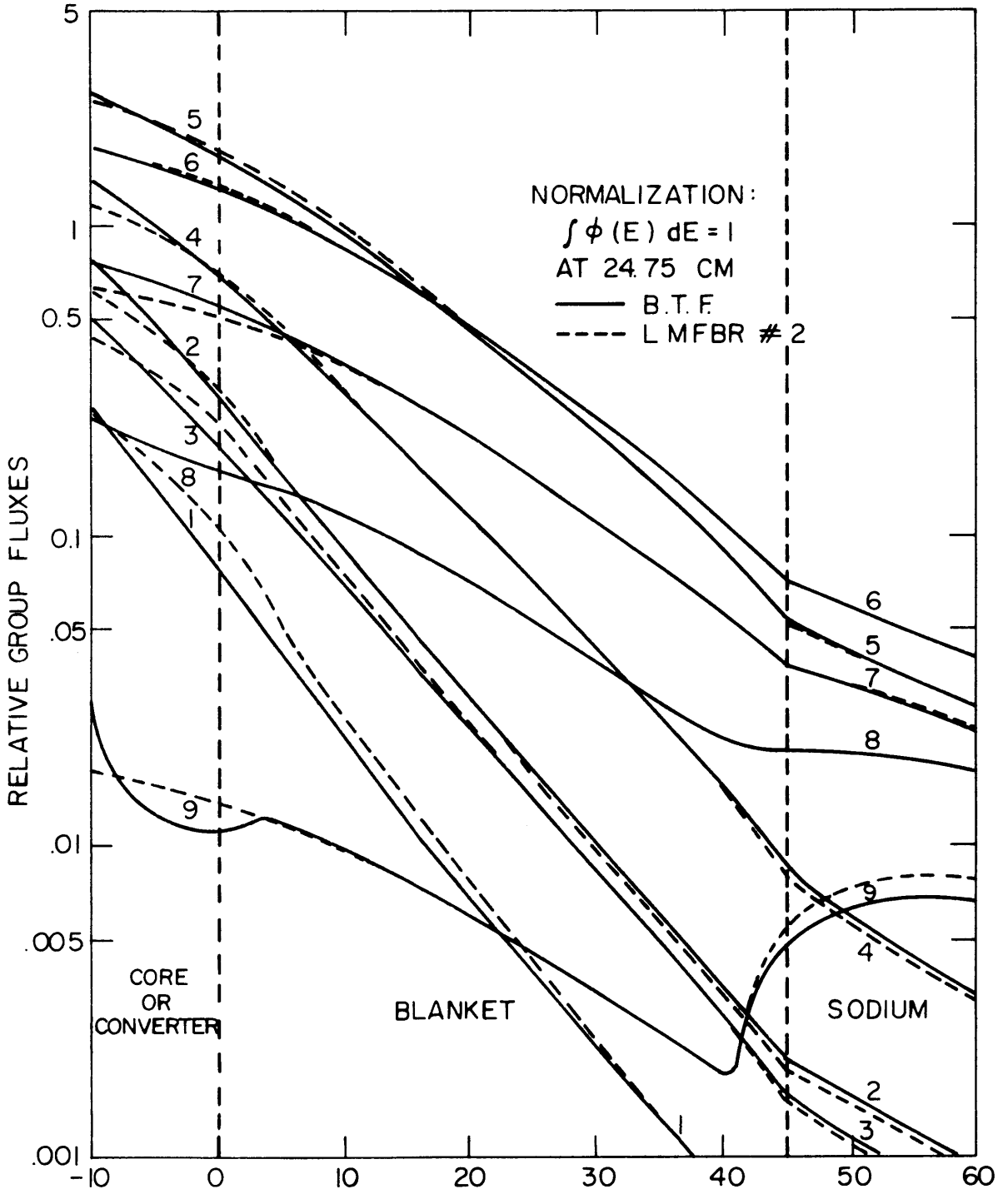

FIG. 2.6 COMPARISON OF THE 16 GROUP BLANKET FLUX DISTRIBUTIONS IN THE CONVERTER-BLANKET ASSEMBLY AND LMFBR # 2

with increasing distance into the blanket, particularly at lower energies; only the first group (3 Mev to 10 Mev) shows any significant discrepancy. The small differences between the group flux distributions at the outer edges of the simulated blanket and the LMFBR radial blanket are due to the inability of the constant lateral leakage from the converter-blanket assembly to simulate perfectly the LMFBR's cylindrical geometry.

Table 2.5 compares the converter-blanket interface spectrum with the LMFBR No. 2 core-blanket interface spectrum. The converter-blanket interface spectrum has been normalized to an incident thermal flux of 5×10^9 n/cm^2-s to yield the absolute fluxes expected; the two spectra are still internormalized by equating $\int \phi(E)\, dE$ at the middle of the blanket. The comparison between the two interface spectra is good from 10 Mev down to 3 ev, but undesirable leakage through the converter plate is evident in the energy range from 3 ev to thermal. However, this low-energy leakage is only 0.21% of the total interface flux, and was reduced by a factor of 6 in the final design by the addition of a 1/8-in. sheet of boral between the converter and blanket assemblies.

Calculations were made with ANISN to determine the effect that the low-energy leakage would have on the activation ($\int \sigma_c(E)\phi(E)dE$) of materials which it would be desirable to irradiate in the Blanket Test Facility, such as U^{238} and Au^{197}. It was found that without the boral sheet the low-energy leakage increased the activation of U^{238} by less than 0.4%, and the activation of Au^{197} by less than 10%. With the 1/8-in. boral sheet between the converter and blanket assemblies, the activation of U^{238} and Au^{197} were increased by less than 0.04% and 1.5%, respectively.

TABLE 2.5

Comparison of the 16-Group Spectra at the Inner Edge of the Simulated Blanket and the LMFBR Blanket

Group	E_L	Converter-Blanket Interface*	Core-Blanket Interface
1	3 Mev	1.29×10^{7}	1.82×10^{7}
2	1.4 "	4.60×10^{7}	4.90×10^{7}
3	0.9 "	3.18×10^{7}	3.73×10^{7}
4	0.4 "	1.11×10^{8}	1.13×10^{8}
5	100 kev	2.79×10^{8}	2.82×10^{8}
6	17 "	2.20×10^{8}	2.14×10^{8}
7	3 "	9.24×10^{7}	7.98×10^{7}
8	0.55 "	2.64×10^{7}	2.60×10^{7}
9	100 ev	1.82×10^{6}	2.22×10^{6}
10	30 "	3.01×10^{4}	4.58×10^{4}
11	10 "	6.00×10^{2}	1.15×10^{2}
12	3 "	1.29×10^{1}	1.91×10^{1}
13	1 "	6.81×10^{5}	2.81×10^{0}
14	0.4 "	5.65×10^{5}	1.53×10^{0}
15	0.1 "	2.85×10^{5}	1.03×10^{0}
16	thermal	1.70×10^{5}	2.37×10^{-1}

* Normalized to 5×10^{9} n/cm^2-s incident thermal flux.

2.4.3 Effect of the Graphite and Fuel Region Thicknesses Upon the Converter-Blanket Interface Spectrum

As mentioned in 2.4.1, the optimum converter configuration was found to consist of a 20-cm-thick graphite region and a 16.5-cm-thick UO_2 fuel region. Figure 2.7(A) shows the percentage change in group fluxes at the converter-blanket interface resulting from a 2.2-cm decrease in the fuel region thickness (equivalent to 2 rows of the 1/2-in.-diameter fuel rods), while Figure 2.7(B) shows the change resulting from a 10-cm decrease in the graphite region thickness. It is evident from these figures that a change in the thickness of the fuel region affects mainly that fraction of the converter leakage spectrum above about 300 kev, while a change in the thickness of the graphite region affects mainly that fraction of the spectrum below about 20 kev. This result implies that the present converter configuration is extremely flexible, inasmuch as it is possible to produce a wide range of converter leakage spectra merely by varying the thicknesses of the graphite and fuel regions.

2.5 THE EFFECT OF BACKSCATTER UPON THE SIMULATED BLANKET SPECTRUM

As mentioned in section 1.2, construction of the Blanket Test Facility in the MIT Reactor necessitated the use of concrete biological shielding for the converter-blanket assembly. In order to ascertain the effect of the backscattering of leakage neutrons by the concrete shielding, two-dimensional six-group calculations were made with TWENTY GRAND on a model of the B.T.F. which had a graphite

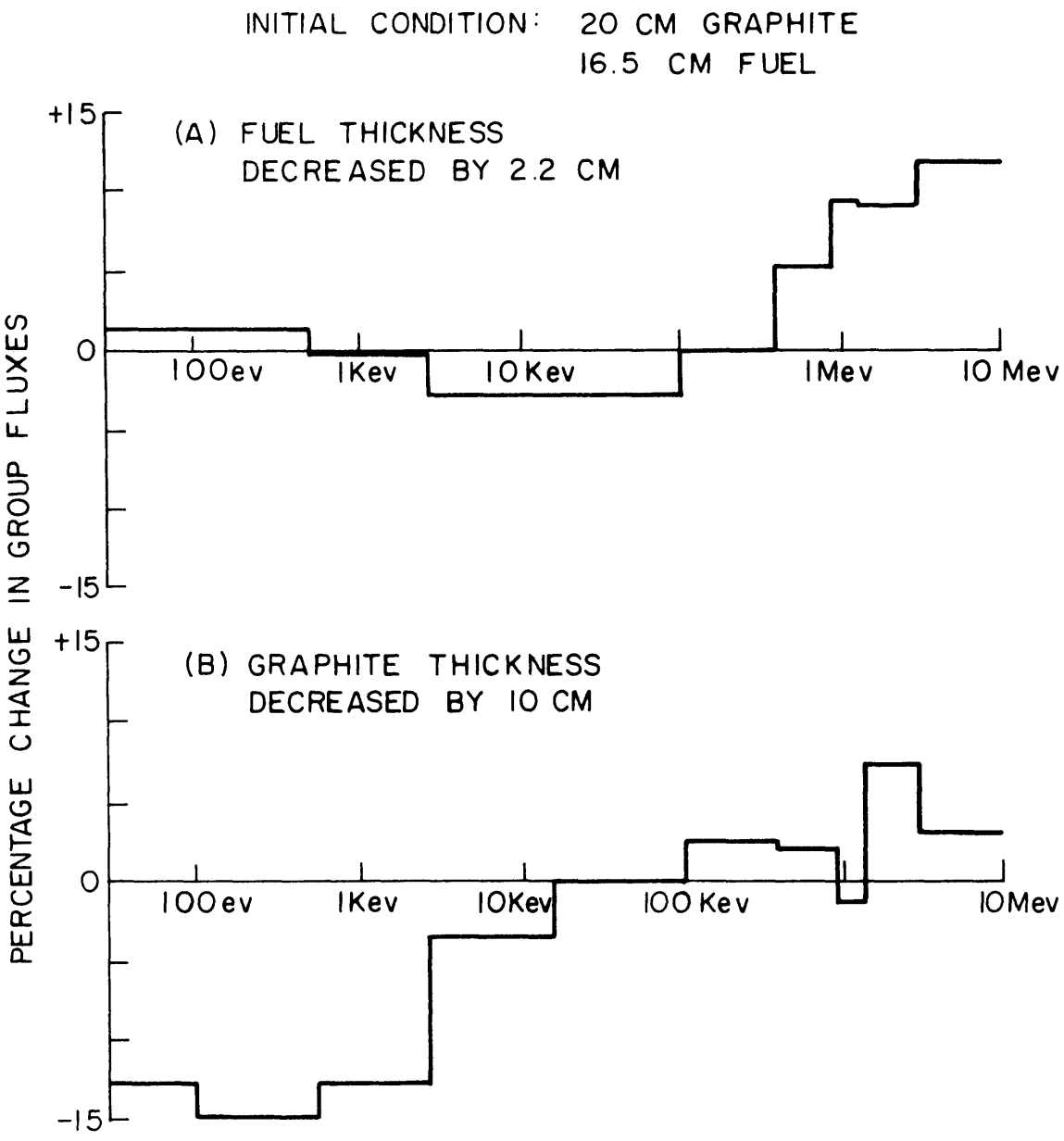

FIG. 2.7 – EFFECT OF GRAPHITE AND FUEL REGION THICKNESSES UPON THE CONVERTER–BLANKET INTERFACE SPECTRUM.

reflector on either side of the converter, and a concrete reflector on either side of the blanket assembly (see Figure 2.8). The composition and effective height of the converter, blanket and sodium reflector are the same as for the one-dimensional calculations (section 2.4.1). The composition used for the magnetite concrete[29] is given in Table 2.6; magnesium, silicon and calcium in the concrete have been accounted for by using an equivalent aluminum atom density.

TABLE 2.6

Magnetite Concrete Composition

Material	Atom Density, $cm^{-3} \times 10^{-24}$
C	0.00040
O	0.04366
H_2O	0.00448
Al	0.01484
Fe	0.01575

Figure 2.9 shows the 6-group flux distributions calculated by TWENTY GRAND across the simulated blanket and concrete reflector at a distance of 27 cm from the converter-blanket interface. It is seen that the concrete produces a considerable perturbation of the spectrum in the outer 20 cm to 30 cm of the blanket, owing to moderation and backscattering of the blanket leakage flux. However, over the central 80 cm of the blanket (-40 cm $< x <$ 40 cm), the neutron spectrum is

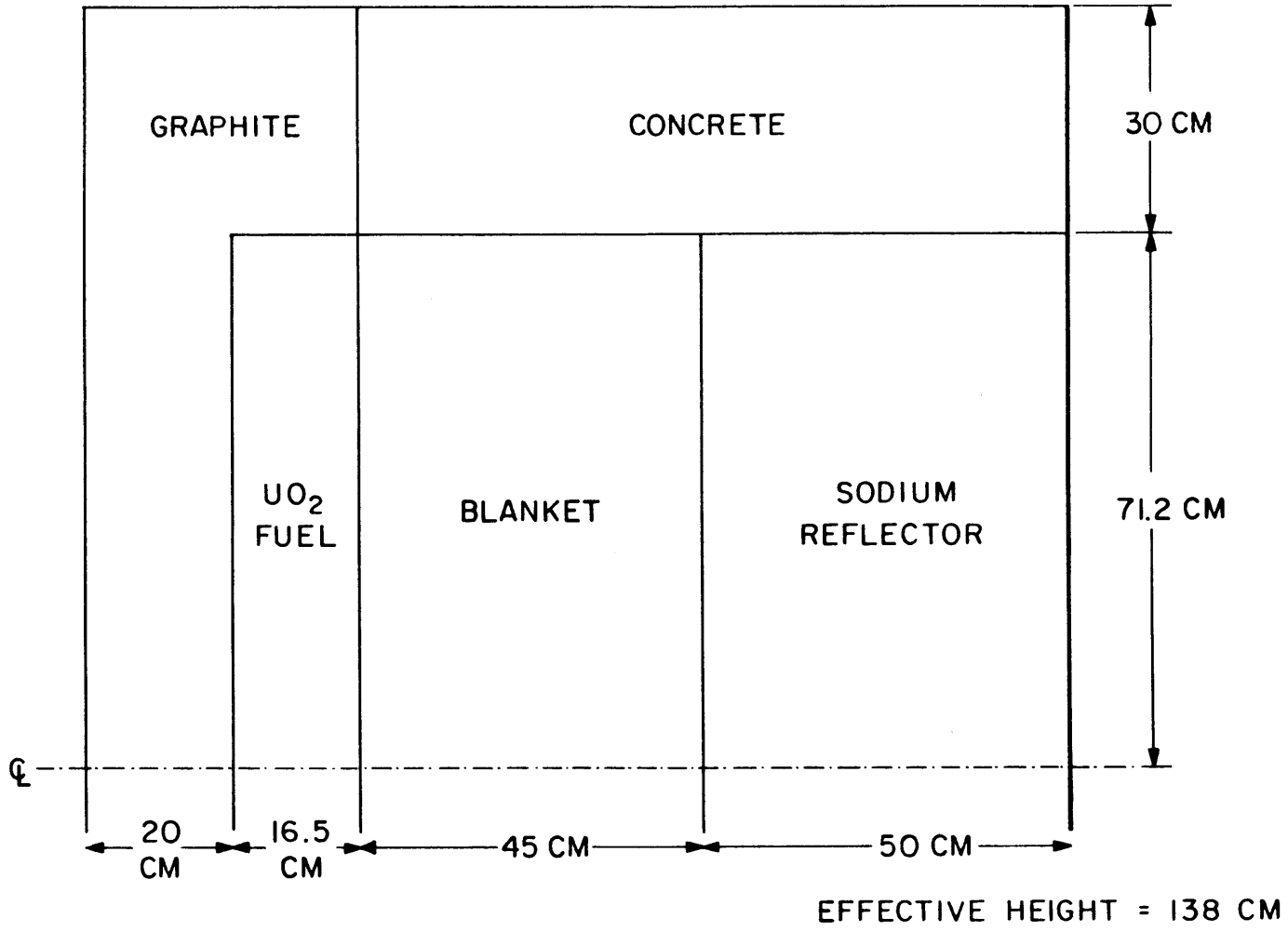

FIG. 2.8 B.T.F. MODEL FOR CALCULATIONS WITH TWENTY GRAND.

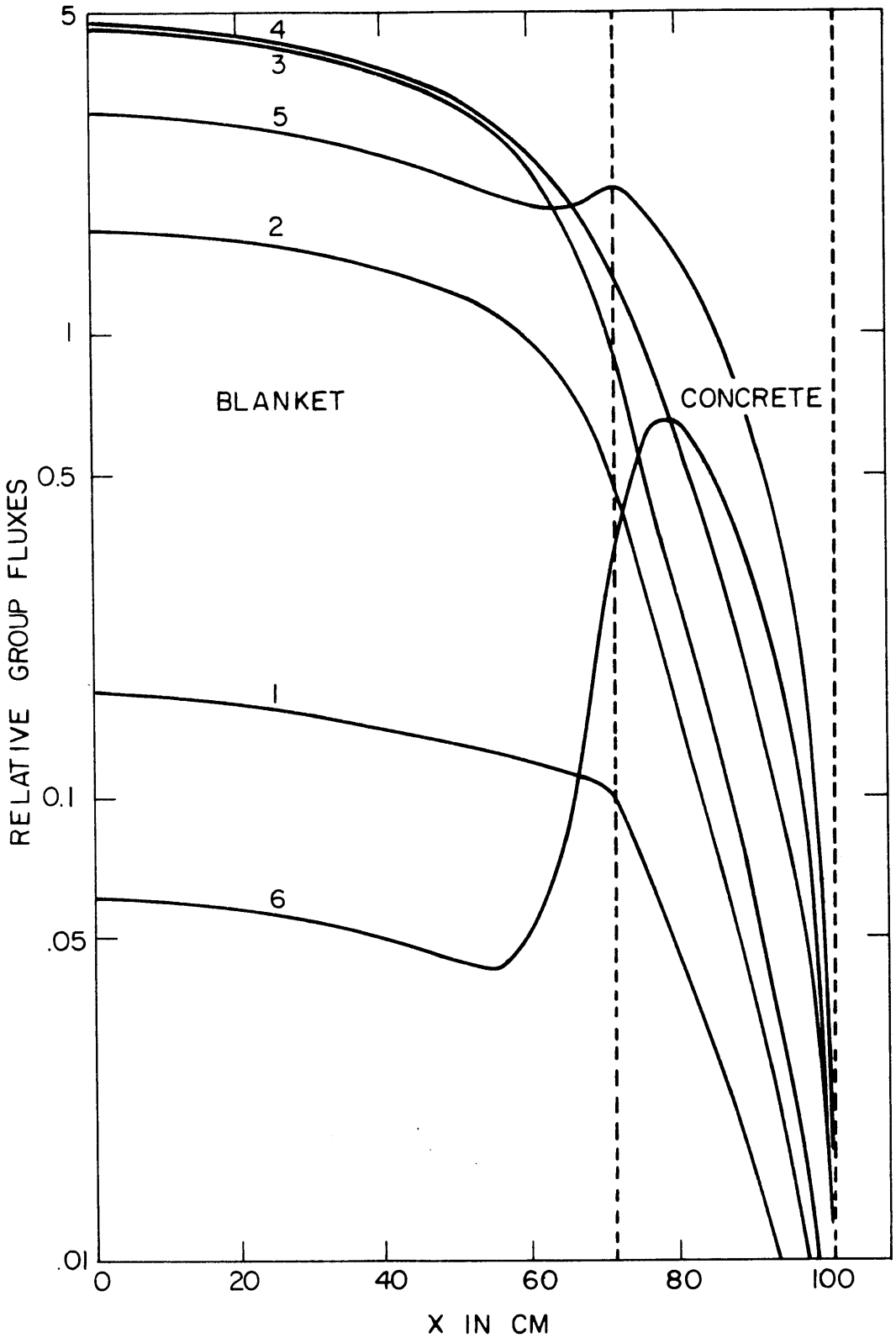

FIG. 2.9 6 GROUP FLUX DISTRIBUTIONS ACROSS THE SIMULATED BLANKET 27CM FROM THE CONVERTER BLANKET INTERFACE.

evidently laterally asymptotic (or separable), since the group flux distributions can all be fitted to the form

$$\phi_i = A_i \cos\left(\frac{\pi x}{202.5}\right)$$

with greater precision than the convergence limits of the calculation. This function also fits the shape of the incident thermal flux.

These results lead to two important conclusions. First, the lateral (x- and y-direction) shape of the fast neutron flux is predominantly determined by the lateral shape of the incident thermal flux; obviously, though, it is preferable to ensure that the thermal source flux has the same shape as that determined by the effective height and width of the simulated blanket. Second, backscattering from the concrete shielding perturbs the blanket spectrum only in the outer 20 cm to 30 cm of the blanket assembly. Since the blanket assembly has a height of about 140 cm and a width of about 150 cm, the unperturbed region in the simulated blanket should be greater than 80 cm by 90 cm, more than adequate for any experimental measurements. As will be noted in chapter 3, however, these calculations led to installation of a boral liner in the irradiation region to further control edge effects of the type evidenced in these calculations.

2.6 MULTIGROUP CALCULATIONS FOR THE FIRST B.T.F. BLANKET ASSEMBLY

It was desired that the blanket assembly to be used for initial evaluation of the completed Blanket Test Facility (B.T.F. Blanket No. 1) be relatively inexpensive and easy to construct. To this end, ANISN

calculations were performed for a variety of simulated blanket compositions, containing different combinations of iron, magnetite (Fe_3O_4) and anhydrous borax ($Na_2B_4O_7$). It was found that the group flux distributions in a simulated blanket composed of 50 v/o iron and 50 v/o anhydrous borax best approximated those in the radial blanket of the reference LMFBR's. This mixture contains oxygen, sodium and iron, and simulates uranium with iron and boron. The atom densities calculated for the actual loading of Blanket No. 1 are given in Appendix C.

Figure 2.10 compares the multigroup neutron spectra in B.T.F. Blanket No. 1 and LMFBR No. 2 at a distance of 24.75 cm into both blankets; the two spectra are again normalized by setting $\int \phi(E)\, dE = 1$. It is evident that the iron-borax blanket spectrum is a reasonable approximation to the LMFBR radial blanket spectrum from 10 Mev down to 500 ev, at this position.

Table 2.7 compares the 16-group spectra at the inner edge of Blanket No. 1 and the inner edge of the radial blanket of LMFBR No. 2, with the same normalizations as Table 2.5. Again the converter-blanket interface spectrum is a good approximation to the core-blanket interface spectrum from 10 Mev down to 500 ev, but is considerably softer at lower energies.

A comparison of Table 2.7 with Table 2.5 shows the reduction in the converter plate leakage flux below 3 ev effected by the 1/8-in. sheet of boral added to the rear of the converter for the ANISN calculations on B.T.F. Blanket No. 1.

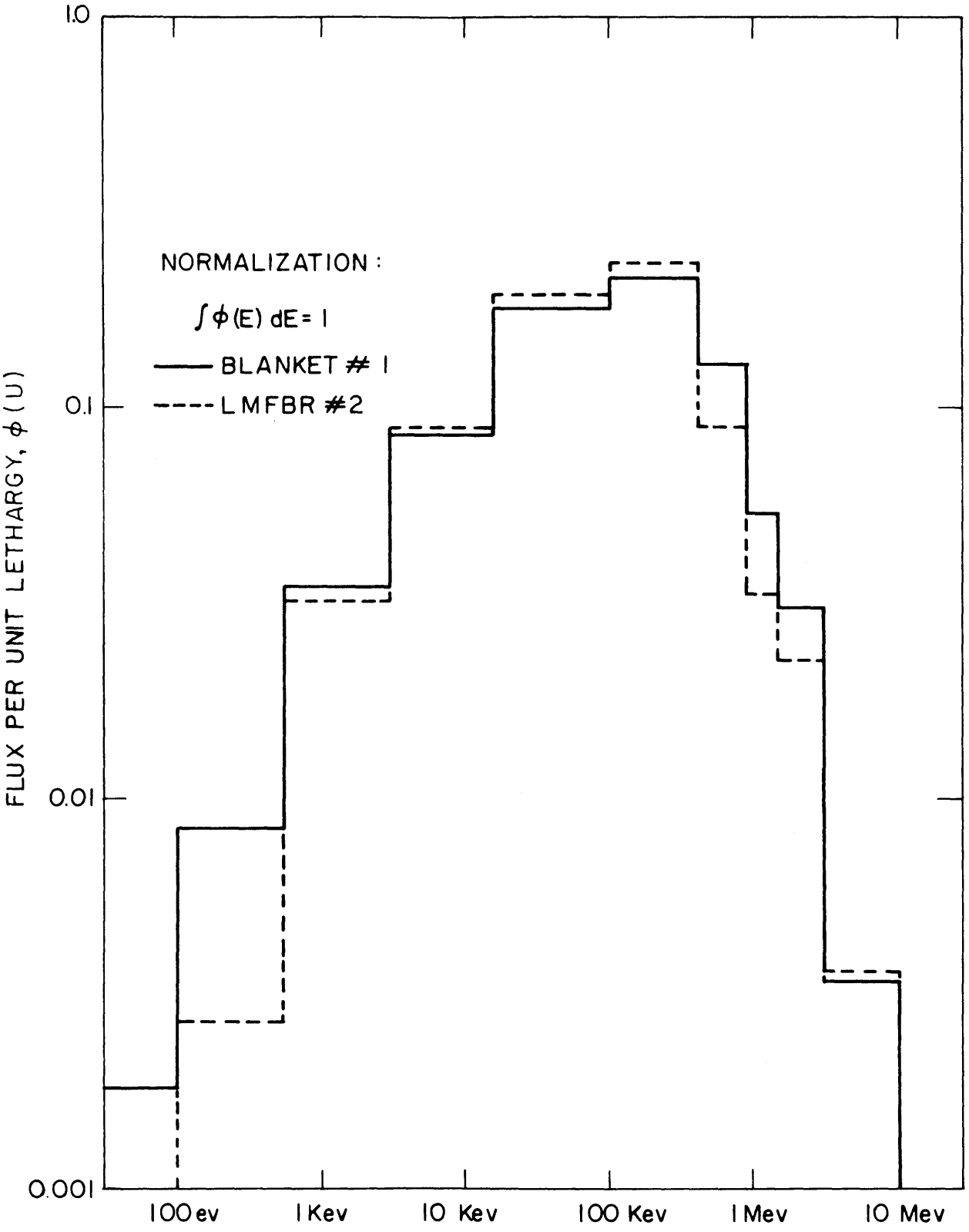

FIG. 2.10 MULTIGROUP SPECTRA 24.75 CM INTO BTF BLANKET AND LMFBR # 2 RADIAL BLANKET

TABLE 2.7

Comparison of the 16-Group Spectra at the Inner Edge of B.T.F. Blanket No. 1 and the LMFBR Blanket

Group	E_L	Converter-Blanket Interface*	Core-Blanket Interface
1	3 Mev	1.12×10^7	1.43×10^7
2	1.4 "	4.29×10^7	3.85×10^7
3	0.9 "	2.98×10^7	2.83×10^7
4	0.4 "	9.96×10^7	8.87×10^7
5	100 kev	2.21×10^8	2.22×10^8
6	17 "	1.70×10^8	1.68×10^8
7	3 "	7.48×10^7	6.26×10^7
8	0.55 "	2.29×10^7	2.04×10^7
9	100 ev	2.87×10^6	1.75×10^6
10	30 "	2.58×10^5	3.59×10^4
11	10 "	3.66×10^4	9.09×10^1
12	3 "	6.12×10^3	1.50×10^1
13	1 "	7.77×10^4	2.20×10^0
14	0.4 "	2.88×10^4	1.20×10^0
15	0.1 "	3.21×10^3	8.08×10^{-1}
16	thermal	5.32×10^1	1.86×10^{-1}

*Normalized to 5×10^9 n/cm^2-s incident thermal flux.

2.7 POWER GENERATION AND FAST NEUTRON FLUX IN THE B.T.F.

By normalizing the foregoing multigroup analyses of the B.T.F. to the measured thermal neutron flux in the hohlraum of the MITR, it was possible to predict the operating power level of the converter plate and the magnitude of the fast neutron fluxes expected.

For an incident thermal flux of 5×10^9 n/cm^2-s, the estimated power production in the 4-ft.-high by 5-ft.-wide converter assembly is about 55 watts, 80% of which is generated in the first 4 rows (4.6 cm) of UO_2 fuel of the 15-row-thick fuel assembly. This provides fast neutron fluxes of about 7×10^8 n/cm^2-s at the converter-blanket interface and about 2.5×10^7 n/cm^2-s at a distance of 45 cm into the simulated blanket, adequate for any planned experiments. For example, the specific activity of gold foils after four hours' irradiation in the B.T.F. would be about 3500 dpm/mgm at the converter-blanket interface and about 320 dpm/mgm at a distance of 45 cm into the blanket.

It is interesting to note that a fast critical assembly with a core volume of 3000 liters would have to operate at a power level of about 350 watts to provide blanket neutron flux levels comparable to those provided by the B.T.F. operating at 55 watts. Furthermore, the volume of the radial blanket of such a fast critical assembly would be over 5000 liters, and the volume of the axial blankets (upper plus lower) would be about 2500 liters, while the volume of the B.T.F. blanket is only about 1000 liters.

2.8 SUMMARY

The calculations described above show that the "optimized" converter assembly (with 20 cm of graphite and 16.5 cm of fuel) should have a leakage spectrum typical of the leakage spectrum from the core of a large LMFBR. The fact that the multigroup calculations with the three computer programs (using two different cross-section libraries) all predicted the same optimum configuration encourages confidence in the chosen converter plate design. It has also been shown that if the simulated blanket dimensions are properly chosen (an effective height of 138 cm and an effective width of 163 cm), the spatial flux distributions in the simulated blanket should be typical of those in the radial blanket of a large LMFBR. Furthermore, the chosen blanket dimensions are large enough to prevent leakage neutrons, backscattered from the concrete shielding surrounding the assembly, from perturbing the neutron flux distributions in the center of the blanket assembly.

Finally, the B.T.F. has been shown to have certain inherent advantages over a fast critical assembly, which would have to be operated at a power level of about 350 watts to obtain blanket fluxes comparable to those generated by 55-watt operation of the B.T.F., and could require as much as eight times as much blanket material for a full-scale mockup.

Chapter 3

DESIGN AND CONSTRUCTION OF THE BLANKET TEST FACILITY

3.1 INTRODUCTION

As outlined in section 1.2, the Blanket Test Facility is located at the rear of the graphite-lined hohlraum, which was originally constructed to feed thermal neutrons from the MITR thermal column up into the heavy water exponential tank (see Figure 1.1). In 1959, the former thermal column door was moved back from the face of the graphite thermal column to form part of the rear shield wall of the D_2O Thermal Lattice Project. In the present reconstruction, the B.T.F. irradiation region was formed by removing the rear graphite wall of the hohlraum and the thermal column door, and installing a five-sided aluminum box to line the resulting cavity. The interior volume of this cavity is about 6 ft by 6 ft by 6 ft. Since the aluminum liner box is seam-welded, it maintains the sealed nature of the hohlraum and prevents the leakage of radioactive argon from the hohlraum into the irradiation region and the reactor building.

Shielding for the irradiation region is provided by four heavy concrete shield blocks, two stationary and two portable. The two portable shield blocks weigh approximately 15 tons each and can be removed by means of the reactor building's overhead crane to provide access to the irradiation region.

A set of rails, extending from the front of the aluminum liner box out to the reactor building containment wall, permits the insertion of experimental assemblies mounted on carts into the irradiation region. For operation of the Blanket Test Facility, the converter assembly is rolled to the front of the irradiation region, the simulated blanket assembly is installed directly behind it, and the concrete shield doors replaced. For operation of the D_2O Thermal Lattice Facility and other experiments utilizing the hohlraum thermal flux, the converter assembly is replaced by a third cart, loaded with graphite and having the same external dimensions as the converter assembly, which restores the reflective properties of the hohlraum. The capability of replacing the converter cart with the graphite cart ensures that the Blanket Test Facility does not compromise any of the capabilities of the thermal exponential assembly.

Figures 3.1 and 3.2 show cross-section and plan views, respectively, of the hohlraum and Blanket Test Facility, with the simulated blanket assembly located on the reactor floor rather than in its operating position behind the converter in the irradiation region. Sections 3.2 through 3.5 describe the various components of the facility in greater detail.

3.2 SHIELDING

External shielding for the B.T.F. is provided by four heavy concrete shield blocks, two stationary and two portable. Figure 3.2 shows the shielding configuration and also the stepping to prevent

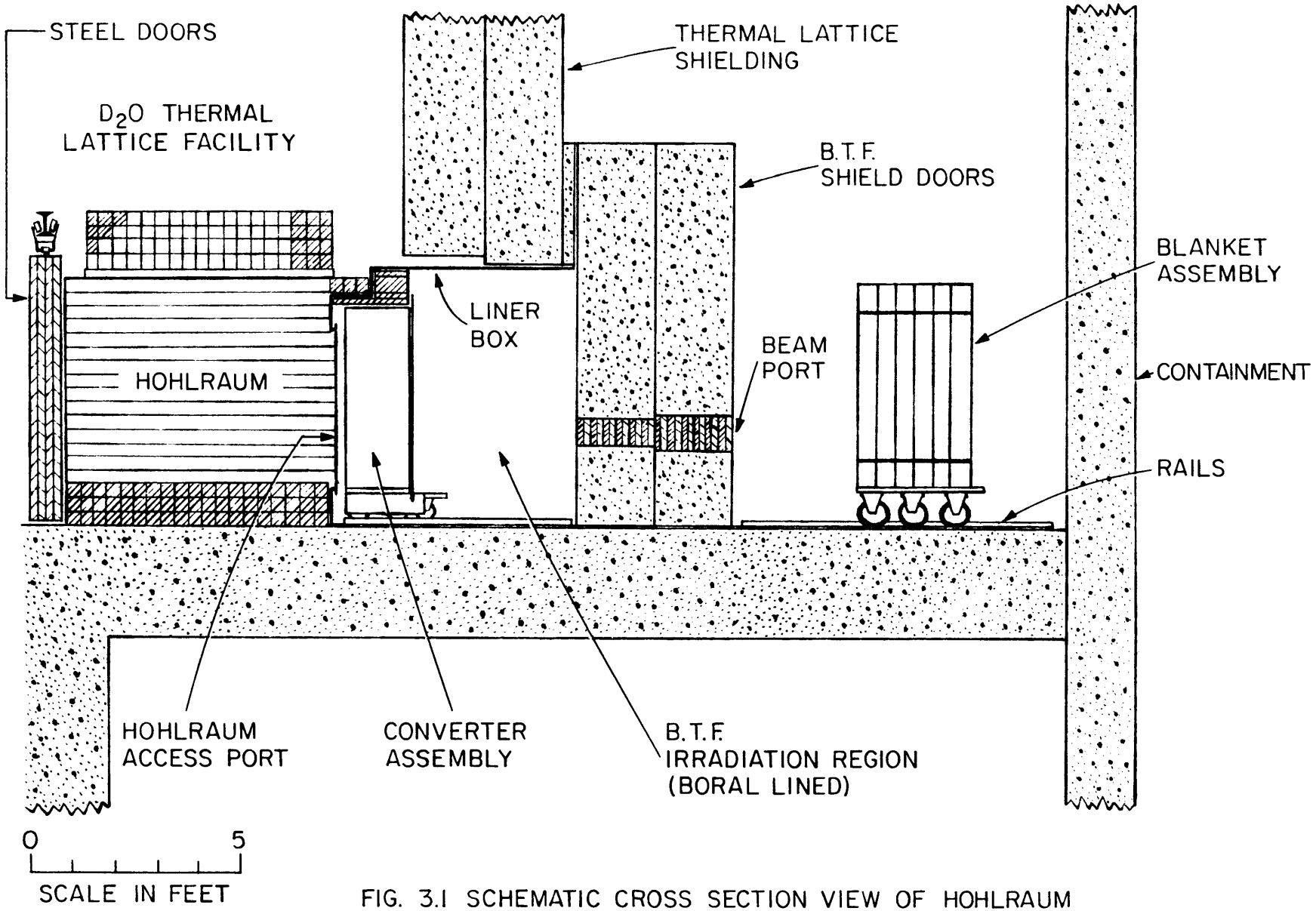

FIG. 3.1 SCHEMATIC CROSS SECTION VIEW OF HOHLRAUM AND BLANKET TEST FACILITY.

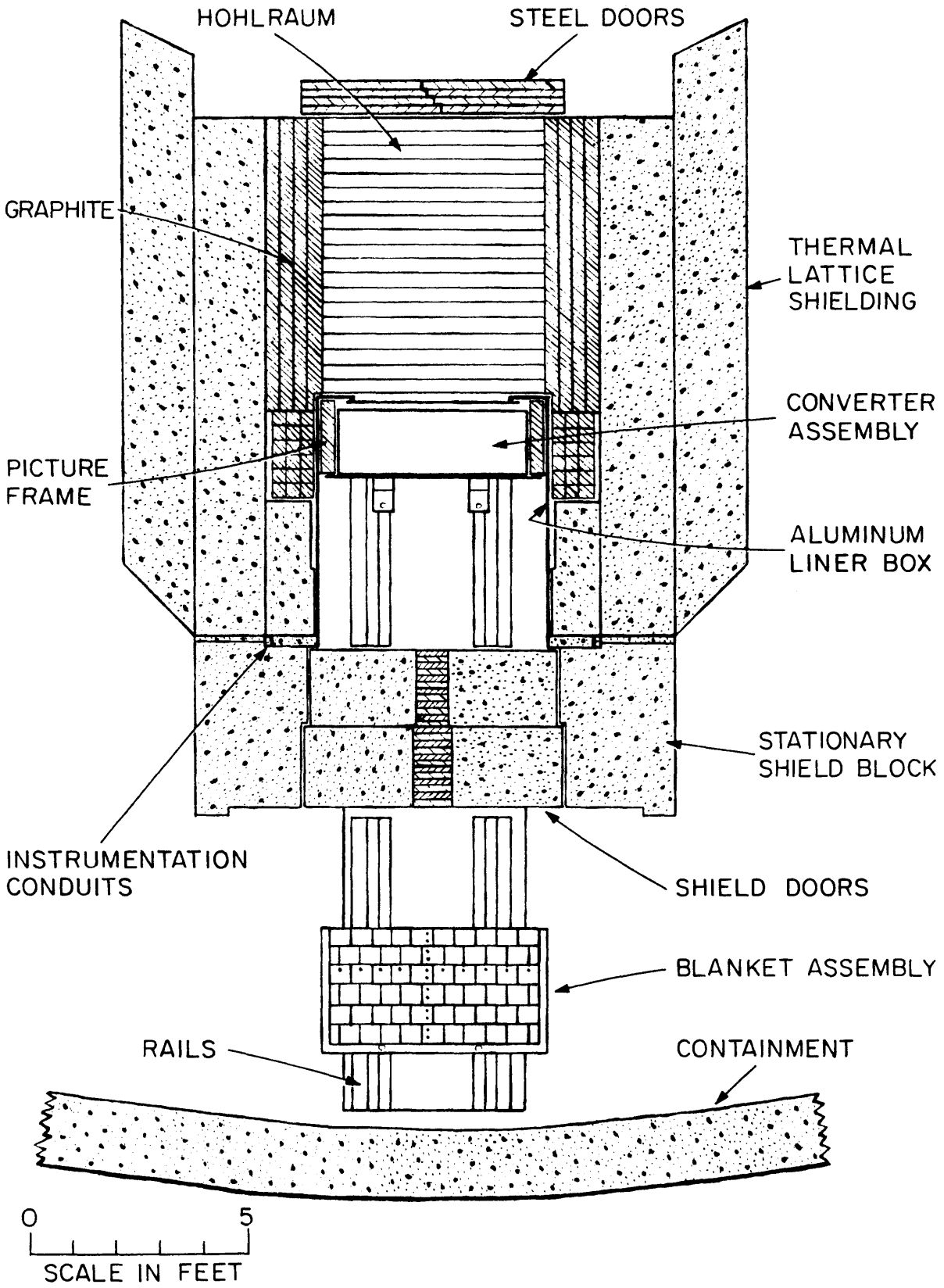

FIG. 3.2 SCHEMATIC PLAN VIEW OF THE HOHLRAUM AND BLANKET TEST FACILITY.

radiation streaming. The two side shield blocks are 3 ft wide and 4 ft thick, while the inner shield door is 6 ft 6 in. wide and 2 ft thick, and the outer shield door is 6 ft 10 in. wide and 2 ft thick; all four blocks are 9 ft 6 in. high. This provides a 4-ft-thick shield for the irradiation region, designed to reduce fast neutron dose to less than 1 n/cm^2-s. and gamma dose to less than 1 mr./hr outside the shielding under the most severe operating conditions (the shielding calculations are described in Appendix D).

The shield blocks are made of magnetite concrete with a density of 240 lbs/ft^3 and are strengthened by a lattice of 1-in. steel reinforcing rods. Four threaded steel inserts (1-1/2-in. I.D.) in each shield block facilitate rigging to the reactor building's overhead crane using cables and shackles. Steel angle on the inside corners of the side shield blocks and all four corners of both shield doors prevents damage to the blocks during manipulation of the shield doors with the overhead crane. A steel boot covers the bottom of each shield door to serve a similar function.

A beam port through both shield doors at a height of 31 in. (10 in. square in the inner shield door and 12 in. square in the outer shield door) provides flexibility for possible future experiments, such as neutron spectrometry and prompt activation analysis. Four 1-ft-thick shield plugs (two in each shield door) of laminated steel and masonite sheet provide the necessary shielding for the beam port.

Since the rear face of the previously existing thermal exponential assembly shielding was uneven, five sections of steel channel were bolted to it and filled with heavy concrete to provide a smooth vertical

surface for the side shield blocks and inner door block to butt up against. The four shield blocks were shimmed after installation to ensure a close fit to the concrete-filled channel. Figure 3.1 shows the horizontal section of channel (3 ft high, 8 ft 10 in. wide and 3-3/4 in. thick) which is attached to the thermal exponential assembly shielding above the entrance to the irradiation region; Figure 3.2 shows the four vertical sections of channel attached at each side of the entrance (an inner section 6 ft 6 in. high, 10 in. wide and 3-3/4 in. thick and an outer section 9 ft 6 in. high, 2 ft wide and 1-3/4 in. thick on each side). Two penetrations in each inner section of channel, and corresponding penetrations in the aluminum liner box, accommodate L-shaped instrumentation conduits of 1-in.-diameter aluminum pipe which run from the top of the shielding down between the inner and outer channel sections and through the inner channel section and aluminum liner box to the irradiation region.

3.3 THE IRRADIATION REGION

3.3.1 The Aluminum Liner Box

The five-sided aluminum box which lines the irradiation region is an all-welded structure with inside dimensions of 6 ft 2 in. high by 6 ft 1 in. wide by 6 ft 1 in. deep. The liner box was fabricated by seam-welding 6061-T6 aluminum sheet (1/2 in. sheet for the floor and 1/4 in. sheet for the sides, top and front) reinforced with 1 in. by 1 in. by 1/4 in. 6061-T6 aluminum angle. The front of the box has a 4-ft-diameter port with a cover plate which can be removed to provide access to the hohlraum region; the cover plate is made of 1/8-in. aluminum sheet to improve thermal neutron transmission.

After installation of the liner box at the rear of the hohlraum, the small space, several inches wide between the sides and top of the liner box and the existing thermal exponential shielding was filled with plywood (coated with fire-resistant paint). Three lengths of steel angle, machined to fit between the liner box and the thermal exponential shielding and bolted to the rear edges of the liner box, were coated with epoxy cement to seal the hohlraum from the irradiation region and the reactor building.

Boral sheet, 1/8 in. thick and 48 in. wide, was tack-welded to the top and sides of the liner box, to reduce backscattering of thermalized neutrons from the concrete shielding. Sections of boral sheet were also installed on the floor of the box between the rails.

3.3.2 The Rail System

The 35-1/2-inch-gauge rail system for installation and removal of the experimental carts runs from the front of the irradiation region out to the reactor building containment wall, a distance of 17 ft. A 4 ft 4in.-long center section of each rail can be removed when the shield doors are replaced to close the irradiation region, in order to prevent streaming. Each rail is a 3-3/4-in.-wide plate of 1-in.-thick aluminum plate bolted to a 12-in.-wide base plate of 3/16-in. steel (in the form of an inverted "T"). The experimental cart casters run on the base plate, and the aluminum plate acts as a guide rail. The blanket casters run on the outside of the guide rail, while the converter and graphite cart casters run on the inside of the guide rail. The 5 ft 8 in.-long rail sections in the irradiation region were

positioned with aluminum clips welded to the floor of the aluminum liner box; the 7-ft-long rail sections on the reactor floor were tack-welded to a 1/2-in.-thick steel plate which extends from the rear of the liner box out to the reactor building containment wall (see Fig. 3.2). This steel floor plate has the same thickness as the floor of the aluminum liner box and also provides a flat lay-down surface for the shield doors and distributes the experimental cart loads. Whenever it is desired to remove experimental carts from the irradiation region, the 4 ft 4 in.-long removable center rail sections are positioned and bolted to the steel floor plate with 1/4-in.-diameter countersunk flathead screws.

3.3.3 The "Picture Frame"

In order to prevent streaming of the thermal source flux from the hohlraum around the converter assembly during fast operation of the B.T.F., or around the graphite cart during thermal operation, a 2-ft-deep "picture frame" of graphite and masonite backed with boral sheet was built at the front of the irradiation region (see Fig. 3.3). Both the converter assembly and the graphite cart fit into this picture frame with approximately 1/2 in. clearance at the top and sides and 1 in. clearance at the bottom.

The 4-in.-wide side walls of the picture frame are 4 in. by 4 in. graphite stringers stacked to a height of 5 ft 4 in., and tied together with 1/4-in.-diameter aluminum rods (two 5 ft 4 in.-long rods in each wall). The top of the picture frame consists of a 4-in. thickness of masonite sheet, resting at each side on top of the graphite side walls.

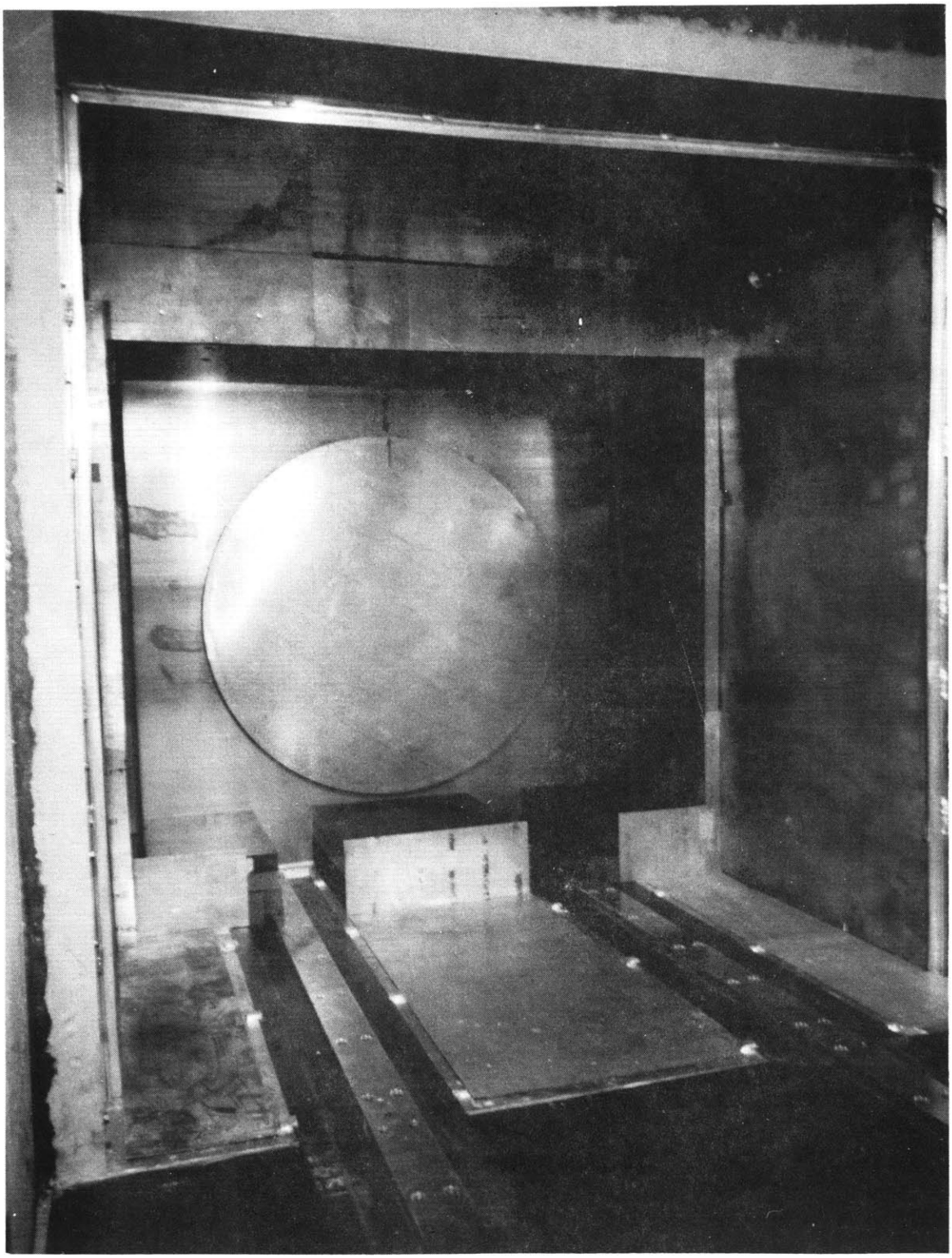

FIG. 3.3 VIEW OF THE BLANKET TEST FACILITY IRRADIATION REGION

The 6-in.-high space between the masonite and the roof of the aluminum liner box was filled with graphite stringers. Standard 4 in. by 4 in. graphite stringers were also laid on the floor of the irradiation region between the rails and covered with a 4-in. thickness of masonite sheet. The completed picture frame has inside dimensions of 66 in. wide by 56 in. high (starting 8 in. above the floor) by 2 ft deep. To absorb thermal neutron leakage through the picture frame, the entire rear surface is covered with 1/8-in. boral sheet.

3.4 THE EXPERIMENTAL ASSEMBLIES

3.4.1 The Experimental Carts

The three experimental assemblies, the graphite wall assembly, the converter assembly and the simulated blanket assembly, are each mounted on a separate cart. Two identical carts, with a maximum load capacity of 6 tons, were built for the graphite wall and converter assemblies, while a third cart, with a maximum load capacity of 24 tons, was built to carry the simulated blanket assembly.

The 6-ton capacity carts have a platform of 1-in. 6061-T6 aluminum plate, 65 in. wide, 22 in. long and 10-1/8 in. high, mounted on two 6-in.-wide by 33-in.-long plates of 1-in. steel, which improve the stability of the carts by extending the wheelbase out behind the platform. Three 1-ton load capacity casters (Bassick 6HB1-2) are bolted to each bearing plate on a 29-in. gauge. Two fairings of 0.020-in. cadmium sheet around the steel plates and casters prevent activation of these components by the thermal neutron flux from the hohlraum.

The 24-ton capacity cart has a platform of 1-in. steel plate, 65 in. wide, 39 in. long and 11-1/2 in. high, supported by six 4-ton load capacity casters (Bassick 8921-2) on a 43-in. gauge. Since the blanket cart has a higher platform and wider wheel gauge than the converter cart, the front of the blanket cart platform can overlap the rear of the converter cart platform by up to 2 in., to ensure that the converter and blanket assemblies can fit together with no void space between them.

Two 2-in.-diameter holes are provided at the rear of each cart to allow removal of the carts from the irradiation region by using chain falls connected between the cart and two anchors mounted in the reactor building containment wall. To date, however, it has been possible to remove the experimental assemblies manually.

3.4.2 The Graphite Wall Assembly

The graphite wall cart carries an assembly of graphite stringers, held in place by an aluminum retaining structure. It was designed to have the same external dimensions as the converter assembly, so that it can replace the latter at the front of the irradiation region during thermal operations, that is, when it is desired to operate the thermal exponential facility or other experiments utilizing the hohlraum thermal flux.

A 64-3/4 in. by 20-7/8 in. rectangular base made from 1-1/2 in. by 1-1/2 in. by 3/8 in. 6061-T6 aluminum angle was tack-welded to the platform of one of the 6-ton-capacity experimental carts.

Vertical lengths of the same type of aluminum angle, 53-1/4 in. high, were then welded at each corner of the base. Lengths of 1 in. by 3/8 in. 6061-T6 aluminum bar were welded in an "X" configuration between the aluminum uprights, and also horizontally between the tops of the uprights, at the sides front and rear, to form a reinforced retaining structure. Standard 4 in. by 4 in. graphite stringers were loaded into the open-topped aluminum framework (which can be seen in Fig. 3.4), to obtain a graphite wall 53-1/2 in. high, 64 in. wide and 20 in. thick.

Sheets of 1/4-in.-thick boral were fastened to the rear of the aluminum framework to provide a 58-in. high by 71-in. wide boral backing to the graphite wall assembly. When the graphite cart is in position at the front of the irradiation region, the boral backing on the graphite cart overlaps the boral backing on the picture frame by about 2 in. at the top and sides and about 1/4 in. at the bottom. This prevents the leakage of thermal flux into the space behind the graphite cart where the converter assembly is generally stored during thermal operation, ensuring that the converter fuel is not activated.

3.4.3 The Converter Assembly

As outlined in section 2.4.1, the converter assembly consists of an 8-in.-thick graphite external moderator region of 4 in. by 4 in. reactor grade graphite stringers, and a 6.865-in.-thick fuel region of 1/2-in.-diameter aluminum-clad UO_2 fuel rods in a close-packed, triangular-pitch array. The graphite stringers and UO_2 fuel rods are mounted vertically, between upper and lower grid plates in a closed aluminum container. The container is designed to prevent any

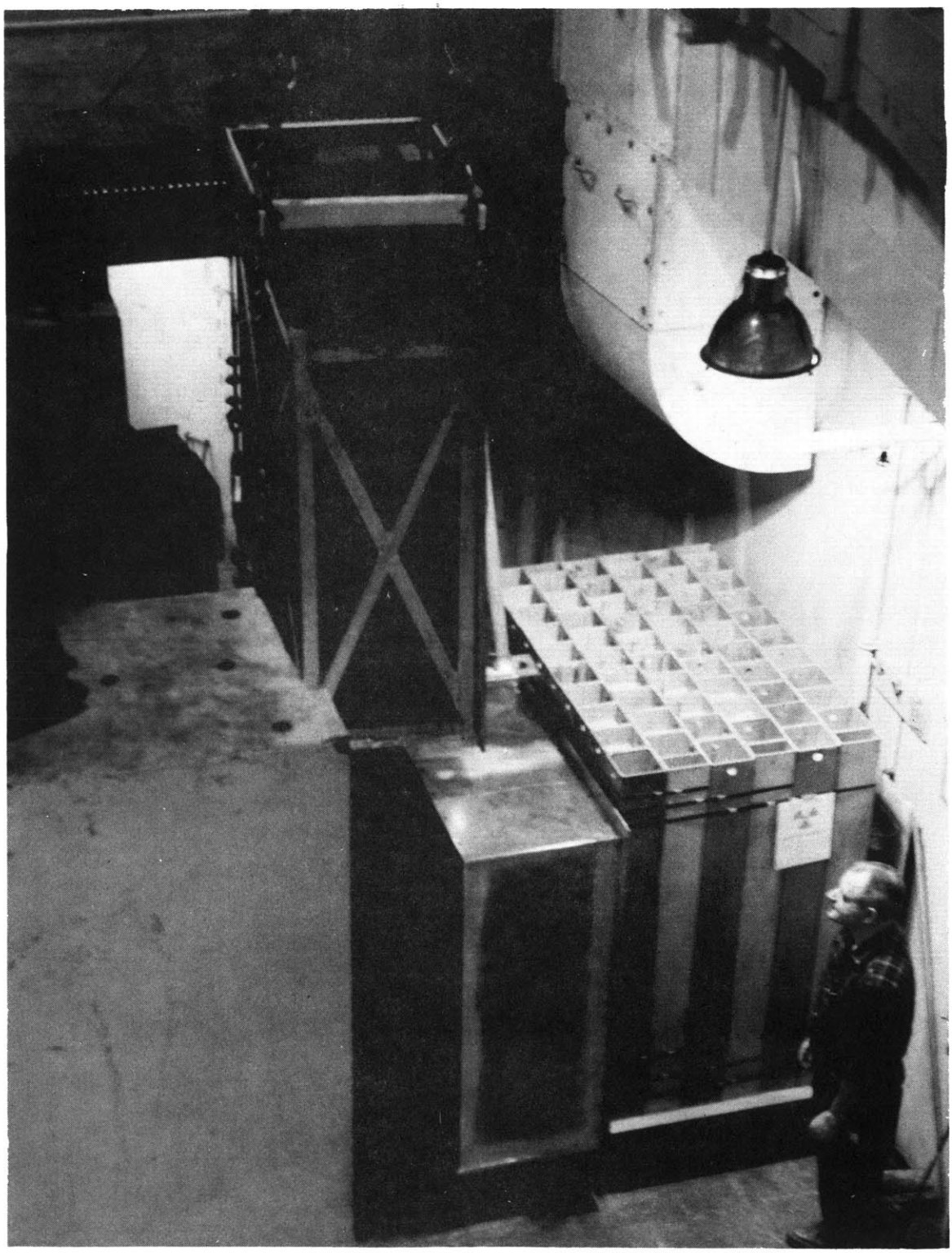

FIG. 3.4 – VIEW OF THE EXTERIOR OF THE BLANKET TEST FACILITY SHOWING THE EXPERIMENTAL ASSEMBLIES

accidental rearrangement of fuel that might approach a critical assembly even if the assembly were flooded. The box will also contain any radioactive argon generated in the converter. A cutaway view of the converter assembly is shown in Figure 3.5.

The all-aluminum (6061-T6 alloy) converter assembly container has external dimensions of 53-1/2 in. high by 64-5/8 in. wide by 21-1/8 in. thick. The bottom of the container was made from 1-in. aluminum plate, while the sides, front and rear were made from 1/8-in. aluminum plate; the five plates were joined with continuous seam welds. A vertical upright of 1 in. by 1 in. aluminum bar was welded into each corner of the container box to reinforce the structure. Two upper grid plate supports of 1 in. by 1 in. aluminum bar, 20-7/8 in. long, were welded to the uprights (one at each side of the container box) so that the tops of the grid plate supports were 2-1/16 in. below the top of the container box (see Figure 3.5). Lengths of 1 in. by 1 in. by 1/4 in. aluminum angle, welded inside the top edge of the front and rear plates, and 1 in. by 1 in. aluminum bar, welded inside the top edge of the side plates, provide further reinforcement, and were also drilled and tapped for the 1/4-in.-diameter bolts which hold down the top cover plate. The 64-5/8 in. by 21-1/8 in. cover plate was made from 1/4-in.-thick aluminum plate.

The completed container box was mounted on one of the 6-ton-capacity experimental carts and fastened with four 1/2-in.-diameter cadmium-plated bolts. The floor of the container box was covered with 1/4-in.-thick boral sheet (the intention being to force the incident thermal flux to assume a double cosine shape by imposing a zero

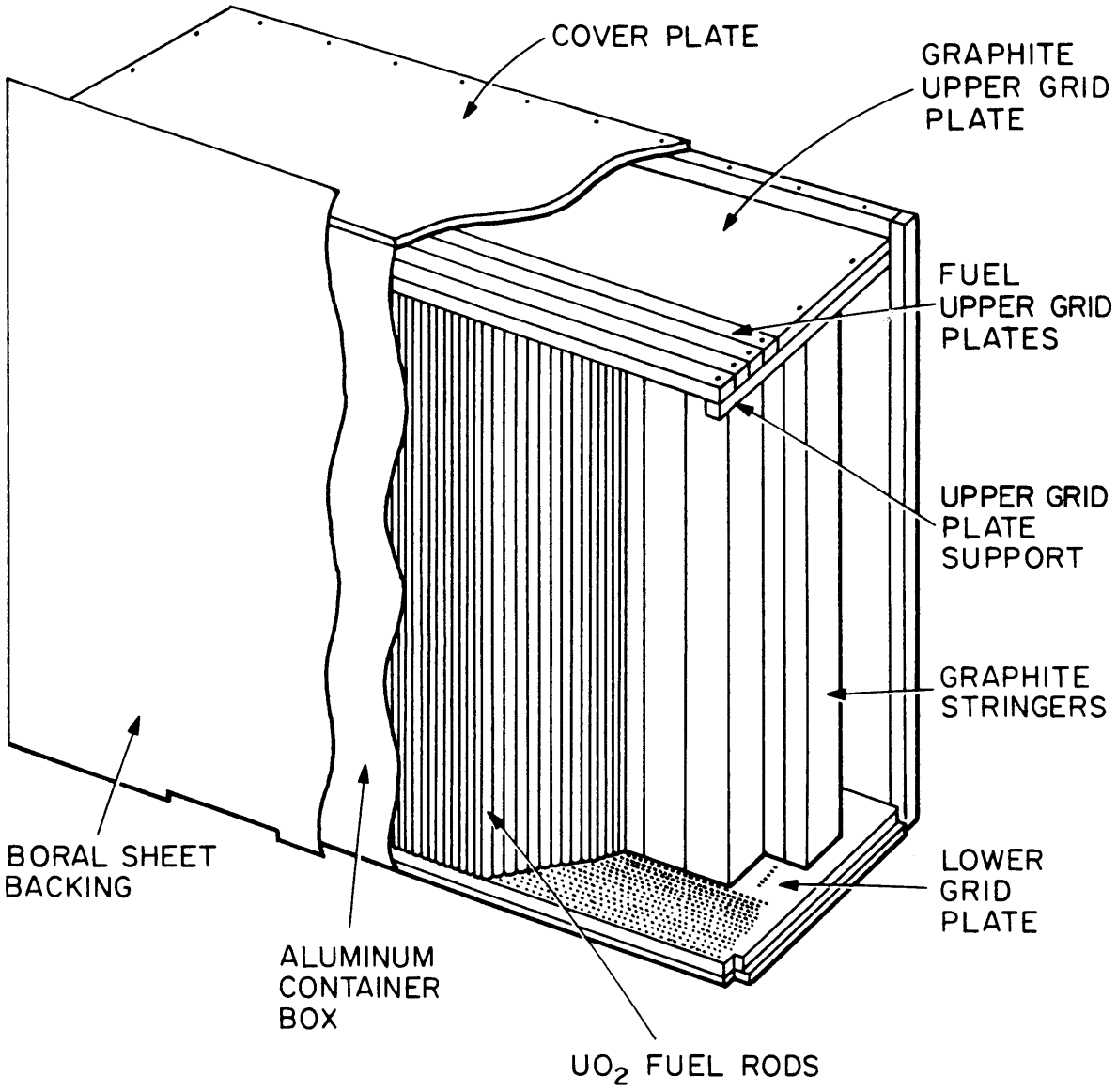

FIG. 3.5 CUTAWAY VIEW OF THE CONVERTER ASSEMBLY.

thermal flux boundary condition at the sides, and top and bottom of the converter assembly). The 64-1/4 in. by 19-3/4 in. lower grid plate of 1/2-in.-thick 6061-T6 aluminum plate was then installed in the bottom of the container box (see Figure 3.5).

The lower grid plate and five upper grid plates have 9/32-in.-diameter, 1/2-in.-deep holes to accommodate the 1/4 in.-diameter, 1/4-in.-long nipples on each end of the UO_2 fuel rods and 4 in. by 4 in. graphite stringers. On the front section of the lower grid plate, the holes were drilled on a 4.020-in.-square pitch to permit the loading of up to 3 rows of 4 in. by 4 in. graphite stringers, 15 stringers to a row. On the rear section of the lower grid plate, the holes were drilled on a 0.510-in. triangular pitch to permit the loading of up to 17 rows of 1/2-in.-diameter UO_2 fuel rods, with 117 or 118 rods in alternate rows. Although the optimum loading was determined from the multigroup calculations to be 2 rows of graphite stringers and 15 rows of UO_2 fuel, the flexibility introduced by permitting any loading up to 3 rows of graphite stringers and 17 rows of fuel will allow the choice of a wide range of converter leakage spectra.

The spacing of the holes in the upper grid plates is identical to that in the lower grid plate. However, to facilitate loading, a single upper grid plate is used to tie down the graphite stringers, while four upper grid plates are used to tie down the fuel rods (see Figure 3.5). Both the upper and lower grid plates are designed so that the fuel rods in the last row of the fuel region (at the rear of the converter assembly) are in contact with the rear wall of the converter container; this ensures that there are no streaming voids between the converter and

blanket assemblies.

Two rows of 4 in. by 4 in. reactor grade graphite stringers, 49-1/2 in. long, were loaded into the container box, to form a graphite region 49-1/2 in. high, 60 in. wide and 8 in. thick. Gaps between the stringers were staggered by loading a 2 in. by 4 in. stringer at each side of the front row, in order to prevent streaming. Aluminum pins, 1/4 in. in diameter, mounted in each end of the stringers, fit into the holes in the upper and lower grid plates to hold the stringers in position. A 62-1/4 in. by 12-5/8 in. top grid plate of 1-in.-thick 6061-T6 aluminum plate was installed over the top of the graphite stringers and fastened to the upper grid plate supports with four 1/4-in.-diameter aluminum bolts.

Next, fifteen rows of fuel rods (a total of 1763 rods) were loaded into the container box. The 1/2-in.-diameter UO_2 fuel rods are 49-1/2 in. long, exclusive of the 1/4-in.-long, 1/4-in.-diameter nipples on each end. The thickness of the 0.500-in.-O.D., Type 1100 aluminum clad is 0.032 in. The 10.20 gm/cm^3 density UO_2 fuel pellets have a diameter of 0.430 in. and an active length of 48 in. The front (closer to the graphite) seven rows of fuel rods have a U^{235} enrichment of 1.99%, while the rear eight rows of fuel rods have a U^{235} enrichment of 1.0999%. The resulting fuel region is 49-1/2 in. high, 60 in. wide and 6.865 in. thick. Four 62-1/4 in. by 1-3/4 in. top grid plates of 1-in.-thick 6061-T6 aluminum plate were installed over the top of the fuel rods and fastened to the upper grid plate supports.

To permit the converter assembly fuel temperature to be monitored during irradiation, two chromel-alumel thermocouples

were mounted (using epoxy resin) on the surface of the aluminum cladding of two fuel rods, both located at the center of the front row of the fuel region. The thermocouples are wired through a 1/4-in.-diameter hole in the converter container's top cover plate to standard thermocouple connectors. When the converter is installed in the irradiation region, the connectors are plugged into sockets which are wired through the instrumentation conduits to an external pyrometer (see section 3.5).

Following loading of the graphite and fuel, the upper grid plates were covered with 1/8-in.-thick boral sheet and the top cover plate installed. Sheets of 1/8-in.-thick boral were fastened to the rear of the container box to provide a 58-in. high by 70-in. wide boral backing to the converter assembly. This boral backing overlaps the boral backing on the picture frame, in the same manner as that on the graphite cart, absorbing thermal flux streaming between the converter assembly and the picture frame, and reducing the low energy leakage from the converter (see section 2.4.2). Finally, a 1/4-in.-thick boral sheet was epoxied to the underside of the converter cart to supplement the internal cadmium sheet in maintaining a black thermal boundary around the periphery of the converter.

3.4.4 The First Blanket Assembly

The multigroup calculations reported in section 2.6 showed that the neutron spectra and spatial flux shapes generated in a simulated blanket assembly composed of 50 v/o iron and 50 v/o anhydrous borax are reasonably similar to those generated in a typical LMFBR radial

blanket. B.T.F. Blanket No. 1 was designed and built to this loading specification,[30] to provide a relatively simple and inexpensive first blanket assembly with which to evaluate the completed facility experimentally.

B.T.F. Blanket No. 1 consists of sixty-three subassemblies, 60 in. tall and loaded to a height of 55.4 in. Fifty-seven of these subassemblies are 6 in. square, and six are 3 in. by 6 in. These are loaded in six rows, each approximately 5 ft wide by 6 in. deep; the 3 in. by 6 in. subassemblies are loaded at each end of alternating rows, so as to stagger the gaps between subassemblies and prevent streaming. Vertical tubes are provided in fifteen of the subassemblies (two tubes in six of the subassemblies, and one tube in nine of the subassemblies) and are aligned during loading to permit vertical, horizontal and axial foil activation traverses to be made through the blanket assembly. Figure 3.2 shows a typical subassembly and foil tube configuration.

The subassemblies were fabricated from 5-ft lengths of low-carbon steel rectangular mechanical tubing; the wall of the tubing is 3/16 in. thick. A steel plate, 1/8 in. thick and recessed 1/2 in., was seam-welded to the bottom of each subassembly. The bottom ends of the 59-1/2-in.-long, 9/16-in.-O.D., 1/2-in.-I.D. vertical foil holder tubes were welded to this lower plate. In subassemblies with a single foil tube, the tube was positioned 1-1/2 in. from one side of the subassembly, and 3 in. from the two adjacent sides; in subassemblies with two foil tubes, both tubes were positioned 1-1/2 in. from the same side of the subassembly and 3 in. apart.

The subassemblies were filled with a mixture of low-carbon steel punchings and anhydrous borax powder (U.S. Borax, commercial grade). The steel punchings are approximately 1/8 in. thick and from 1/4 in. to 1 in. in diameter. The 6-in.-square subassemblies were each loaded with 191.6 pounds of steel punchings and 45.48 pounds of borax powder, while the 3 in. by 6 in. subassemblies were each loaded with half these amounts. An electric hammer was used during the loading of each subassembly to compact the steel-borax mixture to a mean fill height of 55.4 in. Thus the homogenized densities of borax and steel (both the punchings and the subassembly container walls) are 38.39 lbs/ft^3 and 217.9 lbs/ft^3, respectively.

The steel-borax mixture in each subassembly was covered with a 20-gauge steel plate which was sealed with epoxy resin to the subassembly walls. For the 15 subassemblies with foil tubes, 9/16-in.-diameter holes were punched in the cover plates to accommodate the tubes. Each subassembly was given a thin (about 5 mils) coating of red lead paint; the volume of this coating is estimated to be approximately 0.35 v/o of the total blanket volume. Corrections were made for the phenol (C_6H_5OH) content of the red lead coating in calculating the homogenized atom densities for B.T.F. Blanket No. 1 (given in Appendix C).

Samples of the borax loaded into each subassembly were analyzed for water content. Each sample was heated to its melting point, cooled in a dry atmosphere, and the resulting weight loss measured. The average water content of the borax samples was found to be 0.86 w/o. This value was confirmed by nuclear magnetic resonance analysis of

several borax samples dissolved in D_2O.

The completed subassemblies were loaded onto the 24-ton-capacity experimental cart, in the configuration shown in Figure 3.2, by means of the reactor building's overhead crane. A commercial banding machine was used to wrap 1/2-in.-wide steel strap around the top and bottom of the entire blanket assembly to hold the subassemblies in position. The completed blanket assembly is 55.4 in. high, 60.75 in. wide and 30.5 in. deep.

3.5 INSTRUMENTATION

Instrumentation for the Blanket Test Facility consists of a hohlraum thermal flux monitor, an irradiation region gamma dose monitor, and two thermocouples to monitor the converter fuel temperature.

The neutron flux detector is an uncompensated ion chamber (Westinghouse Model 6377), mounted in the graphite floor of the hohlraum just in front of the right-hand side of the aluminum liner box. The ion chamber is wired to a D.C. microammeter (0 to 50 μa), which has a 1000-ohm shunt to provide approximately midscale deflection at a reactor power level of 5 Mw, or a hohlraum thermal flux of about 5×10^9 n/cm^2-s.

The gamma detector (Tracerlab Model RMI-110) is mounted in the top right-hand corner of the irradiation region just behind the picture frame, and is wired to a logarithmic scale meter calibrated in dose units (0.1 mr/hr to 10 r/hr).

The two chromel-alumel thermocouples, mounted on the clad of two fuel rods in the front row of the converter assembly fuel region, are wired to a single three-position switch which is in turn connected to a pyrometer (Simpson Model 3324). The switch allows either thermocouple temperature to be selected on the pyrometer.

The microammeter, gamma dose meter, pyrometer and thermocouple selection switch are mounted in a console which is located on the reactor floor to the right of the B.T.F. shielding.

3.6 OPERATING PROCEDURE FOR THE B.T.F.

3.6.1 Fast Operation

For fast operation of the B.T.F., that is, when a blanket assembly is to be irradiated, the converter assembly is rolled into the picture frame at the front of the irradiation region and the blanket assembly is installed immediately behind the converter. To ensure that there is no void space between the converter and simulated blanket, two 30-in.-long carpenter clamps are connected between the rear of the converter cart and the rear of the blanket cart and tightened. The two center rail sections are then removed, and the inner and outer shield doors are replaced using the overhead crane. D_2O is pumped into the heavy water exponential tank (see Figure 1.1) to maintain the desired reflective properties of the hohlraum and to provide additional shielding over the top of the hohlraum.

To initiate irradiation of the blanket assembly, the thermal column lead shutters and hohlraum steel doors (see Figure 3.2) are

opened. During the irradiation, which is typically about 4 hours for foil activation experiments, the incident (hohlraum) thermal neutron flux and fuel element temperature can be continuously monitored. In practice, however, the fuel element temperature rise during irradiation has been found to be insignificant (less than 1° C after a 4-hour irradiation).

After the irradiation is complete, the lead shutters and steel doors are closed again to isolate the hohlraum from the thermal column and the reactor. The converter and blanket are allowed to cool for 4 to 6 hours to reduce radiation levels. The gamma dose in the irradiation region is monitored to ensure that the radiation level is sufficiently low before the shield doors are opened. The inner and outer shield doors are then removed, and the center rail sections installed. The blanket cart is rolled out onto the reactor floor where foil holders, or other experimental equipment, can be retrieved.

To date, irradiations have been scheduled so that the shield doors are opened only after the weekly reactor shutdown. However, with the lead shutters and steel doors closed, and the converter assembly (which provides considerable gamma shielding) installed in the picture frame, the radiation level in the irradiation region has been found to be less than 100 mr/hr when the reactor is at full power. This should be sufficiently low to permit opening the shield doors to remove the blanket assembly when the reactor is at power; experiments will be performed in the near future to verify this. Changeovers from fast operation to thermal operation, and vice versa, will continue to be made only when the reactor is shut down.

3.6.2 Thermal Operation

In order to convert the B.T.F. for thermal operations, the blanket and converter carts are rolled out of the irradiation region to the reactor building containment wall. The graphite cart is rigged to the overhead crane, by means of a specially designed steel frame and cable sling, and lifted onto the rails in front of the converter and blanket carts. This operation is shown in Figure 3.4. The graphite cart is then rolled into the picture frame at the front of the irradiation region and the converter cart is rolled in behind it for storage. The center rail sections are then removed and the inner and outer shield doors replaced.

The reverse procedure is used for the changeover from thermal operation to fast operation.

Only the graphite cart, which is the lightest (just over 2 tons) of the three experimental carts, need ever be lifted off the rails. However, the graphite cart lifting sling has a sufficient load capacity to lift the converter assembly cart (about 3-1/2 tons), should this be necessary.

3.6.3 Summary

Despite the size and weight of the equipment involved, the Blanket Test Facility has proven relatively easy to operate. Removal or replacement of the shield doors requires careful manipulation of the overhead crane, but can be accomplished in about 30 minutes. The experimental carts can be manually installed in, or removed from, the

irradiation region by two or three persons. Finally, since the converter fuel temperature rise is less than 1° C during irradiation, the B.T.F. does not require continuous monitoring during operation.

Chapter 4

EXPERIMENTAL EVALUATION OF THE BLANKET TEST FACILITY

4.1 INTRODUCTION

When construction of the Blanket Test Facility was complete, a series of experimental runs was made to evaluate the performance of the facility with the converter assembly and the first blanket assembly in place.

During the initial runs, fast neutron and gamma dose measurements were made at full power to determine the effectiveness of the biological shielding. Gamma dose measurements were made following shutdown to determine the accessibility of the irradiation region and the residual activation of the experimental assemblies. The cadmium ratio in the hohlraum was measured during both fast and thermal irradiations. The facility instrumentation was also checked for correct operation.

To evaluate the performance of the converter and blanket, foil activation traverses were made with gold and indium foils. The 64.8-hour half-life $Au^{197}(n, \gamma) Au^{198}$ reaction was chosen because its cross section is large enough at higher energies (about 0.4 barns at 100 kev) to provide adequate foil activity from fast neutron activation, while its high thermal cross section (about 92 barns) and resonance integral (about 1560 barns) would indicate any undesirable thermal or epithermal neutron leakage into the blanket assembly. The 4.5-hour half-life

$In^{115}(n, n')In^{115m}$ reaction was chosen because its 400-kev threshold and relatively high cross section (about 0.27 barns at 2 Mev) make it suitable as an indicator of high energy neutron behavior. Previous irradiation of indium foils in the MIT D_2O Exponential Facility[31] had shown that adequate foil activities could be obtained. Figure 4.1 is a schematic view of the converter and blanket assemblies showing the positions in which the activation traverses were made.

Activation traverses with bare and cadmium-covered gold foils were made along the sides, top and bottom of the blanket assembly to establish the degree to which neutrons were either streaming around the blanket or being backscattered into the blanket from the surrounding concrete shielding.

A matrix of gold foils mounted on a 1/8-in.-thick aluminum sheet inserted between the converter and blanket was irradiated to provide a complete mapping of the converter leakage flux at the converter-blanket interface.

Horizontal and vertical (X- and Y-direction) activation traverses were made with gold and indium foils at varying distances into the blanket assembly to determine the horizontal and vertical flux shapes in the blanket, and to permit calculation of the transverse leakage, or buckling, of the blanket. The gold-to-indium activation ratios were also calculated for these horizontal and vertical traverses to ensure that transverse spectral equilibrium existed throughout most of the blanket volume; this is indicated by a constant gold-to-indium activation ratio for any horizontal or vertical traverse.

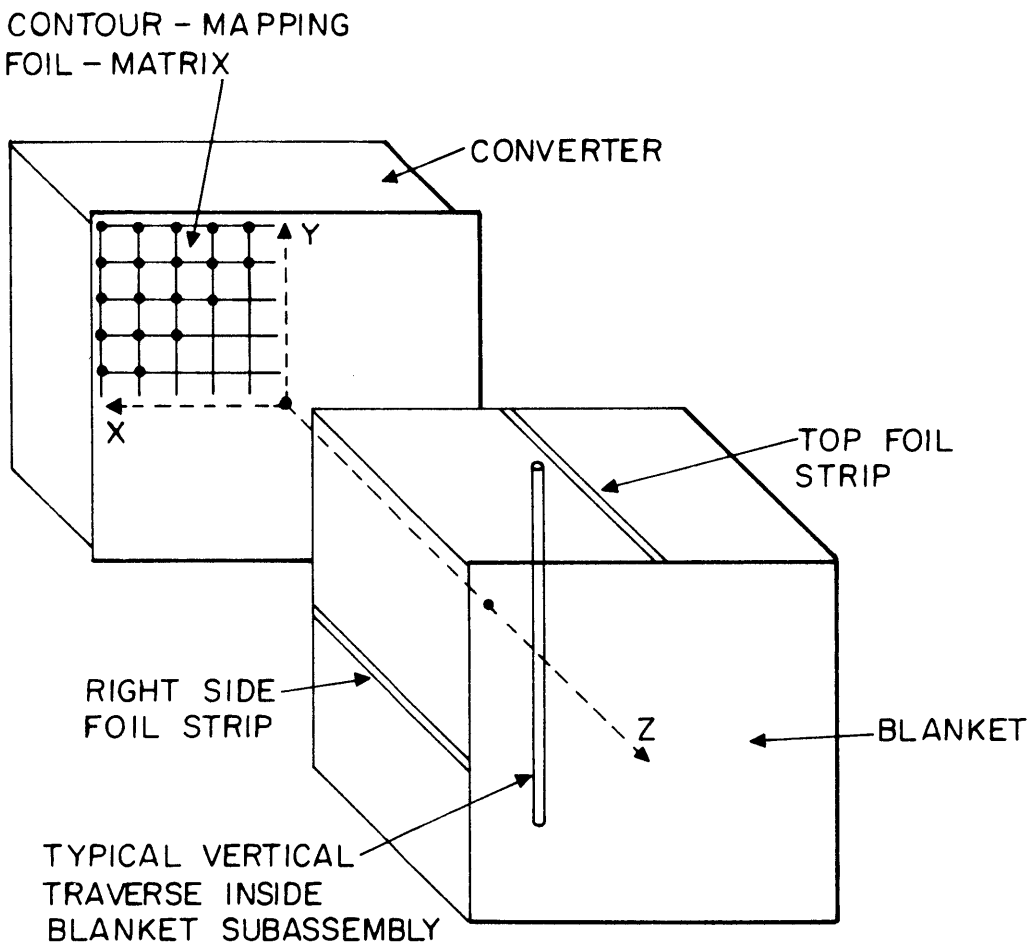

FIG. 4.1 SCHEMATIC VIEW OF THE CONVERTER AND BLANKET ASSEMBLIES SHOWING THE FOIL IRRADIATION POSITIONS

Finally, axial (Z-direction) activation traverses were made in the blanket assembly with gold and indium foils, and the measured activities were compared with calculations made with the ANISN code.

The horizontal, vertical and axial foil activation traverses inside the blanket assembly were made by taping the foils (with 0.001-in.-thick mylar tape) into recessed spots milled in 7/16-in.-diameter aluminum foil holder rods. The foil holders were inserted into the 1/2-in.-I.D. steel foil holder tubes in the blanket subassemblies (see Section 3.4.4) prior to irradiation. All foil activation measurements were made with the subassembly configuration shown in Figure 3.2.

Table 4.1 gives a summary of the measurements performed in five B.T.F. irradiations to evaluate the performance of the facility.

4.2 DOSE RATE AND INSTRUMENTATION EVALUATION

4.2.1 External Dose Rates During B.T.F. Operation

During initial runs, fast neutron and gamma dose measurements were made outside the biological shielding to ensure that the shielding met design requirements.

Area background radiation, particularly from the MITR D_2O heat exchangers directly underneath the facility in the basement of the reactor building, made precise gamma dose measurements difficult. However, for both fast and thermal operations, the gamma dose through the bulk shielding was found to be less than 0.5 mr/hr on contact, while the gamma dose through any streaming slots between the shield blocks was found to be less than 5 mr/hr.

TABLE 4.1

Summary of B.T.F. Evaluation Experiments

B.T.F. Run No.	Measurements Performed	Comments
1	Shielding External Dose Rates Neutron Spectrometer Background Reactor Building A^{41} Level Instrumentation Evaluation	
2	External Blanket Traverses Au and In Horizontal Traverses Au and In Vertical Traverses Residual Activation of Assemblies	Concrete Anti-Streaming Blocks in Place
3	Au and In Horizontal Traverses Au and In Vertical Traverses Au Axial Traverses Hohlraum Cadmium Ratio Fuel Element Temperature Rise Irradiation Region Gamma Dose	Concrete Anti-Streaming Blocks Removed
4	Au and In Horizontal Traverses Au and In Vertical Traverses Au and In Axial Traverses	Additional Boral on Bottom of Converter
5	Converter Source Flux Mapping	

Measurements also indicated that the fast neutron dose outside the shielding was less than 1 n/cm^2-s during fast operation. The increases in the reactor building A^{41} activity and in the fast neutron background count rate of neutron spectrometers in the reactor building were also negligible.

4.2.2 Irradiation Region Gamma Dose Rates

After a 4-hour irradiation of the converter and blanket assemblies (Run No. 3), the irradiation region gamma monitor (see Section 3.5) reading was followed for a period of 5 hours to determine the cooling rate in the irradiation region. Figure 4.2 shows the gamma monitor reading during the cooling period after the steel doors and lead shutters were closed to terminate irradiation. It was observed that the gamma monitor reading decreased from about 2 r/hr immediately following irradiation (during irradiation the meter is off scale, > 10 r/hr) to about 100 mr/hr after 4-1/2 hours of cooling. At this time, reactor shutdown occurred, and an immediate drop in the gamma monitor reading from 100 mr/hr to 33 mr/hr was observed. This indicates that most of the post-shutdown dose rate inside the irradiation region is due to the MITR and not to the B.T.F. components. It also shows that access to the irradiation region during reactor operation might be possible (as discussed in Section 3.6.1).

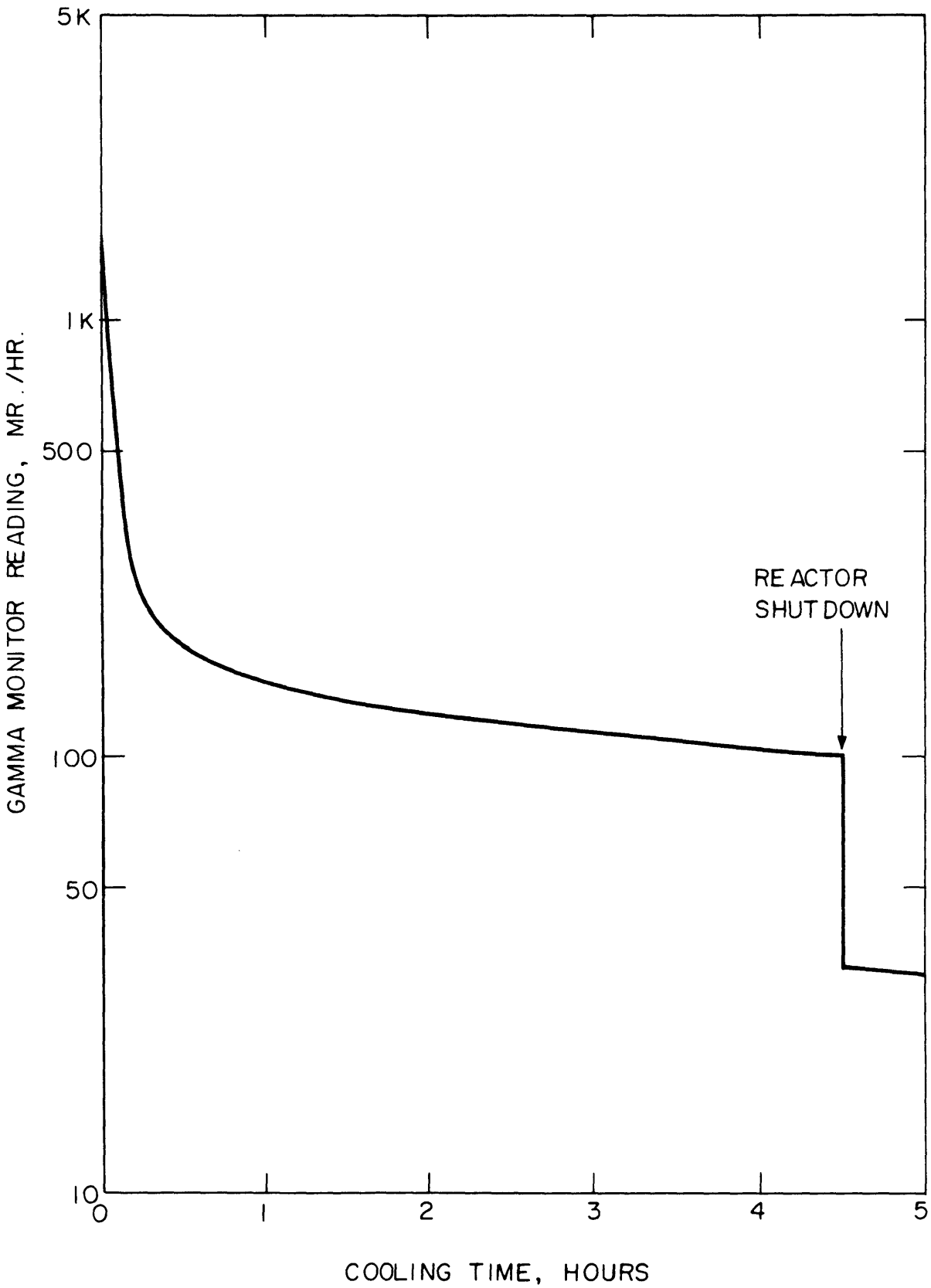

FIG. 4.2 IRRADIATION REGION GAMMA DOSE FOLLOWING A 4 HOUR B.T.F. IRRADIATION

4.2.3 Experimental Assembly Gamma Dose Rates

Measurements were made of the residual activation of the three experimental assemblies following irradiation and cooling. The gamma dose at the center of the rear surface of the converter assembly container was found to be about 220 mr/hr on contact after 2-1/2 hours irradiation and 7 hours cooling, decreasing to about 30 mr/hr after 24 hours cooling.

The gamma dose at the center of the front surface of the blanket assembly (the hottest area) was found to be about 30 mr/hr on contact after 2-1/2 hours irradiation and 7 hours cooling, decreasing to about 5 mr/hr after 24 hours cooling. After irradiation periods of up to 40 hours, the gamma dose at the center of the rear surface of the graphite wall assembly was about 2 mr/hr on contact; some hot spots, particularly weld beads on the front of the assembly and the experimental cart wheel areas, had gamma doses between 15 and 20 mr/hr on contact. Residual activation of both the blanket assembly and graphite wall assembly are sufficiently low for storage of these assemblies on the floor of the reactor building.

4.2.4 Instrumentation Evaluation

During the first and second B.T.F. runs, the pyrometer connected to the two thermocouples at the center of the front row of the converter fuel region (see Section 3.5) was continuously monitored. Neither thermocouple showed any discernible increase in fuel element temperature (the pyrometer cannot discern temperature changes of less than 5° C).

The thermocouple wiring and pyrometer were subsequently checked and found to be in working order. For the third B.T.F. run, the pyrometer was replaced by a bridge circuit which could detect temperature changes as low as 0.1° C. The fuel element temperature rise was observed to be less than 1° C during a 4-hour irradiation.

The microammeter connected to the hohlraum neutron flux detector (see Section 3.5) was shunted to provide approximately mid-scale deflection (21.5 μa.) at a reactor power level of 5 Mw.

4.3 FOIL COUNTING TECHNIQUES

4.3.1 The Gold Foils

The gold foils used for the activation traverses and flux mapping were 1/8 in. in diameter and 0.010 in. thick. The activity of the gold foils was recorded by an automatic counting and sample-changing system, using standard techniques developed in connection with the MIT D_2O Exponential Facility.[28]

A thalium-activated sodium iodide crystal was used for counting the 412-kev principal photopeak (and also the higher energy photopeaks) of Au^{198}. The baseline discriminator of the single-channel analyzer was set at the lowest point in the spectrum below the photopeak, at about 300 kev.

After counting, the raw data were corrected for decay, background and deadtime, and reduced to relative activity per milligram of foil at the end of irradiation.

4.3.2 The Indium Foils

The indium foils used for the activation traverses were 1/4 in. in diameter and 0.010 in. thick. Techniques developed in connection with the MIT D_2O Exponential Facility[31] were used to count the activity of the indium foils.

Detection of the $In^{115}(n, n')In^{115m}$ reaction is complicated by the competing neutron capture reaction, $In^{115}(n, \gamma)In^{116}$. The resonance integral for the capture reaction is about 2640 barns; as a result, the 54-min. half-life In^{116} activity may not be negligible even 8 to 12 hours after the end of irradiation, when the counting of the In^{115m} activity should begin. The In^{116} activity consists of gamma rays with energies greater than the 335-kev In^{115m} activity, so that there can be Compton-effect counts from In^{116} activity underneath the 335-kev photopeak.

The indium foils were counted individually by hand. A well-type, thalium-activated sodium iodide crystal was used for counting the 335-kev photopeak of In^{115m}. A single-channel analyzer was used to straddle the peak; the channel width was approximately 120 kev.

After counting, the raw data were corrected for decay, background and deadtime, and reduced to relative activity per milligram of foil at the end of irradiation.

4.4 EXPERIMENTAL EVALUATION OF THE PERFORMANCE OF THE CONVERTER ASSEMBLY AND BLANKET NO. 1

4.4.1 Hohlraum Cadmium Ratio Measurements

The cadmium ratio for gold was measured in the hohlraum, at a position approximately 3 in. in front of the center of the irradiation region's hohlraum access port (see Figure 3.1). The measurement was made during both fast and thermal operation of the facility.

The cadmium ratio in the hohlraum was found to be 1700 for thermal operation and 140 for fast operation. These results indicate that the graphite wall assembly does indeed provide the hohlraum with the reflective properties and high cadmium ratio necessary for thermal operations, and also that the hohlraum cadmium ratio is quite high even during fast operation.

4.4.2 Measurement of Streaming and Backscattering Around the Blanket

To establish the degree to which neutrons were either streaming around the blanket, or being backscattered into the blanket from the surrounding concrete shielding, gold foil activation traverses were made in the axial (Z) direction along the sides, top and bottom of the blanket assembly. The gold foils for each traverse were attached to a 1/16-in.-thick strip of aluminum sheet with 0.001-in.-thick mylar tape. The aluminum sheet was then mounted on the surface of the blanket assembly.

Figure 4.3 shows the relative gold foil activities obtained from these activation traverses (the standard deviation in the foil activities is smaller than the diameter of the points in the figure). It is seen that

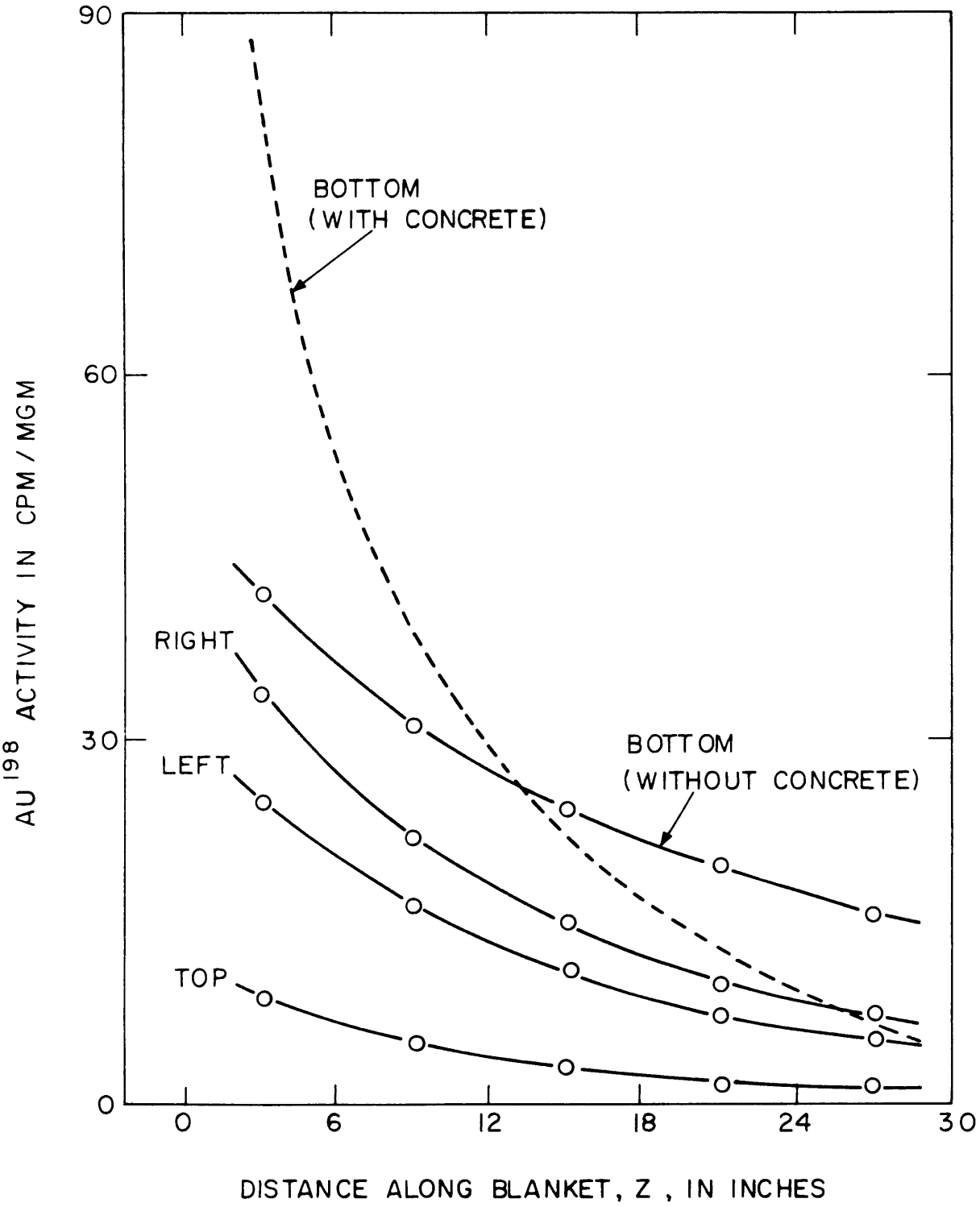

FIG. 4.3 GOLD AXIAL ACTIVATION TRAVERSES ALONG OUTER SURFACES OF BLANKET NO. 1

the foil activities drop off rapidly with increasing axial distance along the surface of the blanket, indicating that there is relatively little streaming around the outer surfaces of the blanket assembly.

Two separate measurements of the gold foil activity along the bottom of the blanket are shown in Figure 4.3. The first, marked "WITH CONCRETE" was obtained during Run No. 2. For this run, 8-in.-thick concrete blocks had been laid on the floor of the irradiation region (and covered with boral sheet) to fill the volume beneath the blanket assembly. The purpose of these concrete blocks was to minimize neutron streaming along the bottom of the blanket. While they did indeed minimize streaming (note the relatively low foil activities at large Z), the blocks increased backscatter into the bottom of the blanket, as can be seen from the fact that the gold foil activities on the bottom of the blanket are considerably higher than those on the top or sides of the blanket. To improve this situation, the concrete blocks were removed for Run No. 3 (see Table 4.1), and the boral sheet laid on the floor of the irradiation region instead. The activation traverse along the bottom of the blanket marked "WITHOUT CONCRETE" shows that removal of the concrete blocks did indeed decrease backscattering, although at the expense of an increase in streaming. The net result, however, is an improvement, and the concrete blocks were not used in the final B.T.F. configuration.

The disparity between corresponding gold foil activities at the top and bottom of the blanket is due to the fact that the vertical centerline of the blanket assembly is 3.7 in. above the vertical centerline of the converter assembly's active fuel region. Thus, neutron leakage from

the top of the blanket is lower than that from the bottom.

Cadmium ratios measured at the center of each of the traverses were all less than 1.05, indicating that there is relatively little backscattering of thermalized neutrons into the blanket. The small increase in the (bare) gold-to-indium activation ratio toward the outside edges of the blanket (see Figures 4.7 and 4.10) confirmed that backscattering is low even for epithermal neutrons.

4.4.3 Mapping of the Converter Source Flux Shape

To provide a complete mapping of the spatial shape of the fast neutron flux at the converter-blanket interface, 110 gold foils, in a matrix of 11 columns by 10 rows (see Figure 4.1), were irradiated during Run No. 5. The gold foils were attached with mylar tape to 1/8-in.-thick, 60-in.-square aluminum sheet. The aluminum sheet was mounted between the converter and blanket assemblies.

Figure 4.4 shows a "contour map" of the relative gold foil activity obtained at the converter-blanket interface. The map was generated by finite-difference interpolation between the experimental data points. The gold foil activity decreases smoothly in all directions from the center of the converter assembly's active fuel region (X = 0, Y = 0). Symmetry about the two axes is reasonably good, particularly about the horizontal (Y = 0) axis; some asymmetry about the vertical (X = 0) axis is evident, but this may be due to nonuniform loading of the iron and borax in the blanket subassemblies (this problem is discussed further in the next section). Examination of Figure 4.4 shows that the spatial shape of the gold foil activity, and hence that of the converter

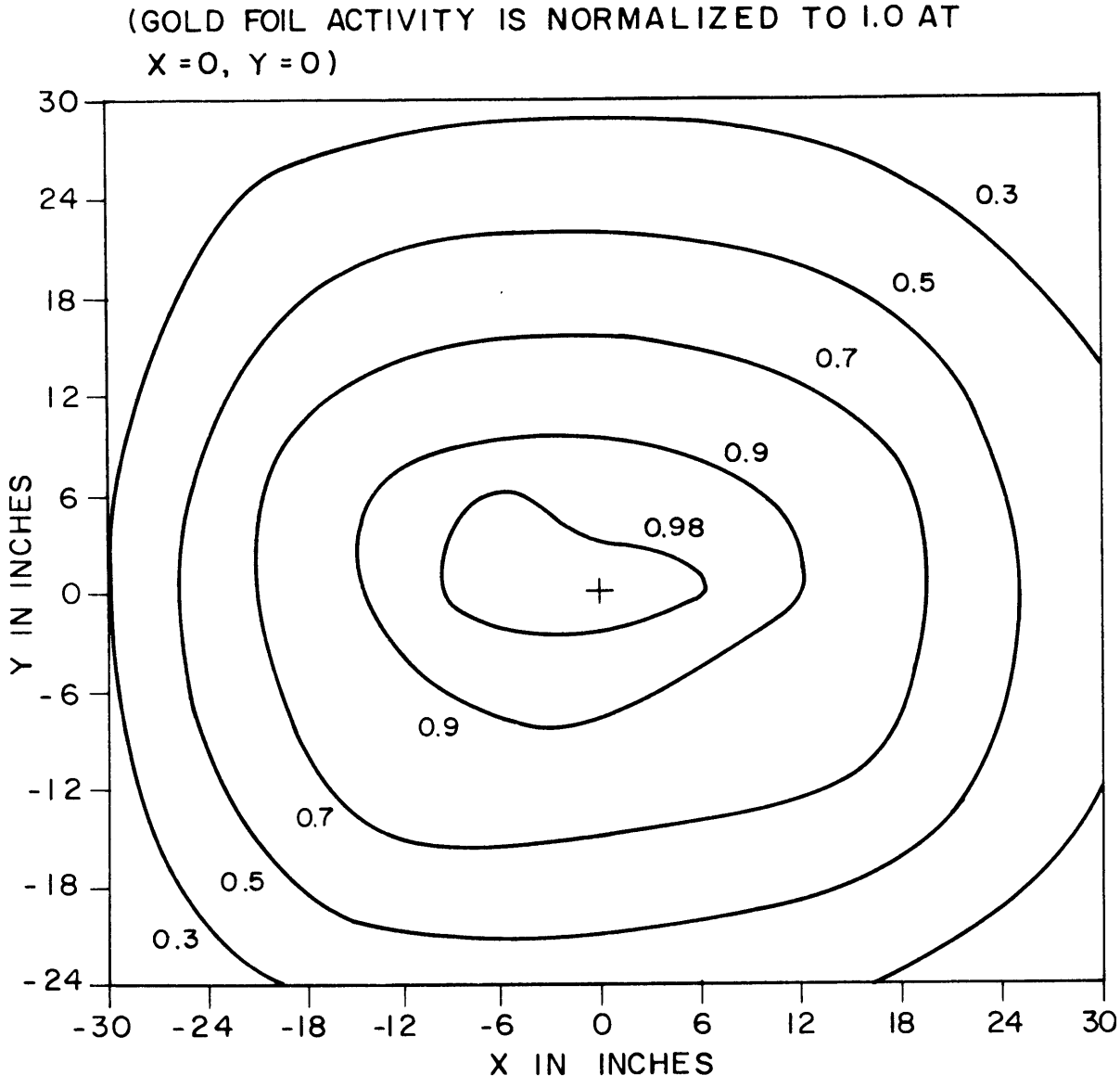

FIG. 4.4 CONTOUR MAP OF GOLD FOIL ACTIVITY AT THE CONVERTER - BLANKET INTERFACE

fast neutron source flux, may in fact be described approximately by a double cosine function,

$$\phi(X, Y) \simeq A \cos\left(\frac{\pi X}{75}\right) \cos\left(\frac{\pi Y}{63}\right),$$

where A is an arbitrary constant and X and Y are in inches.

4.4.4 Gold and Indium Horizontal Activation Traverses in Blanket No. 1

Horizontal (X-direction) activation traverses were made with gold and indium foils at several distances into the blanket assembly to determine the horizontal distribution of the neutron flux in the blanket. The horizontal traverses were made across the vertical centerline (Y = 0).

Figures 4.5 and 4.6 show the horizontal activation traverses for gold and indium, respectively (standard deviation in the foil activities is smaller than the diameter of the points in the figures). It is evident from these figures that the two gold activation traverses and the single indium activation traverse are well approximated by the relation,

$$A(X) = A(0) \cos\left(\frac{\pi X}{75}\right),$$

where A is the gold or indium foil activity, and X is in inches. For the gold and indium horizontal activation traverses at Z = 13.5 in., it is observed that the measured activity at X = 9 in. is considerably below the fitted cosine curve. Since the deviation is approximately the same for both the gold and the indium activities, it is likely that this effect results from a nonuniform density or local inhomogeneity of the borax powder and iron punchings in the blanket subassemblies.

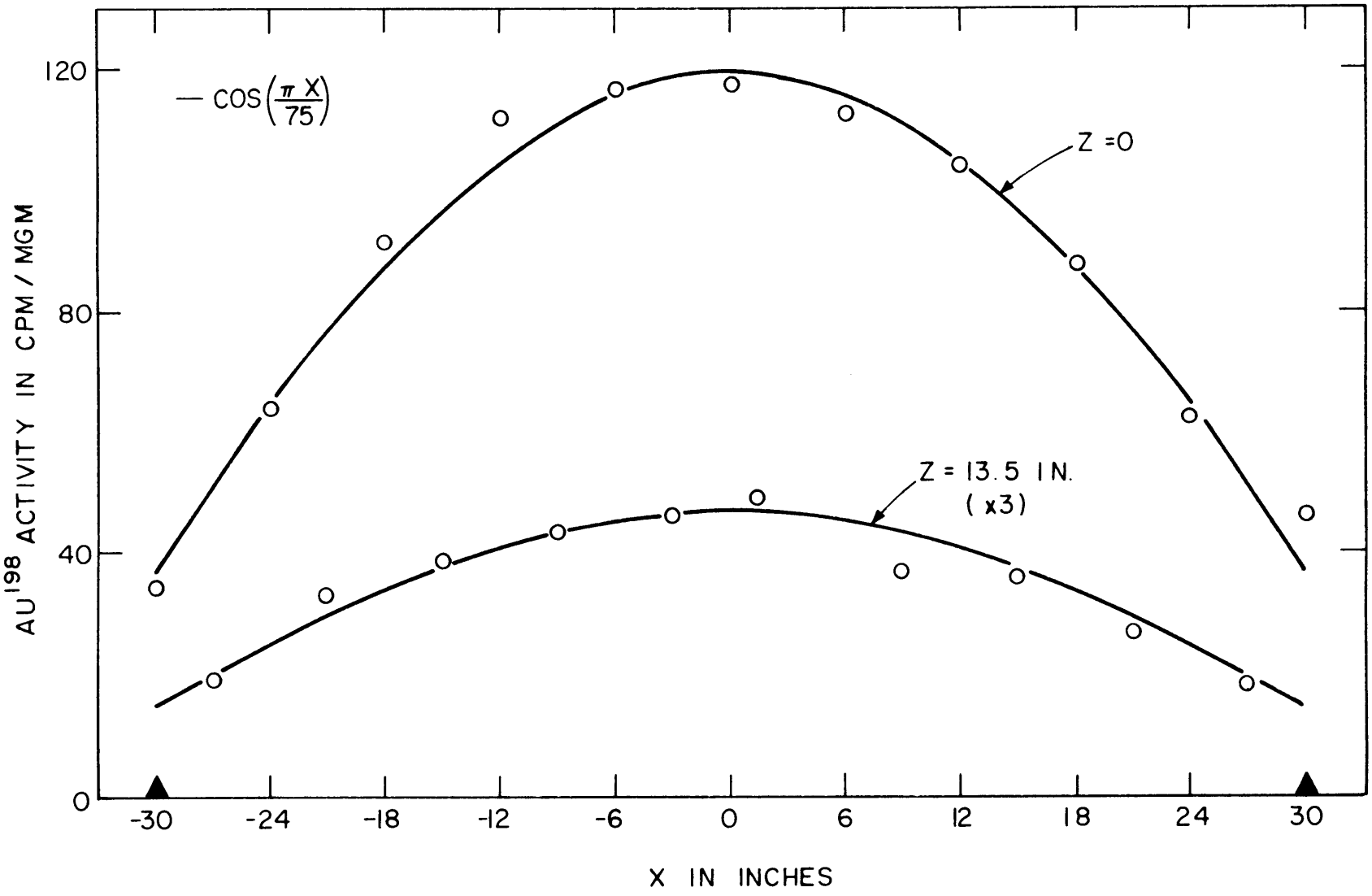

FIG. 4.5 GOLD HORIZONTAL ACTIVATION TRAVERSES IN BLANKET NO. 1

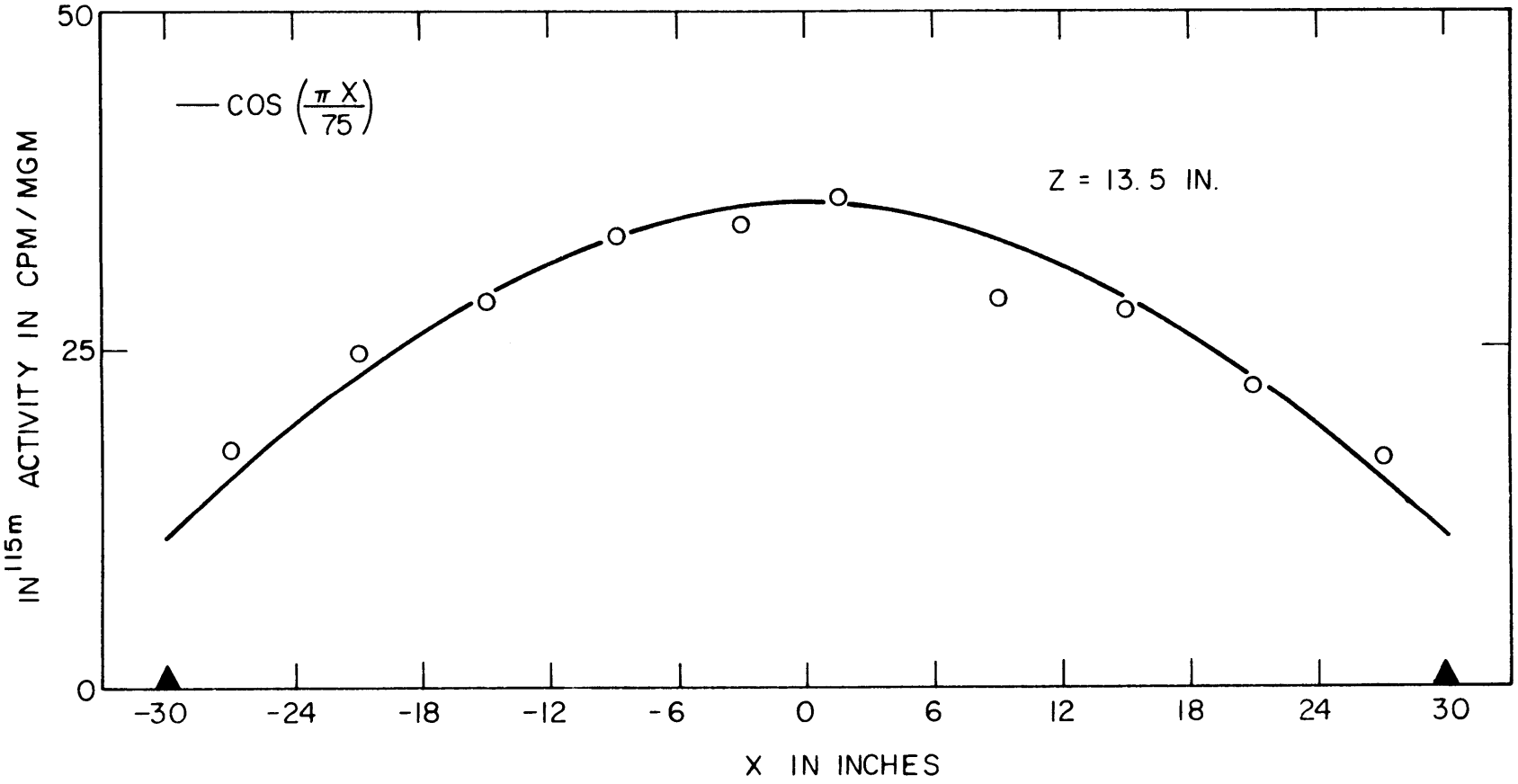

FIG. 4.6 INDIUM HORIZONTAL ACTIVATION TRAVERSE IN BLANKET NO. 1

Figure 4.7 shows the horizontal gold-to-indium activation ratio calculated from the horizontal gold and indium activation traverses at Z = 13.5 in. It is seen that the gold-to-indium activation ratio is constant from about X = -21 in. to about X = 18 in., indicating that horizontal spectral equilibrium is reached over a central region of the blanket about 3 ft wide.

4.4.5 Gold and Indium Vertical Activation Traverses in Blanket No. 1

Vertical (Y-direction) activation traverses were made with gold and indium foils at several distances into the blanket assembly to determine the vertical distribution of the neutron flux in the blanket. The vertical traverses were made 1.5 in. off the horizontal centerline (X = -1.5 in.).

Figures 4.8 and 4.9 show the vertical activation traverses for gold and indium, respectively (the standard deviation in the foil activities is smaller than the diameter of the points in the figures). It is seen from these figures that the gold and indium activation traverses are reasonably well approximated by the relation,

$$A(Y) = A(0) \cos\left(\frac{\pi Y}{63}\right),$$

where A is the gold or indium foil activity, and Y is in inches. The gold vertical activation traverse at Z = 1.5 in. shows the largest discrepancies between the measured activities and the fitted cosine curve, but again this may be due to nonuniform loading of the blanket subassembly.

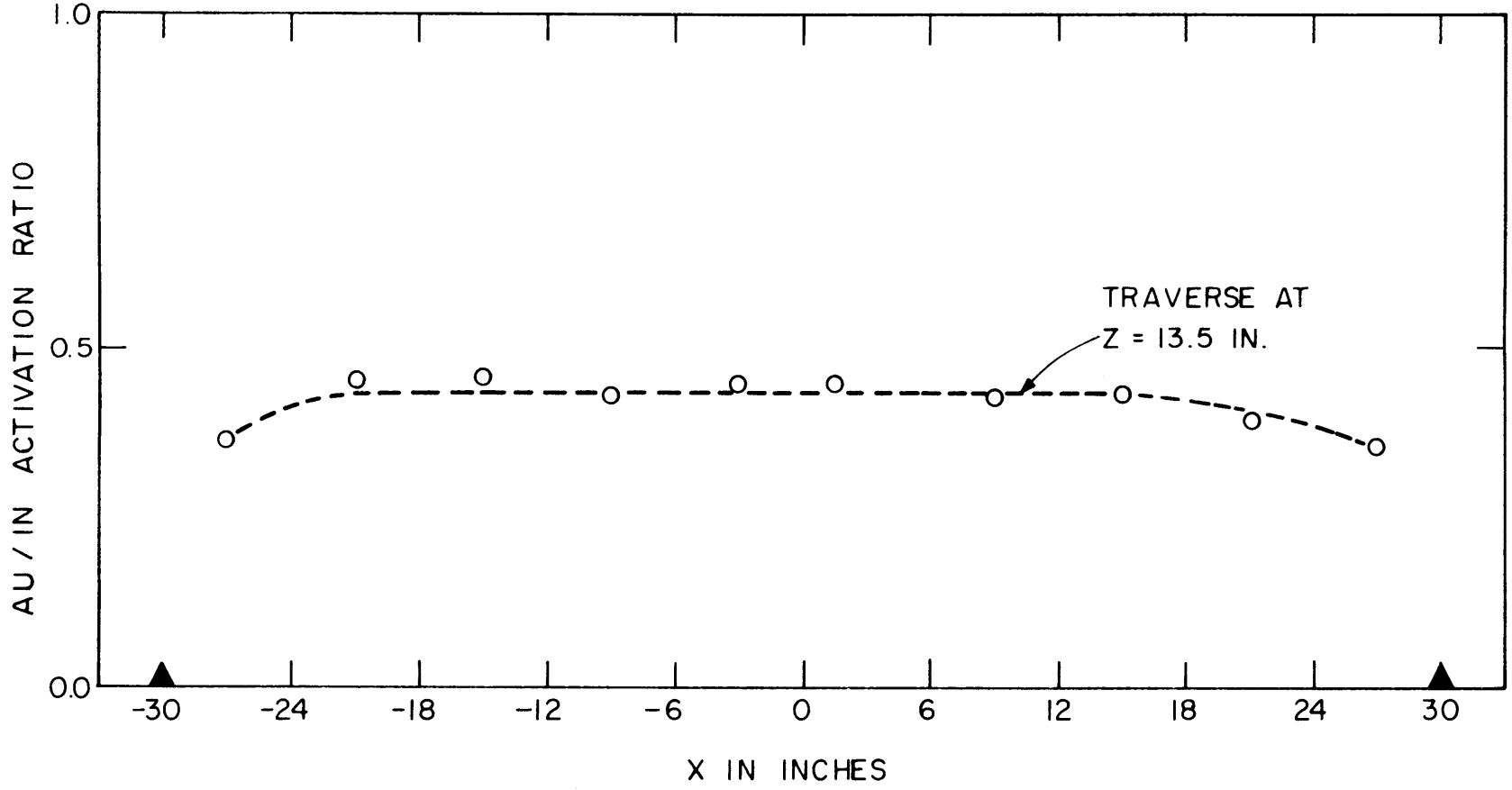

FIG. 4.7 GOLD TO INDIUM HORIZONTAL ACTIVATION RATIO IN BLANKET NO.1

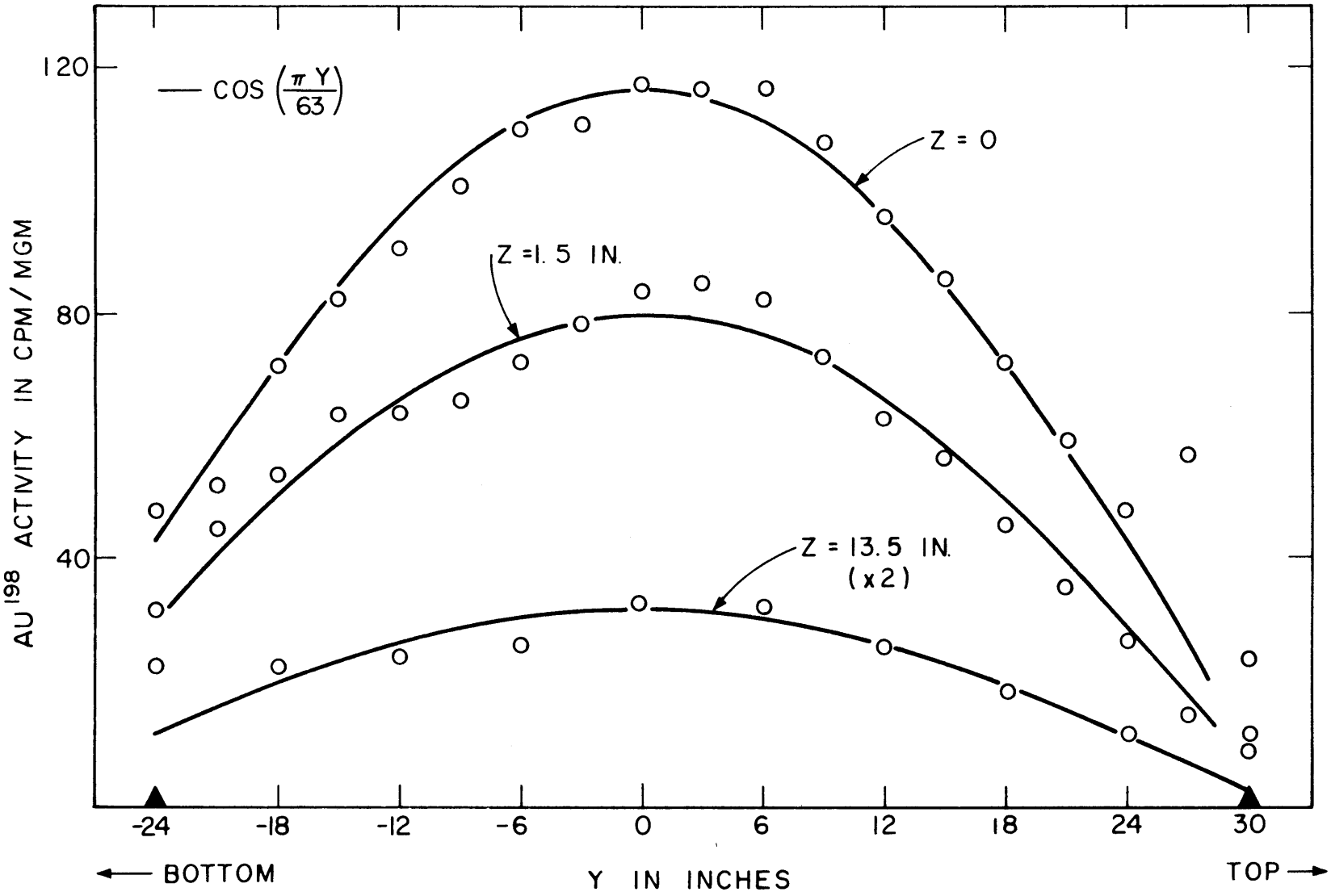

FIG. 4.8 GOLD VERTICAL ACTIVATION TRAVERSES IN BLANKET NO. 1

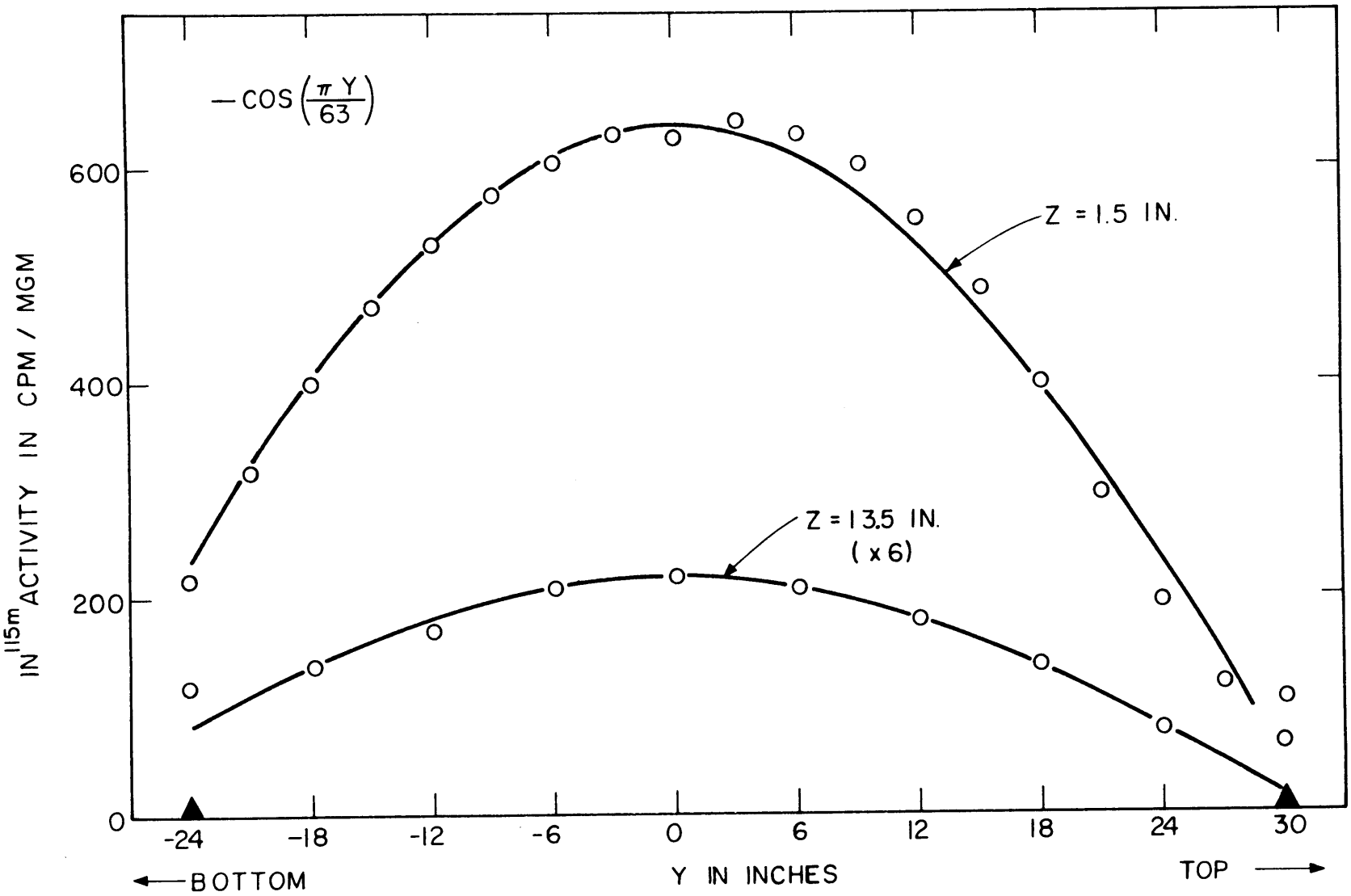

FIG. 4.9 INDIUM VERTICAL ACTIVATION TRAVERSES IN BLANKET NO. 1

Figure 4.10 shows the vertical gold-to-indium ratios calculated from the vertical gold and indium activation traverses at Z = 1.5 in. and Z = 13.5 in. It is seen that the gold-to-indium activation ratios are constant from about Y = -12 in. to about Y = 30 in., indicating that vertical spectral equilibrium is reached over a central region of the blanket about 3-1/2 ft in height. Below Y = -12 in., both gold-to-indium ratios increase appreciably; this result indicates a softening of the spectrum due to inscattering at the bottom of the blanket.

4.5 GOLD AND INDIUM AXIAL ACTIVATION TRAVERSES IN BLANKET NO. 1

4.5.1 The Experimental Measurements

Axial (Z-direction) activation traverses were made with both gold and indium foils through the center (X = -1.5 in., Y = 0) of the blanket assembly. The experimentally measured gold and indium axial activation traverses are shown in Figures 4.11 and 4.12, where they are compared with calculations made with the ANISN code.

4.5.2 The ANISN Calculations

The ANISN calculations (16-group, S_8 transport theory) of the gold and indium activation through the blanket were made using the final dimensions and compositions of the converter assembly and Blanket No. 1 (given in Appendices B and C). The 16-group cross section set used for the calculations was the same as that used for the multigroup calculations described in Chapter 2. Since 16-group activation cross sections for gold

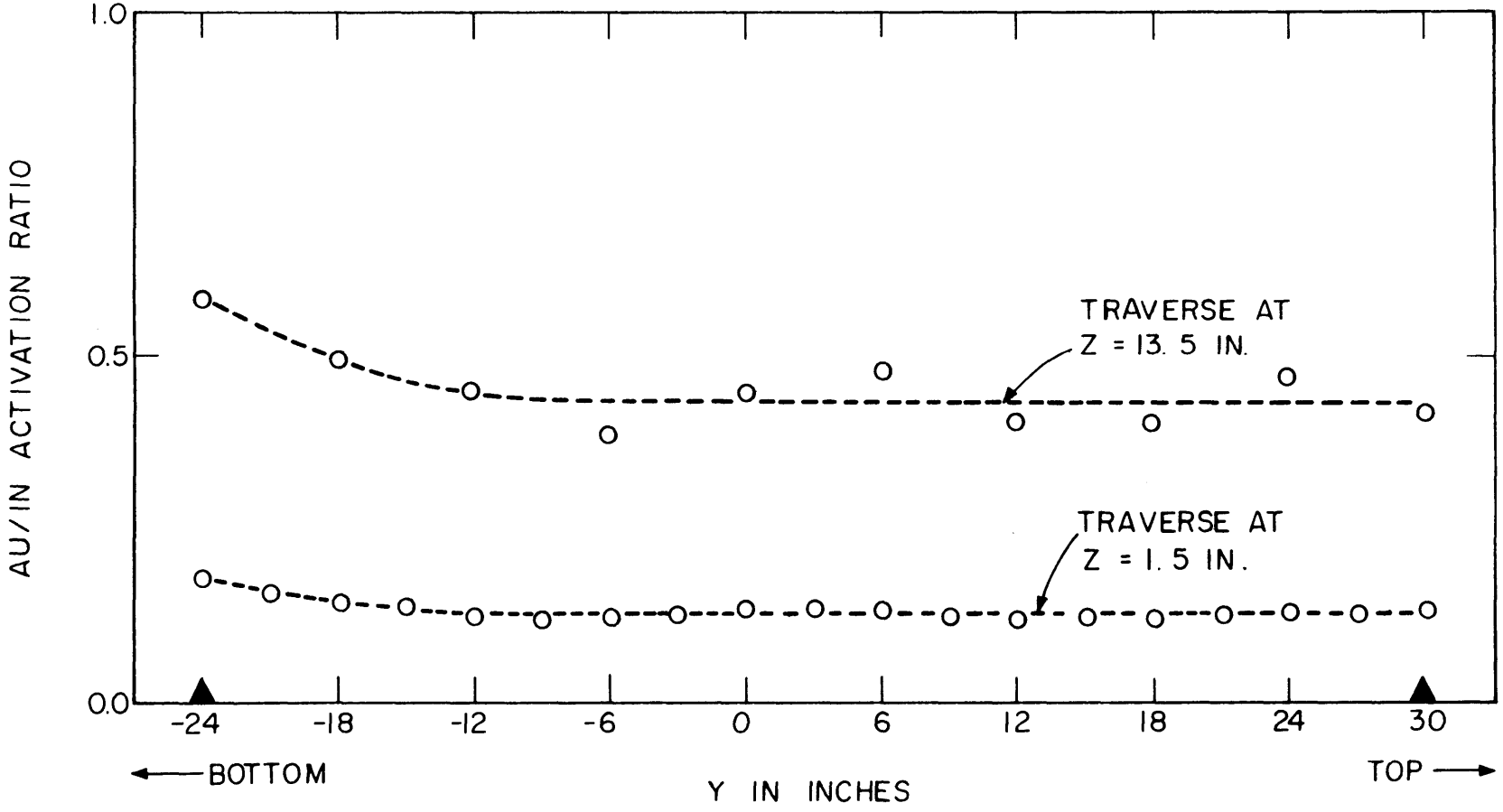

FIG. 4.10 VERTICAL GOLD TO INDIUM ACTIVATION RATIOS IN BLANKET NO. 1

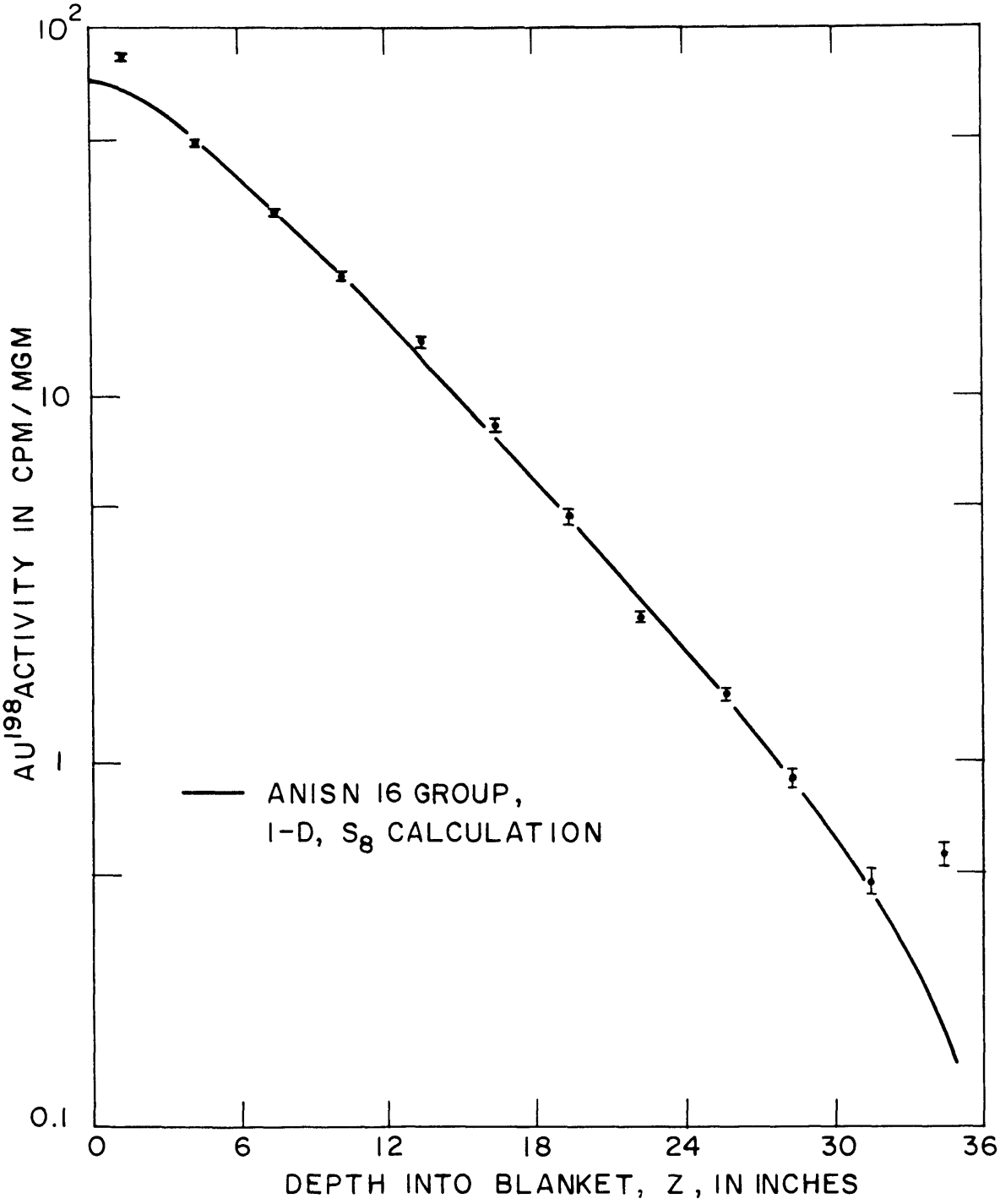

FIG. 4.11 GOLD AXIAL ACTIVATION TRAVERSE IN BLANKET NO. 1

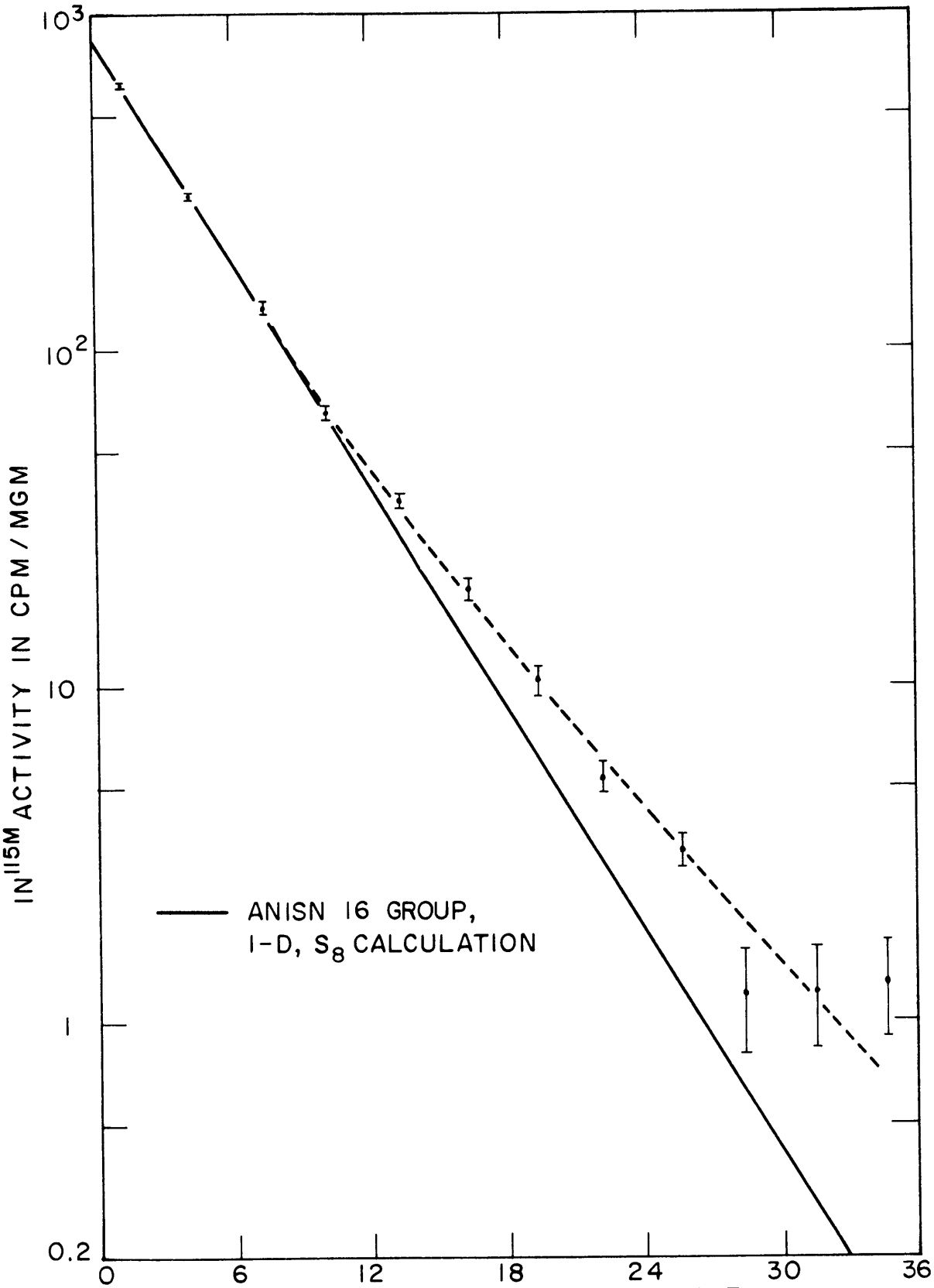

FIG. 4.12 INDIUM AXIAL ACTIVATION TRAVERSE IN BLANKET NO. 1

and indium were not included in this set, they were obtained by collapsing the 620 group activation cross sections of the SAND-II library[32] over a typical LMFBR core asymptotic spectrum. The 16 group activation cross sections for the $Au^{197}(n, \gamma)Au^{198}$ and $In^{115}(n, n')In^{115m}$ reactions are given in Table 4.2.

TABLE 4.2

16 Group Activation Cross Sections for Gold and Indium

Group	E_L	Activation Cross Section, barns	
		$Au^{197}(n, \gamma)Au^{198}$	$In^{115}(n, n')In^{115m}$
1	3.5 Mev	0.0215	0.341
2	1.4 "	0.0586	0.275
3	0.9 "	0.0974	0.0960
4	0.4 "	0.141	0.0161
5	100 kev	0.287	0.000319
6	17 "	0.630	0.0
7	3 "	1.59	0.0
8	0.55 "	6.02	0.0
9	100 ev	11.8	0.0
10	30 "	23.2	0.0
11	10 "	7.02	0.0
12	3 "	700	0.0
13	1 "	35.4	0.0
14	0.4 "	23.8	0.0
15	0.1 "	43.2	0.0
16	thermal	92.3	0.0

Since ANISN is a one-dimensional code, lateral neutron leakage from the converter and blanket assemblies was taken into account by means of a lateral buckling factor. For the calculations shown in Figures 4.11 and 4.12, the lateral buckling was calculated from the experimentally determined values of the effective height and width of the neutron flux distribution in the blanket,

$$H = 63 \text{ in.} = 160 \text{ cm},$$

and $$A = 75 \text{ in.} = 190 \text{ cm},$$

so that $$B^2 = \left(\frac{\pi}{H}\right)^2 + \left(\frac{\pi}{A}\right)^2 = 0.000660 \text{ cm}^{-2}.$$

However, it was found that if the lateral buckling was calculated instead from the theoretical extrapolated height and width of the blanket assembly (145 cm and 160 cm, respectively, from which $B^2 = 0.000890 \text{ cm}^{-2}$), the calculated values of the gold and indium activation through the blanket were not appreciably affected. In fact, the deviation between the values calculated for gold or indium by the two methods increased from zero at the inner edge of the blanket (Z = 0) to only 5% at the outer edge of the blanket (Z = 36 in.); this variation is smaller than the uncertainty in the experimental measurements, particularly at deep penetrations.

4.5.3 Comparison of Experiment and Calculations

From Figure 4.11 it is seen that the experimentally measured gold activity in the axial direction through the blanket compares extremely well with the calculated activity, except at the first (Z = 1.5 in.) and last (Z = 34.5 in.) data points. The deviation at Z = 34.5 in. is due to

inscattering at the back of the blanket assembly.

From Figure 4.12 it is seen that the experimentally measured indium activity in the axial direction through the blanket compares extremely well with the calculated activity through the first 12 in. of the blanket. Beyond Z = 12 in., the experimental values and the ANISN calculation diverge progressively. It is possible that the discrepancy at deep penetrations may have resulted from a contribution from residual In^{116} activity in the indium foils during counting (see Section 4.3.2), although efforts were made to prevent this in the counting procedure. This possibility is suggested by the fact that the indium activity at deep penetrations parallels the gold activity; in other words, the indium activity simulates that of a nonthreshold type (n, γ) reaction at deep penetrations.

4.6 SUMMARY

The experimental measurements described above show that the Blanket Test Facility operates safely and that the desired spatial and energy dependence of the neutron flux in the converter and blanket assemblies is obtained.

Gamma and fast neutron dose measurements indicate that the biological shielding attenuates gamma-ray and fast neutron fluxes to values below the design requirements. The fuel temperature rise in the converter assembly fuel rods during irradiation has been found to be negligible; this permits operation of the facility without continuous monitoring. Measurements of the irradiation region gamma dose and residual activation of the converter and blanket assemblies following

irradiation periods of up to 4 hours show that gamma doses are low enough to permit safe handling of the experimental assemblies after a 4 to 6 hour cooling period.

The horizontal and vertical activation traverses with gold and indium foils at the converter-blanket interface and through the blanket assembly itself show that both the horizontal and vertical spatial distributions of the neutron flux in the blanket assembly have the desired cosine dependence; furthermore, these cosine distributions have constant width and height through the thickness of the blanket. Hence the neutron flux in the blanket assembly can be described by the relation,

$$\phi(X, Y, Z, E) = \cos\left(\frac{\pi X}{75}\right) \cos\left(\frac{\pi Y}{63}\right) \phi(Z, E) ,$$

and lateral leakage from the assembly can be accounted for with a constant buckling factor in numerical calculations. It has been shown that only a small amount of neutron streaming occurs around the blanket, that backscattering into the blanket from the surrounding concrete shielding is also small, and that lateral spectral equilibrium is attained in a large (approximately 3 ft square) central region of the blanket assembly.

The gold axial activation traverse through the blanket shows remarkably good agreement with ANISN calculations, even at distances of up to 31.5 in. into the blanket assembly. The indium axial activation traverse and the ANISN calculations show excellent agreement through the first 12 in. of the blanket, but diverge progressively at deeper penetrations. Irradiation periods of less than 4 hours have been sufficient

to provide adequate foil activity.

In short, it is concluded that the facility is ready in all respects for its intended use – the experimental investigation of LMFBR blankets.

Chapter 5

CONCLUSIONS AND DISCUSSION OF FUTURE WORK

5.1 CONCLUSIONS

The work presented in this report has shown that a facility can be constructed to conduct experimental studies of the breeding blanket region of an LMFBR independently of the plutonium-fueled core region, using a uranium-loaded converter assembly to generate a fast neutron driving flux for a simulated blanket assembly. Apart from the low cost and inherent safety, this type of facility has certain important advantages over a critical facility. First, it requires only about one-tenth of the volume of blanket material needed for full-scale cylindrical critical mockup; second, at full-power operation (about 55 watts) the converter is capable of generating blanket region fluxes equivalent to those in a critical assembly operating at the relatively high power of 350 watts.

Analytical calculations, described in Chapter 2, showed that the spatial distribution of the neutron flux in the blanket assembly would closely simulate that in the radial blanket of a large LMFBR if the effective height and width of the blanket assembly were correctly chosen. Numerical multigroup calculations with the ANISN, AIM-6 and TWENTY GRAND codes showed that a converter assembly composed of a 20-cm-thick graphite external moderator region and a 16.5-cm-thick fuel region would generate a fast neutron leakage spectrum which

closely approximated the leakage spectrum from an LMFBR core. It was found that the converter leakage spectrum could be varied to achieve a wide variety of energy distributions by changing the thicknesses of the graphite moderator and fuel regions. This suggested great flexibility in the converter concept, and the converter assembly was subsequently designed and built so as to permit changes in the graphite and UO_2 fuel loadings to be made easily.

Two-dimensional multigroup calculations made with the TWENTY GRAND code showed that backscattering from concrete shielding should perturb the blanket spectrum only in the outer 20 cm to 30 cm of the blanket assembly. The TWENTY GRAND calculations also indicated that the lateral shape of the fast neutron flux in the blanket assembly should be determined predominantly by the lateral shape of the thermal source flux incident upon the converter fuel.

From a study of various blanket compositions it was found that a mixture of 50 v/o iron and 50 v/o anhydrous borax could provide neutron spectra and spatial flux shapes reasonably similar to those in real blanket assemblies. For reduced cost and ease of construction, this composition was specified for the first blanket assembly (B.T.F. Blanket No. 1), which was used to test the completed facility, while the more protracted construction of a realistic blanket assembly (B.T.F. Blanket No. 2) was still underway.

Details of the design and construction of the Blanket Test Facility were discussed in Chapter 3. Principal features of the facility are a shielded irradiation region, located at the rear of the graphite-lined hohlraum of the MIT Reactor, and three experimental carts carrying

the converter and blanket assemblies and a graphite wall assembly. The carts are mounted on a rail system which allows the assemblies to be rolled from the reactor floor into the irradiation region. The graphite wall assembly was provided to replace the converter assembly at the front of the irradiation region and restore the reflective properties of the hohlraum during the operation of other experiments utilizing the hohlraum thermal flux.

The completed facility has proven flexible and easy to operate. Removal or replacement of the shield doors and the experimental assemblies requires careful manipulation, particularly with the overhead crane, because of the size and weight of the equipment involved. However, retrieval of foil irradiation packages from the blanket assembly or a changeover from fast operation to thermal operation (and vice versa) can be accomplished in the relatively short time of one to two hours. Radiation dose levels during full-power operation of the facility are low, and the temperature rise of the converter assembly fuel has been found to be negligible ($< 1°$ C); this obviates the necessity for continuous monitoring of the facility during operation. The residual activation of the experimental assemblies after irradiation periods of up to 4 hours is low enough to permit the assemblies to be removed from the irradiation region after 4 to 6 hours cooling.

The results of the horizontal and vertical activation traverses with gold and indium foils (reported in Chapter 4) showed that both the horizontal and vertical spatial distributions of the neutron flux in the blanket assembly have the desired cosine dependence. Hence, lateral leakage from the blanket can be taken into account by means of a

constant buckling factor in numerical calculations. The effective height of the vertical cosine distribution was found to be 160 cm, and the effective width of the horizontal cosine distribution was found to be 190 cm, yielding a total lateral buckling of 0.000660 cm^{-2}. From the analytical methods developed in Section 2.2, it can be shown that this lateral buckling yields an axial spatial flux distribution in the blanket assembly equivalent to the radial spatial flux distribution in the radial blanket of an LMFBR having core volume of 7100 liters (that is, an equivalent core height of 117 cm, given by the 160 cm effective height minus 2 × 21.5 cm axial reflector savings, and an equivalent core radius of 139 cm, given by Eq. 2.14 for A = 190 cm and z = 22.5 cm). However, calculations with the ANISN code showed that an increase in the lateral buckling to 0.000890 cm^{-2} (equivalent to an LMFBR core volume of about 3200 liters) had no significant effect on the axial distribution of gold and indium activities. In other words, for large, low-leakage systems, the spatial distribution of the blanket flux is not sensitive to core radius. The horizontal and vertical gold-to-indium activation ratios indicated that lateral spectral equilibrium was attained in a large central volume of the blanket assembly. The ratios showed that backscattering perturbed the blanket spectrum in no more than the outer 30 cm of the blanket assembly, or to about the same extent as predicted by the TWENTY GRAND calculation.

Axial activation traverses with gold and indium foils showed that the fast source flux generated by the converter is sufficient to provide adequate foil activity through the entire 3-ft thickness of Blanket No. 1, after irradiation periods of less than 4 hours. This means that deep

penetration measurements can be made in the reflector region of the reflected blanket assembly (B.T.F. Blanket No. 2) which will be used in subsequent experiments with the Blanket Test Facility. Good agreement was obtained between the measured axial activities of gold and indium and ANISN calculations; this provides additional confidence in the calculations performed to optimize the converter assembly design. The progressively increasing discrepancy between the measured and calculated indium axial activity beyond about Z = 12 in. may possibly be due to a contribution from a small amount of residual In^{116} activity in the foils during counting. Work will be carried out on Blanket No. 2 with both indium and other threshold foils to investigate whether this discrepancy is a real one.

In conclusion, it has been shown both theoretically and experimentally that the Blanket Test Facility can reproduce the energy and spatial distributions of the neutron flux in a typical LMFBR blanket, and that the completed facility is ready for the planned experimental program of LMFBR blanket research.

5.2 FUTURE WORK

While evaluation of the completed facility with B.T.F. Blanket No. 1 was being carried out, construction of the second blanket assembly was proceeding concurrently and is now nearing completion. B.T.F. Blanket No. 2 [33] is an accurate mockup of a real LMFBR blanket composition. Subassembly boxes of low-carbon steel rectangular mechanical tubing (similar to those used in Blanket No. 1) will be loaded with 121 uranium metal fuel rods arranged on a square lattice

spacing of 0.51 in.; the 0.25-in.-diameter uranium metal fuel is clad in low-carbon steel tubing. The inter-rod volume in each subassembly will be filled with anhydrous sodium chromate (Na_2CrO_4) powder. In its initial configuration, Blanket No. 2 will be 18 in. thick with an 18-in.-thick iron (carbon steel) reflector. The estimated homogenized atom densities for Blanket No. 2 are given in Table 5.1, where they are compared with those in a typical LMFBR blanket (composed of 40 v/o sodium, 40 v/o depleted UO_2 and 20 v/o stainless steel) and with those in the radial and axial blankets of the ZPPR assembly planned for the AEC's Demonstration Reactor Benchmark Program.[36]

Experimental measurements to be made on Blanket No. 2 will include activation traverses through the blanket and reflector with depleted and enriched uranium and plutonium foils (to measure U^{238} capture and fission, U^{235} fission and Pu^{239} fission) and selected other foils, such as gold and indium. An attempt will be made to use prompt capture gamma spectroscopy to perform a neutron balance inside the blanket assembly. Measurements of the differential neutron spectrum will be made at various distances into the blanket assembly with a proton recoil spectrometer, using methods similar to those developed by E. F. Bennett[34, 35] at ANL. The differential neutron spectrum in the blanket assembly will also be determined by unravelling the incident neutron spectrum from the component gamma activities induced in a mixed-powder foil, and also, possibly, by measuring the recoil doppler broadening of the hydrogen capture gamma peak. A heterogeneity experiment involving the measurement of U^{238} capture and fission rates inside a blanket fuel rod is to be performed early in the test program for Blanket No. 2.

TABLE 5.1

Comparison of Blanket Atom Densities

Isotope	B.T.F. Blanket No. 2	Typical LMFBR Radial Blanket*	ZPPR Benchmark Demonstration Reactor	
			Radial Blanket	Axial Blanket
U^{235}	0.000093	0.000018	0.000026	0.000016
U^{238}	0.008407	0.0089	0.01099	0.00708
H	0.000071**	---	---	---
O	0.01575	0.0178	0.01993	0.0141
C	0.000712	---	0.0009955	---
Na	0.00788	0.0102	0.00589	0.008899
Fe	0.01042	0.0126	0.00778	0.00967
Cr	0.00394	0.0030	0.00230	0.002290
Ni	---	0.0014	0.00091	0.000913

* Composed of 40 v/o sodium, 40 v/o depleted UO_2 and 20 v/o stainless steel.

** Assuming 0.1 w/o H_2O in Na_2CrO_4 powder.

It is later planned to investigate the effects of varying the thickness of the blanket region and of varying the thickness or composition of the reflector region. A combined experimental and theoretical study of blanket-reflector interactions is planned, including the effects of external or even internal moderation with materials such as graphite. In fact, replacement of the 18-in. iron reflector by graphite is under consideration for Blanket No. 3. An economic analysis is being made to determine the most probable evolutionary trends in LMFBR blanket design so as to provide a rational basis for the selection of these future experimental configurations. All of this work is being carried out under USAEC Contract AT(30-1)4105.

It is intended that the program of experimental and theoretical research planned for the Blanket Test Facility will achieve the long-range goal of providing the information required for the optimization of LMFBR breeding blanket design.

Appendix A

THE SIX-GROUP CROSS SECTION SET

The six-group fast-thermal cross section set used for calculations with the TWENTY GRAND code was adapted from a five-group set by I. P. Moorhead,[13] with the addition of a thermal group. Table A.1 gives the group lower energy boundaries, and Table A.2 is a listing of the group cross sections.

TABLE A.1

Group Lower Energy Boundaries for the Six-Group Cross Section Set

Group	E_L	x
1	1.35 Mev	0.574
2	0.3 Mev	0.360
3	67 kev	0.058
4	9.1 kev	0.008
5	0.4 ev	0.0
6	thermal	0.0

TABLE A.2

Six-Group Microscopic Cross Sections

Material	Group	σ_{tr}	σ_c	σ_f	ν	$\sigma_{i\to i+1}$	$\sigma_{i\to i+2}$	$\sigma_{i\to i+3}$
U^{235}	1	4.50	0.100	1.29	2.70	1.45	0.215	0.0
	2	5.44	0.153	1.24	2.53	0.541	0.066	0.0018
	3	9.21	0.342	1.62	2.48	0.076	0.0018	0.0
	4	12.70	0.884	2.73	2.47	0.029	0.0	—
	5	14.30	2.520	6.00	2.47	0.008	—	—
	6	704	112	582	2.47	—	—	—
U^{238}	1	4.59	0.041	0.513	2.60	1.81	0.361	0.0
	2	5.78	0.135	0.0007	2.48	0.310	0.0	0.0
	3	9.38	0.211	0.0	—	0.168	0.0	0.0
	4	12.70	0.481	0.0	—	0.054	0.0	—
	5	14.30	0.800	0.0	—	0.008	—	—
	6	11.03	2.73	0.0	—	—	—	—
Pu^{239}	1	4.60	0.061	1.97	3.13	0.814	0.126	0.0
	2	6.14	0.135	1.76	2.97	0.330	0.038	0.001
	3	9.42	0.392	1.73	2.92	0.061	0.001	0.0
	4	13.62	0.863	2.10	2.91	0.043	0.0	—
	5	16.80	2.100	3.50	2.91	0.007	—	—
	6	1036	280	746	2.90	—	—	—
Pu^{240}	1	4.60	0.053	1.54	2.60	1.13	0.224	0.0
	2	6.16	0.195	0.644	2.47	0.271	0.0	0.0
	3	9.42	0.307	0.011	2.47	0.124	0.0	0.0

(continued)

TABLE A.2 (continued)

Material	Group	σ_{tr}	σ_c	σ_f	ν	$\sigma_{i\to i+1}$	$\sigma_{i\to i+2}$	$\sigma_{i\to i+3}$
Pu^{240}	4	13.62	0.816	0.0	–	0.050	0.0	–
	5	16.80	1.50	0.0	–	0.007	–	–
	6	304.6	295	0.0	–	–	–	–
C	1	1.60	0.0	–	–	0.284	0.0	0.0
	2	2.82	0.0	–	–	0.417	0.0	0.0
	3	3.96	0.0	–	–	0.389	0.0	0.0
	4	4.29	0.0	–	–	0.268	0.0	–
	5	4.33	0.0	–	–	0.080	–	–
	6	4.53	0.0	–	–	–	–	–
O	1	2.08	0.0	–	–	0.307	0.0	0.0
	2	3.73	0.012	–	–	0.370	0.0	0.0
	3	3.35	0.0	–	–	0.192	0.0	0.0
	4	3.35	0.0	–	–	0.149	0.0	–
	5	3.60	0.0	–	–	0.045	–	–
	6	4.02	0.0002	–	–	–	–	–
Na	1	2.19	0.0003	–	–	0.412	0.020	0.0
	2	3.26	0.0007	–	–	0.316	0.026	0.0
	3	3.47	0.001	–	–	0.165	0.0	0.0
	4	4.90	0.002	–	–	0.162	0.0	–
	5	10.0	0.005	–	–	0.022	–	–
	6	4.39	0.505	–	–	–	–	–

(continued)

TABLE A.2 (concluded)

Material	Group	σ_{tr}	σ_c	σ_f	ν	$\sigma_{i\rightarrow i+1}$	$\sigma_{i\rightarrow i+2}$	$\sigma_{i\rightarrow i+3}$
Al	1	1.64	0.0004	—	—	0.393	0.034	0.0
	2	2.75	0.0010	—	—	0.194	0.0	0.0
	3	4.78	0.0030	—	—	0.172	0.0	0.0
	4	3.76	0.0086	—	—	0.056	0.0	—
	5	1.60	0.012	—	—	0.008	—	—
	6	1.585	0.230	—	—	—	—	—
Fe	1	2.02	0.0050	—	—	0.641	0.093	0.0
	2	3.37	0.0054	—	—	0.133	0.008	0.0
	3	4.18	0.0076	—	—	0.111	0.0	0.0
	4	5.35	0.020	—	—	0.055	0.0	—
	5	8.00	0.014	—	—	0.033	—	—
	6	13.4	2.53	—	—	—	—	—
H_2O	1	3.08	0.012	—	—	2.24	0.58	0.019
	2	6.59	0.0	—	—	5.15	1.54	0.04
	3	9.75	0.0	—	—	10.11	0.30	0.0
	4	14.51	0.0	—	—	7.89	0.0	—
	5	16.55	0.035	—	—	4.14	—	—
	6	68.60	0.57	—	—	—	—	—

Appendix B

DIMENSIONS AND COMPOSITION OF THE CONVERTER ASSEMBLY

The converter assembly consists of an 8-in.-thick graphite external moderator region, a 6.865-in.-thick fuel region containing 1/2-in.-diameter aluminum-clad UO_2 fuel rods in a close-packed triangular pitch array, 0.510 in. on center, and a 1/8-in. boral sheet backing. The UO_2 fuel pellets have a diameter of 0.430 in. and a density of 10.20 gm/cm^3; the 0.500-in.-O.D., Type 1100 aluminum clad is 0.032 in. thick. The UO_2 fuel rods have U^{235} enrichments of 1.99% and 1.0999%, and are separated into two enrichment regions with the higher enrichment region at the front (closer to the graphite), to provide higher thermal-to-fast conversion.

Table B.1 gives the dimensions of the converter assembly and Table B.2 gives the homogenized atom densities for the four regions. To properly account for the lower fuel density at the graphite-fuel region interface (see Figure B.1), the atom densities in the first 0.265 in. of the first fuel region should be reduced by 16%.

TABLE B.1

Dimensions of the Converter Assembly

Active Fuel Height	48.0 in.
Active Fuel Width	60.0 in.
Graphite Region Thickness	8.00 in.
First Fuel Region Thickness	3.150 in.
Second Fuel Region Thickness	3.715 in.
Boral Sheet Thickness	0.125 in.

TABLE B.2

Converter Assembly Atom Densities

Material	Atom Density – $cm^{-3} \times 10^{-24}$			
	Graphite Region	First Fuel Region	Second Fuel Region	Boral Sheet
U^{235}	–	0.000286	0.000158	–
U^{238}	–	0.013952	0.014080	–
B	–	–	–	0.026239
C	0.083110	–	–	0.006560
O	–	0.028477	0.028477	–
Al	–	0.012221	0.012221	0.044263

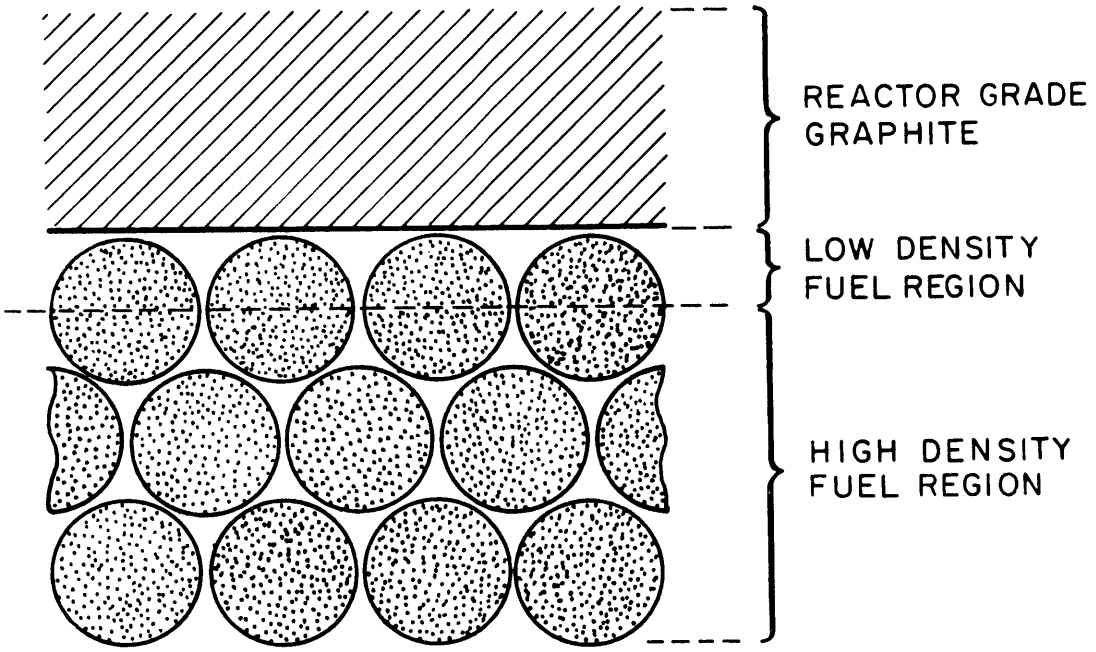

FIG. B.1 SCHEMATIC DIAGRAM OF THE CONVERTER ASSEMBLY GRAPHITE-FUEL REGION INTERFACE.

Appendix C

DIMENSIONS AND COMPOSITION OF B.T.F. BLANKET NO. 1

B.T.F. Blanket No. 1 contains approximately 50 v/o low-carbon steel and 50 v/o anhydrous borax ($Na_2B_4O_7$), has an average height of 55.4 in., a width of 60.75 in. and is 36.5 in. thick. Loaded densities are 3.490 gm/cm^3 of low-carbon steel (in the form of punchings approximately 1/8 in. thick and from 1/4 in. to 1 in. in diameter) and 0.6149 gm/cm^3 of anhydrous borax powder. Table C.1 gives the atom densities for Blanket No. 1; corrections have been made for the 0.86 w/o water content of the borax and for the phenol (C_6H_5OH) content of the red lead coating on the blanket subassemblies (0.35 v/o).

TABLE C.1

Blanket No. 1 Atom Densities

Material	Atom Density, $cm^{-3} \times 10^{-24}$
H	0.000488
B	0.007370
C	0.000197
O	0.013098
Na	0.003685
Fe	0.037634

Appendix D

SHIELDING CALCULATIONS

D.1 INTRODUCTION

The Blanket Test Facility is shielded by 4 ft of heavy concrete (magnetite concrete with a density of 240 lbs/ft^3) designed to reduce the fast neutron dose to less than 1 n/cm^2-s and the gamma dose to less than 1 mr/hr outside the shielding under the most severe operating conditions. For thermal operation the most severe operating condition is to have only the graphite cart in the B.T.F. irradiation cave, while for fast operation the most severe condition is to have only the converter cart (operating at full power) in the irradiation cave.

Calculations to predict the fast neutron and gamma doses outside the shielding followed the methods used in references 37 and 38; the data used were taken principally from reference 38.

For the gamma shielding calculations only two sources of gamma radiation were considered; these were the 5-Mev graphite capture gammas produced in the MITR thermal column and the graphite-lined hohlraum. Dose rates due to MITR core and converter plate fission gammas were found to be negligible compared to those due to the thermal column and hohlraum capture gammas. The only fast neutron source considered was that produced by the converter plate operating at full power.

D.2 GAMMA SHIELDING CALCULATIONS

The equivalent point sources of 5-Mev graphite capture gammas were calculated from the relations

$$S_o = A\phi_{\gamma i}/F, \tag{D.1}$$

where

$$\phi_{\gamma i} = \phi_\gamma/(B e^{-\mu_\gamma t}), \tag{D.2}$$

and

$$\phi_\gamma = -\frac{\mu_n \phi_o}{2(\mu_\gamma - \mu_n)} (e^{-\mu_n t} - e^{-\mu_\gamma t}). \tag{D.3}$$

In the above expressions, A is the area of the graphite, t is the thickness of the graphite, F is a geometry factor, B is the gamma buildup factor, μ_γ and μ_n are the gamma and neutron reciprocal relaxation lengths, respectively, and ϕ_o is the neutron flux incident on the graphite. Assuming ϕ_o to be 1×10^{13} n/cm^2-s for the thermal column and 5×10^9 n/cm^2-s for the hohlraum (at a reactor power level of 5 Mw), the calculated gamma source intensities are

$$S_{o_1} = 7.2 \times 10^{16} \ \gamma\text{'s/s in the thermal column,}$$

and

$$S_{o_2} = 1.1 \times 10^{14} \ \gamma\text{'s/s in the hohlraum.}$$

The gamma doses are then calculated from the relation

$$\phi_\gamma = \frac{S_o}{4\pi R^2} \sum_i B_i \, e^{-\sum_i x_i/d_i}, \tag{D.4}$$

where B_i is the buildup factor, x_i is the shielding thickness and d_i is the shielding decade length for 5-Mev gammas. Table D.1 summarizes

the calculations for thermal operation of the facility, while Table D.2 summarizes the calculations for fast operation. The total gamma dose outside the concrete shielding is estimated to be 0.54 mr/hr for thermal operation and 0.024 mr/hr for fast operation.

TABLE D.1

Gamma Dose Calculations for Thermal Operation

(a) Thermal Column Gamma Dose

Material	x_i, ft	d_i, ft	x_i/d_i	B_i
Graphite	5.33	1.66	3.21	4.5
Concrete	4.00	0.623	6.42	12.8
Sum			9.63	17.5

$1/4\ \pi R^2 = 1.35 \times 10^{-7}\ cm^{-2}$

$\phi_{\gamma_1} = 40\ \gamma's/cm^2\text{-}s \equiv 0.22\ mr/hr$

(b) Hohlraum Gamma Dose

Material	x_i, ft	d_i, ft	x_i/d_i	B_i
Graphite	1.67	1.66	1.00	2.5
Concrete	4.00	0.623	6.42	12.8
Sum			7.42	15.5

$1/4\ \pi R^2 = 8.96 \times 10^{-7}\ cm^{-2}$

$\phi_{\gamma_2} = 58\ \gamma's/cm^2\text{-}s \equiv 0.32\ mr/hr$

TABLE D.2

Gamma Dose Calculations for Fast Operation

(a) Thermal Column Gamma Dose

Material	x_i, ft	d_i, ft	x_i/d_i	B_i
Graphite	4.27	1.66	2.67	4.1
UO_2 Fuel	0.54	0.27	2.00	3.1
Concrete	4.00	0.623	6.42	12.8
Sum			11.09	20.0

$1/4\ \pi R^2 = 1.35 \times 10^{-7}\ cm^{-2}$

$\phi_{\gamma_1} = 1.6\ \gamma's/cm^2\text{-}s \equiv 0.009\ mr/hr$

(b) Hohlraum Gamma Dose

Material	x_i, ft	d_i, ft	x_i/d_i	B_i
Graphite	0.67	1.66	0.40	2.2
UO_2 Fuel	0.54	0.27	2.00	3.1
Concrete	4.00	0.623	6.42	12.8
Sum			8.82	18.1

$1/4\ \pi R^2 = 8.96 \times 10^{-7}\ cm^{-2}$

$\phi_{\gamma_2} = 2.7\ \gamma's\ /cm^2\text{-}s \equiv 0.015\ mr/hr$

D.3 FAST NEUTRON SHIELDING CALCULATIONS

The fast neutron source generated by 55-watt operation of the converter plate is

$$S_n = 4.4 \times 10^{12} \text{ neutrons/s}.$$

The fast neutron flux is calculated from the expression

$$\phi_n = \frac{C\, S_n}{4\pi R^2} \cdot 10^{-x/d}, \qquad \text{(D.5)}$$

where C is the converter self-absorption factor (0.27), x is the shielding thickness (4 ft) and d is the fast neutron decade length (0.603 ft). From Eq. D.5, the fast neutron dose outside the converter is estimated to be 0.24 n/cm^2-s (fast operation only).

D.4 SUMMARY

The gamma dose rates (0.54 mr/hr for thermal operation and 0.024 mr/hr for fast operation) and fast neutron dose rate (0.24 n/cm^2-s for fast operation only) calculated above show that the desired shielding criteria can be met, even under the most severe operating conditions. Since the converter cart is usually stored behind the graphite cart during thermal operation, and the blanket assembly is usually positioned behind the converter cart during fast operation, the dose rates will be considerably less under most operating conditions.

Appendix E

REFERENCES

1. "Proceedings of the International Conference on Fast Reactors (Critical Experiments)," ANL-7320 (October, 1966).

2. "Reactor Physics Efforts Required in Support of the Fast Breeder Development Program," WASH-1066 (January, 1966).

3. Chezem, C. G., "A Uranium-Metal Exponential Experiment," NSE, 8, 652-669 (1960).

4. Martens, F. H., ed., "The Fast Exponential Experiment," ANL-5379 (1955).

5. Borgwaldt, H., et al., "SUAK, a Fast Subcritical Facility for Pulsed Neutron Measurements," Proceedings of the Symposium on Pulsed Neutron Research, Session V, Karlsruhe (May, 1965).

6. "LMFBR Program Plan," Vol. 9, Physics, WASH-1109 (August, 1968).

7. Forbes, I. A., "Ph. D. Thesis Prospectus," Nuclear Engineering Department, M. I. T. (April, 1967).

8. Herbst, D. A. and J. H. Talboy, "Preliminary Design Study of a Neutron-Spectrum Converter for Use in the Juggernaut Reactor's East Thermal Column," ANL-7244 (July, 1966).

9. Kato, W. Y., G. J. Fischer and L. R. Dates, "Safety Analysis Report, Argonne Fast Critical Facility (ZPR-VI)," ANL-6271 (December, 1963).

10. Reardon, W. A. and H. H. Hummel, "A Study of the Equilibration Process in the ANL Fast Exponential Pile," NSE, 3, 201 (1958).

11. Tobias, M. L. and T. B. Fowler, "The TWENTY GRAND Program for the Numerical Solution of Ten-Group Neutron Diffusion Equations in Two Dimensions," ORNL-3200 (July, 1961).

12. Plebuch, R. K., "Reactor Physics of Nuclear Rocket Reactors," Sc. D. Thesis, Department of Nuclear Engineering, M. I. T. (1963).

13. Moorhead, I. P., "The Effects of Errors in Cross Section Data on Calculations for a Large Dilute Fast Reactor," Proceedings of the I.A.E.A. Seminar on the Physics of Fast and Intermediate Reactors, Vol. II, Vienna (August, 1961).

14. Flatt, H. P., D. C. Baller and E. R. Cohen, "AIM-5: A Multigroup, One-Dimensional Diffusion Equation Code," NAA-SR-7137 (April, 1962).

15. Flatt, H. P. and D. C. Baller, "The AIM-6 Code," AI-Memo (January, 1961).

16. Engle, W. W., M. A. Boling and B. W. Colston, "DTF-II, A One-Dimensional, Multigroup Neutron Transport Program," NAA-SR-10951 (March, 1966).

17. Engle, W. W., "A User's Manual for ANISN," K-1693 (March, 1967).

18. Boling, M. A. and W. A. Rhoades, "DTF-II / ANISN Conversion to IBM SYSTEM / 360," AI-66-Memo 171 (April, 1967).

19. Hansen, H. E. and W. H. Roach, "Six and Sixteen Group Cross Sections for Fast and Intermediate Critical Assemblies," LAMS-2543 (December, 1961).

20. Codd, J., M. F. James and J. E. Mann, "Some Physics Aspects of Cermet and Ceramic Fast Systems," Proceedings of the I.A.E.A. Seminar on the Physics of Fast and Intermediate Reactors, Vol. II, Vienna (August, 1961).

21. "Proceedings of the Conference on Breeding, Economics and Safety in Large, Fast Power Reactors," ANL-6792 (October, 1963).

22. "Proceedings of the Conference on Safety, Fuels and Core Design in Large, Fast Power Reactors," ANL-7120 (October, 1965).

23. "Proceedings of the International Conference on Sodium Technology and Large Fast Reactor Design," ANL-7520 (November, 1968).

24. Hasnain, S. A. and D. Okrent, "On the Design and Management of Fast Reactor Blankets," NSE, 9, 314-322 (March, 1961).

25. Sesonske, A. and R. P. Hammond, "A Preliminary Investigation of Fast Oxide Breeder Reactors for Sea Water Conversion," LA-2733 (October, 1962).

26. Greebler, P. and E. Goldman, "Doppler Calculations for Large, Fast Ceramic Reactors," GEAP-4092 (December, 1962).

27. Loewenstein, W. B. and G. W. Main, "Fast Reactor Shape Factors and Shape-Dependent Variables," ANL-6403 (November, 1961).

28. Palmedo, P. F., I. Kaplan and T. J. Thompson, "Measurements of the Material Bucklings of Lattices of Natural Uranium Rods in D_2O," NYO-9660, MITNE-13 (1962).

29. Creutz, E. and K. Downes, "Magnetite Concrete for Radiation Shielding," J. Appl. Phys., 20, 1236 (1949).

30. Synan, J. W., "Design and Construction of B.T.F. Blanket No. 1," Course 22.90 Report, Department of Nuclear Engineering, M.I.T. (August, 1969).

31. Woodruff, G. L., I. Kaplan and T. J. Thompson, "A Study of the Spatial Distributions of Fast Neutrons in Slightly Enriched Uranium Rods Moderated by Heavy Water," MIT-2344-5, MITNE-67 (November, 1965).

32. McElroy, W. N. et al., "A Computer-Automated Iterative Method for Neutron Flux Spectra Determination by Foil Activation," AFWL-TR-67-41 (August, 1967).

33. Klucar, J. L., "Design and Construction of B.T.F. Blanket No. 2," Course 22.90 Report, Department of Nuclear Engineering, M.I.T. (August, 1969).

34. Bennett, E. F., "Fast Neutron Spectroscopy by Proton-Recoil Proportional Counting," NSE, 27. 16-27 (1967).

35. Bennett, E. F., "Neutron Spectrum Measurement in a Fast Critical Assembly," NSE, 27, 28-33 (1967).

36. Davey, W. G. and C. E. Till, "The Demonstration Reactor Benchmark Program," Report No. ZPR-TM-10 (December, 1969).

37. Gage, A. M., "Neutron Fluxes, Gamma-Ray Dose Rates and Temperatures in the Iron-Magnetite Concrete Shield of the Omega West Reactor," LA-2155 (December, 1957).

38. "Report on Shielding Calculations for the Exponential Experiment at the MITR," MITR Internal Memorandum (July, 1959).